NEOGENE LOW-LATITUDE SEASONAL ENVIRONMENTAL VARIATIONS: STABLE ISOTOPIC AND TRACE ELEMENTAL RECORDS IN MOLLUSKS FROM THE FLORIDA PLATFORM AND THE CENTRAL AMERICAN ISTHMUS

A Dissertation

by

KAI TAO

Submitted to the Office of Graduate Studies of
Texas A&M University
in partial fulfillment of the requirements for the degree of

DOCTOR OF PHILOSOPHY

August 2012

Major Subject: Geology

Neogene Low-latitude Seasonal Environmental Variations: Stable Isotopic and Trace Elemental Records in Mollusks from the Florida Platform and the Central American Isthmus

NEOGENE LOW-LATITUDE SEASONAL ENVIRONMENTAL VARIATIONS: STABLE ISOTOPIC AND TRACE ELEMENTAL RECORDS IN MOLLUSKS FROM THE FLORIDA PLATFORM AND THE CENTRAL AMERICAN ISTHMUS

A Dissertation

by

KAI TAO

Submitted to the Office of Graduate Studies of
Texas A&M University
in partial fulfillment of the requirements for the degree of

DOCTOR OF PHILOSOPHY

Approved by:

Chair of Committee,	Ethan L. Grossman
Committee Members,	Debora J. Thomas
	Thomas E. Yancey
	Thomas Olszewski
	Niall C. Slowey
Head of Depaartment,	J. Rick Giardino

August 2012

Major Subject: Geology

ABSTRACT

Neogene Low-latitude Seasonal Environmental Variations: Stable Isotopic and Trace Elemental Records in Mollusks from the Florida Platform and the Central American Isthmus. (August 2012)

Kai Tao, B.S., University of Science and Technology of China

Chair of Advisory Committee: Dr. Ethan L. Grossman

This Ph.D. dissertation integrates stable isotope and trace element geochemistry in modern and fossil gastropod shells to study low-latitude marine paleoenvironments. First, stable isotopes ($\delta^{18}O$ and $\delta^{13}C$) and Sr/Ca ratios are used to examine low-latitude temperature and salinity variations recorded in Plio-Pleistocene (3.5-1.6 Ma) fossils from western Florida during periods of high-latitude warming and "global" cooling. The middle Pliocene Pinecrest Beds (Units 7 and 4) and the overlaying Plio-Pleistocene Caloosahatchee Formation generate significantly different $\delta^{18}O$-derived paleotemperatures but identical Sr/Ca ratios. High $\delta^{18}O$ values, together with low $\delta^{13}C$ values and brackish fauna, indicate that Unit 4 was deposited in a lagoonal environment similar to modern Florida Bay. In contrast, relatively low $\delta^{18}O$ and high $\delta^{13}C$ values in Unit 7 and Caloosahatchee Formation represent deposition in an open-marine environment. The observed Unit 7 and Caloosahatchee paleotemperatures are inconsistent with middle Pliocene warming event, but consistent with the Plio-Pleistocene cooling trend.

To quantify modern upwelling and freshening signals and contrast these signals between the tropical eastern Pacific (TEP) and southwestern Caribbean (SWC), methodologies are developed for reconstructing seasonal upwelling and freshening patterns from modern tropical gastropod shells from Panama using: 1) paired oxygen and carbon isotopic profiles and $\delta^{18}O$–$\delta^{13}C$ (δ–δ) correlations, and 2) deviation from baseline $\delta^{18}O$ values that represent conditions free of seasonal upwelling or freshening influences. Shell $\delta^{18}O$ values normalized to the baseline faithfully record modern conditions of little or no upwelling in SWC and Gulf of Chiriquí, and strong upwelling in the Gulf of Panama, as well as strong freshwater input in most areas.

The baseline and δ– δ methods are applied to identify and quantify changes in upwelling and freshening in the Neogene TEP and SWC seawaters associated with the final closure of Central American Isthmus. The records reveal significant upwelling in late Miocene SWC and mid Pliocene TEP waters, strong freshening in SWC waters from 5.7–2.2 Ma, and minimal seasonal upwelling and/or freshening variations in Plio-Pleistocene SWC waters. The reconstructed paleotemperatures agree with the global cooling trend through the late Miocene, but lack evidence for middle Pliocene warming or late Neogene global cooling.

ACKNOWLEDGEMENTS

I would like to thank my committee chair, Dr. Ethan Grossman, and my committee members, Drs. Deborah Thomas, Thomas Yancey, Thomas Olszewski, and Niall Slowey, for their guidance and support throughout the course of this research.

Thanks also go to my friends and colleagues and the faculty and staff of the Department of Geology and Geophysics, especially Post-doctoral researcher John Robbins, for making my time at Texas A&M University a great experience. I also want to extend my gratitude to the Smithsonian Tropical Research Institution for providing partial funds for the field trip and sample collections. I want to specially thank Dr. Aaron O'Dea for the help in sample collection and insightful comments on the paper manuscripts. I also want to thank Roger Portell from Florida Museum of Natural History and Tom Duda from Museum of Zoology in the University of Michigan for providing partial samples. Thanks go to Sindia Sosdian and Luz Romero for the help in trace elemental analyses. Finally, thanks to my mother and father for their love and encouragement.

TABLE OF CONTENTS

Page

LIST OF FIGURES

FIGURE Page

LIST OF TABLES

CHAPTER I

INTRODUCTION

Stable isotopic signatures provide valuable information for understanding global climate change and nutrient deliveries. During the Neogene period, the global climate maintained a long-term cooling trend with exceptions in middle Miocene (17–14.5 Ma) and in middle Pliocene (3.5–2.5 Ma), evidenced by benthic foraminiferal oxygen isotopic records (Zachos et al., 2001), sea level change (Haq et al., 1987), and fossil abundance (Allmon, 1993), etc. However, the tropical sea-surface temperature (SST) changes may differ from the global trend that is largely derived from high-latitudes. For example, the middle Pliocene tropical SST reconstructions from ostracod assemblages (Cronin and Dowsett, 1993; Dowsett et al., 1996) and from planktonic foraminiferal stable isotopes (Billups et al., 1998) both indicate equal or slightly cooler (2–3 ^{o}C) temperatures relative to modern SSTs, while the high-latitude SSTs were estimated to be 4–6 ^{o}C warmer than present (Dowsett et al., 1996; Dowsett and Loubere, 1992). Similar to the middle Pliocene controversy, there has been a recent debate regarding low-latitude climate change during the late Miocene cooling. A study of planktonic foraminiferal δ^{18}O-derived SSTs from 33 late Miocene (7.2–5.6 Ma) Ocean Drilling Project (ODP) and Deep Sea Drilling Project (DSDP) sites suggests markedly cool low-latitude temperatures, in some cases more than 9°C lower than modern SSTs (e.g. DSDP 216 and 709C, Williams et al., 2005). Meanwhile, SST estimates from Mg/Ca analyses of

---

This thesis/dissertation follows the style of Palaios.

planktonic foraminifera in the west Caribbean (ODP 999) suggest cool tropical temperatures that are about 2℃ lower than modern (Groeneveld, 2005, Groeneveld et al., 2008). However, SST estimates from alkenone unsaturation analyses from ODP site 958, northeastern Atlantic (23.9990°N, 20.0008°W), suggest subtropical SSTs that were warmer by 2–4°C (Herbert and Schuffert, 1998). Discrepancies such as these have lead scientists to question the accuracy of the $\delta^{18}O$-derived paleotemperatures from calcitic planktonic foraminifers, citing the potential influences of dissolution and diagenesis, vital effect, and changes in seawater $\delta^{18}O$ (Pearson et al., 2001; Williams et al., 2005).

The formation of Central American Isthmus (CAI) had a dominant impact on late Neogene climate. At present, there are significant differences between tropical east Pacific (TEP) and southwestern Caribbean (SWC) waters across the isthmus, which include differences in mean annual temperature (MAT), salinity, nutrient concentrations, primary productivity, and stable isotopic composition. The modern Caribbean-Pacific contrast of surface water MAT of 2°C and salinity of 1–1.5‰ was established by about 4.2 Ma (Keigwin, 1982; Haug et al., 2001), resulting largely from (1) strong seasonal upwelling of nutrient-rich waters in the Pacific that reduces temperature and increases productivity, and (2) high evaporation in the Caribbean and net Caribbean-Pacific vapor flux that increases salinity in the Caribbean and reduces salinity in the Pacific (Maier-Reimer et al., 1990; D'Croz et al., 1991; D'Croz and O'Dea, 2007). Prior to the isthmian uplift when the seaway was still open, these contrasts were minimal.

To evaluate the low-latitude environmental variation during the "global" warming or cooling period, and the temperature contrast in TEP and SWC seawaters before and after the final closure of CAI, additional SST proxies, such as $\delta^{18}O$ and Sr/Ca ratios of

molluscan (especially gastropods) shells are used in this study. In isotopic studies, mollusks provide a strong complement to planktonic foraminifera for reconstructing ancient climates in that: 1) their long life span provides records of both seasonal and interannual temperature variations, which are unavailable from foraminifera; 2) their aragonitic mineralogy makes it easier to assess chemical preservation; 3) their shallow benthic habitat ensures that they do not sink below the carbonate compensation depth (CCD) and thus less likely to be dissolved.

These advantages have raised interest in using mollusks as a substitute for planktonic foraminifera in isotopic studies of paleoclimate (e.g. Kobashi et al., 2001; Latal et al., 2004). However, isotope records from the mollusks have their own limitations resulting from uncertain local salinity and temperature variation. One possible method to avoid such ambiguities is by combining isotopic and trace metal records (e.g. Sr/Ca). It has already been demonstrated that Sr/Ca in some modern molluscan shells provides a proxy for independently estimating SSTs (Sosdian et al., 2006). By making paired measurements of $\delta^{18}O$ and Sr/Ca on the same shell, we can estimate the record of seawater $\delta^{18}O$ which may be used to reconstruct local changes in salinity. This method has been used in **Chapter 2** to reconstruct the paleoenvironments in the middle Pliocene Pinecrest Beds (Unit 7 and 4) and Plio-Pleistocene Caloosahatchee Formation.

In addition to being a paleo-SST proxy, stable isotopes can also be used for testing nutrients delivered by upwelling and freshwater input in low-latitude and tropical marine ecosystems. **Chapter 2** identifies the origin of high productivity in the Florida Platform in middle Pliocene by comparing the oxygen and carbon isotope pattern to modern Florida Bay conditions. **Chapter 3** describes stable isotope analyses ($\delta^{13}C$ and

$\delta^{18}O$) on 13 serially-sampled modern *Conus* shells collected from southwestern Caribbean (SWC, non-upwelling) and tropical eastern Pacific (TEP) Gulf of Chiriquí (non-upwelling) and Gulf of Panama (upwelling) coastal waters across the Central American Isthmus (CAI), aiming to develop a new method which uses "normal" temperatures that are free of seasonal upwelling during dry season and "normal" salinities that are free of seasonal freshwater runoff during rainy season to establish a baseline for molluscan shell $\delta^{18}O$ values. $\delta^{18}O$ values that significantly exceed baseline $\delta^{18}O$ values can be only caused by the decrease of seawater temperature created by upwelling of cold saline deep water; $\delta^{18}O$ values that are significantly below baseline can be only caused by intensive freshwater runoff which lower the seawater salinity.

The newly-developed baseline method can be complementary to the traditional method of paired oxygen and carbon isotopic correlations. For example, in **Chapter 3** all five shells in the upwelling area of Gulf of Panama show positive $\delta^{18}O$–$\delta^{13}C$ correlations, which are indicative of freshwater input only. However, the baseline method detects both significant upwelling and freshening signals in this area. A closer examination by separating dry-season shell $\delta^{18}O$ values from the rest of year reveals significant negative correlation in four of five shells, confirming the hypothesis that the freshwater signal during rainy season masks the expected upwelling signals in the modern Gulf of Panama.

In **Chapter 4**, the combined stable isotope methods are applied to Neogene molluscan shells across CAI from late Miocene to Plio-Pleistocene (12–1.5 Ma) to test the changes of marine environmental variation between TEP and SWC waters.

CHAPTER II

ORIGIN OF HIGH PRODUCTIVITY IN THE PLIOCENE OF THE FLORIDA PLATFORM: EVIDENCE FROM STABLE ISOTOPES AND TRACE ELEMENTS*

Overview

High productivity on the Florida Platform during the Pliocene has been ascribed to upwelling and to freshwater input of nutrients. To test these hypotheses, high-resolution stable isotopic and Sr/Ca analyses have been performed on 14 *Conus* and *Turritella* gastropod shells collected from the middle Pliocene Pinecrest Beds (Units 7 and 4) and the Plio-Pleistocene Caloosahatchee Formation. Assuming a published Pliocene seawater $\delta^{18}O$ of 1.02‰ derived from a coupled ocean-atmosphere general circulation model (OAGCM), reconstructed paleotemperatures of Units 7 and 4, and the Caloosahatchee are respectively 25.1 ±1.4°C, 16.1 ±0.6°C, and 22.4 ±0.5°C. Unit 7 paleotemperatures are similar to, and Caloosahatchee paleotemperatures slightly lower than, modern sea surface temperatures (SSTs) in the Sarasota Bay (24.5 ±0.4°C). In contrast, Unit 4 paleotemperatures are unrealistically low. Sr/Ca ratios, however, suggest no significant paleotemperature difference between Pinecrest Units 7 and 4 and the Caloosahatchee Formation, indicating seawater $\delta^{18}O$ variations, rather than temperature differences, are responsible for $\delta^{18}O$ differences. High $\delta^{18}O$ and low $\delta^{13}C$ values of these samples likely reflect highly evaporated freshwater input combined with oxidation of terrestrial debris as a brackish environment is indicated by marine and freshwater fauna in Unit 4. This

---

* Reprinted with permission from "Origin of high productivity in the Pliocene of the Florida platform: evidence from stable isotopes and trace elements" by Tao, K. and Grossman, E. L., 2010, *Palaios,* v. 25, p.796-806, copyright [2010] by SEPM.

isotopic pattern is similar to that for modern Florida Bay mollusks which are influenced by discharge of Everglades waters. Furthermore, episodic enrichments in Fe, U, and P in some shells suggest nutrient input from submarine groundwater discharge. The data, therefore, support the contention that the dominant cause of high productivity in this region was enhanced nutrient input from freshwater influx.

Introduction

The great diversity and abundance of the molluscan fauna on the Florida Platform suggest that oceanic productivity was higher during the middle Pliocene (ca. 3.5–2.5 Ma; Piacenzian) than in the Pleistocene and Recent (Allmon, 1993; Allmon et al., 1996). For example, the middle Pliocene Pinecrest Beds in southwest Florida consist of fossiliferous shelly beds up to 10 m thick with as many as 1,000 molluscan species (Petuch, 1982). Moreover, the frequent occurrence of turritellid gastropods, which presently live in nutrient-rich marine environments, also suggest high oceanic productivity (Allmon, 1988). Although the faunal and geological history of the Florida Platform has been well studied, hypotheses for the cause of high productivity are still debated. The two leading hypotheses are enhanced upwelling (Jones and Allmon, 1995; Allmon et al., 1996) and input of nutrient-rich freshwater (Weinlein et al., 2008; Sliko and Herbert, 2009). Our study examines the possible causes for the middle-Pliocene high productivity by utilizing seasonal isotopic and trace elemental profiles from middle Pliocene and Plio-Pleistocene *Conus* and *Turritella* gastropods collected from the Florida Platform.

Jones and Allmon (1995) proposed that seasonal upwelling is responsible for high productivity on the Florida Platform during the middle Pliocene, based on stable isotope

profiles of the bivalve *Mercenaria campechiensis* and turritellid gastropods. Upwelling would bring cool and nutrient-rich deep waters to the Florida coastal area, causing high productivity and lower marine temperatures off western Florida during the middle Pliocene. Reliable stable isotopic evidence for enhanced upwelling is scarce, however. Only one of two specimens of *M. campechiensis* (MC130) and two of eight specimens of *Turritella gladeensis* (specimens 2b and 3) show the distinct upwelling signals (negative $\delta^{18}O$–$\delta^{13}C$ correlation, $p<0.05$) and as stated in Jones and Allmon (1995. p.71), "the [upwelling] signals measured in our Pliocene turritellids are fairly weak".

Other nutrient sources, such as freshwater influx, may also contribute to the high productivity. Such a stable isotopic signal has been noted in one turritellid (*Turritella apicalis*; Allmon et al., 1996). Meanwhile, a study of the Pliocene and Pleistocene productivity on the Florida Platform, using Fe/Ca and Ba/Ca in mollusk shells as proxies for terrigenous input and productivity, also argues that freshwater input was the primary control for productivity (Weinlein et al., 2008). Furthermore, a recent study combining stable isotopic and trace elemental analyses of Pliocene *Siderastrea spp*. corals suggests high winter or spring precipitation on the southeastern North American continent, coincident with pulses of phosphate, and supports the hypothesis that freshwater is the major cause for high productivity (Sliko and Herbert, 2009).

Stable isotopes alone cannot easily distinguish between the environmental causes of high productivity. This is particularly important in shallow, estuarine environments where such localized effects as freshwater input and evaporative loss frequently occur. Salinity-independent proxies are needed to constrain the $\delta^{18}O$-derived paleotemperatures. Studies have shown that Sr/Ca variations in molluscan shells reflect temperature changes

with presumably little influence from evaporation, precipitation or freshwater input (Tripati and Zachos, 2000; Sosdian et al., 2006). Although the exact relationship between Sr/Ca and temperature in mollusks is complex and taxon-specific, Sr/Ca ratios can still be immensely useful in interpreting paleoenvironments (Sosdian et al., 2006; Tripati et al., 2009). Furthermore, other trace elements such as P may serve as nutrient proxies (Montagna et al., 2006; Sliko and Herbert, 2009).

Study Area and Samples

In this study five *Conus* and two *Turritella* shells were collected from Unit 7 (ca. 3.5–2.5 Ma) of the Pliocene Pinecrest Beds in SMC Aggregates Phase 8 Quarry in the vicinity of Sarasota County, Florida (27º22.61'N, 82º23.47'W; Location 1 in Fig. 2-1). Additional shells were provided by the Florida Museum of Natural History, including three *Conus* shells from Unit 4 (ca. 2.5–2.0 Ma) of the Pinecrest Beds in a quarry 6 km west of Phase 8 Quarry, one *Conus* shell from Unit 7 of the Pinecrest Beds in Highlands County (27º21.97'N, 81º0.33'W, Location 2 in Fig. 2-1), and three *Conus* shells from the Plio-Pleistocene Caloosahatchee Formation (ca. 2.0–1.6 Ma) in Hendry County (26º43.22'N, 81º29.45'W, Location 3 in Fig. 2-1). The middle Pliocene Pinecrest Beds has an excellent diversity of well-preserved fossil shells. The 0.6-m-thick Unit 4 is often referred to as the black layer (Petuch, 1982) or bone-bearing layer (Jones et al., 1991) because of its great abundance of both marine and freshwater shells, and fossils of fish and other vertebrates, which indicate an organic-rich brackish and estuarine environment. The 4.6-m-thick Unit 7, with its great diversity of marine molluscan species, is considered to have been deposited in a tropical-subtropical offshore environment with a

water depth of 20–30 m (Jones et al., 1991). Overlying the Pinecrest Beds in the southern Florida peninsula is the late Pliocene-early Pleistocene Caloosahatchee Formation, which

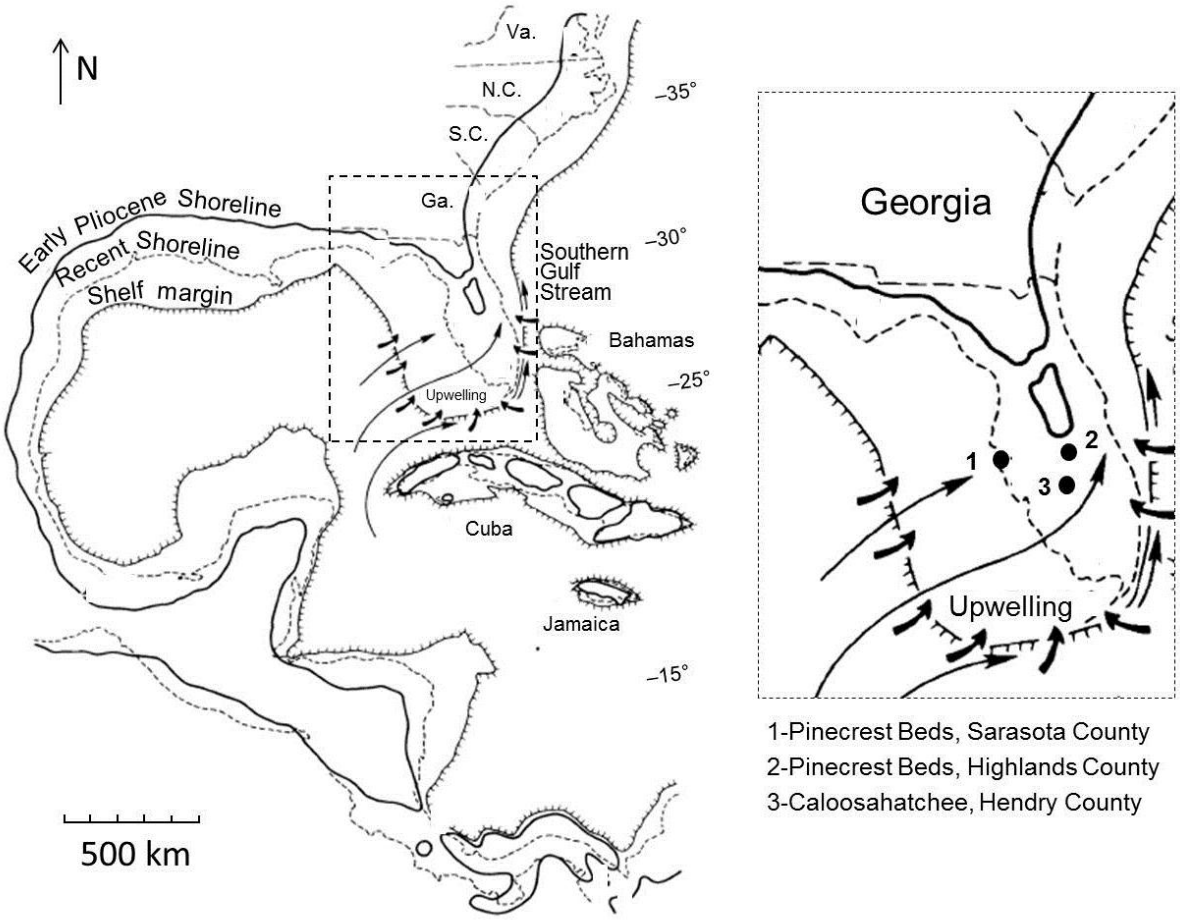

FIGURE 2-1—Study area. Map of the Gulf Coast in the middle Pliocene from Stanley (1986), with numbers indicating sample locations.

consists mostly of fossiliferous sands and carbonates. Molluscan shells are the dominant fossils, and along with corals, bryozoans, echinoids, and vertebrates, indicate a shallow, warm-water estuarine environment (Lyons, 1990).

Twelve *Conus* and two *Turritella* shells were analyzed for stable isotopes, including ten *Conus adversarius* Conrad (1840), one *C. largillierti* Kiener (1845), one *C. spurius*

Gmelin (1791), and two *Turritella gladeensis* Mansfield (1931). Eight of the twelve *Conus* shells and both *Turritella* shells were analyzed for trace elements. These taxa have the advantages of: (1) relatively long life span (2 to >5 years) and large size, which enable inter-annual and seasonal temperature reconstruction (excluding *T. gladeensis*, which usually lives less than 2 years); (2) aragonitic shell mineralogy that facilitates detection of diagenesis; and (3) shallow-dwelling habitat, making possible the estimation of marine surface temperatures.

Methods

Prior to sampling, each specimen was polished and ultrasonicated to remove extraneous materials from shell surfaces. X-ray diffraction analyses have confirmed that all the shells are >99% aragonite. For the serial sampling, a 2–5 mm interval, starting from the apex of shell spiral, was chosen to construct isotopic and trace elemental profiles. Sample powder was collected along shallow linear grooves parallel to growth lines, using a 0.5 mm wide Brasseler carbide dental drill bit. Approximately 300–500 μg powder was collected for each sample, with half for stable isotope analyses and half sent to Rutgers University for elemental analyses. For stable isotopic analyses, about 100 – 150 μg of shell powder was converted to CO_2 gas by reaction with "100%" phosphoric acid at 70°C on a GasBench II automated gas-handling system. The CO_2 gas was then analyzed on a DeltaPlusXP isotope ratio mass spectrometer. All the results were calibrated to Vienna-PDB (VPDB) using NBS-19, with a precision of ±0.05‰ for $\delta^{13}C$ and ±0.08‰ for $\delta^{18}O$. Replicates were run for every two to three samples. The average absolute value for the difference between replicates is 0.10‰ for $\delta^{13}C$ and 0.12‰ for

$\delta^{18}O$. Paleotemperatures were calculated according to Grossman and Ku (1986; eq. 1) and corrected for seawater $\delta^{18}O$ (see later discussion). For trace elemental analysis, the samples were dissolved in 0.065N HNO_3, centrifuged 10 minutes, and diluted to obtain a final Ca concentration of about 4±1 mmol (Sosdian et al., 2006). Then the solution was analyzed on a Vista-Pro CCD Simultaneous Radial ICP-OES based on the method in Andreasen et al. (2006). Long-term precision for Sr/Ca analyses is ±1.5%. Statistical analyses, including *t*-tests and principal component analysis (unrotated factors), were performed using SAS 9.1.3 and StatView 5.0.1, respectively.

Results and Discussion

Oxygen Isotopes

The $\delta^{18}O$ values of specimens from Units 7 and 4 in the Pinecrest Beds generally fall into two groups. Specimens from Unit 7 range from -1.8 to 2.0‰ and average -0.2‰, while those from Unit 4 range from 0.1 to 3.2‰ and average 1.9‰ (Fig. 2-2, Table 2-1). An exception is specimen PTF-1A from Unit 7 (range = 0.7–2.8‰, mean = 1.7‰). The three specimens from the Caloosahatchee Formation range from -0.9 to 1.9‰ and average 0.4‰, slightly higher values than those from Pinecrest Beds Unit 7 but much lower than those from Unit 4.

The oxygen isotope profiles of all specimens are cyclical, reflecting seasonal temperature variation (Fig. 2-2). Most shell oxygen isotope profiles show two or more annual cycles. Large specimens (e.g., 112293) tend to have rapid growth rates in the first and second annual cycles and reduced growth rates in the subsequent cycles (Fig. 2-2 & 2-3). *Conus* specimen 46317-1 shows a sudden increase of both $\delta^{18}O$ and $\delta^{13}C$ following

minima at 115 mm from apex, indicating a cessation of growth between late summer and winter. This hiatus corresponds to a recovery fracture from predation on the shell surface.

The oxygen isotope profiles often have a sawtooth-shaped asymmetry with large increments during spring and summer and small increments during fall and winter, most clearly evident in samples 54437-1 and 54437-2. Note in the profile of 61689 the double-peak pattern in which secondary $\delta^{18}O$ minima (e.g., 40 mm) appear before more extreme summer values (e.g., 70 mm). This may reflect spring drought, which interrupts the decreasing $\delta^{18}O$ trend, caused by warming, with a $\delta^{18}O$ increase due to evaporation and reduced input of low-$\delta^{18}O$ freshwater. Note that spring drought is common in Florida today.

Carbon Isotopes

Similar to the oxygen isotope values, the carbon isotope values of Pinecrest Beds specimens also fall into two groups: specimens from Unit 7 range from 0.4 to 2.9‰ and average 1.9‰ while those from Unit 4 are much lower, ranging from -2.3 to 0.7‰ and averaging -0.9‰ (Fig. 2-2, Table 2-1). The Unit 7 specimen that shows exceptional $\delta^{18}O$ values (PTF-1A) does not significantly differ in $\delta^{13}C$ from other Unit 7 samples. The three specimens from Caloosahatchee Formation range from 0.6 to 3.2‰ and average 1.9‰. These values are slightly higher than those from Pinecrest Beds Unit 7 and much higher than those from Unit 4.

The carbon isotope profiles are more complicated than the oxygen isotope profiles (Fig. 2-2, Table 2-1). In some specimens (e.g., 54437-1, 54437-2, 39147-2), carbon isotope cycles correlate positively with oxygen isotope cycles. Such correlations have

been attributed to salinity variations (Mook, 1971; Surge et al., 2003; Gentry et al., 2008). Other shells (e.g. 112293, PTF-1B2), however, show little $\delta^{13}C$-$\delta^{18}O$ covariance. Other

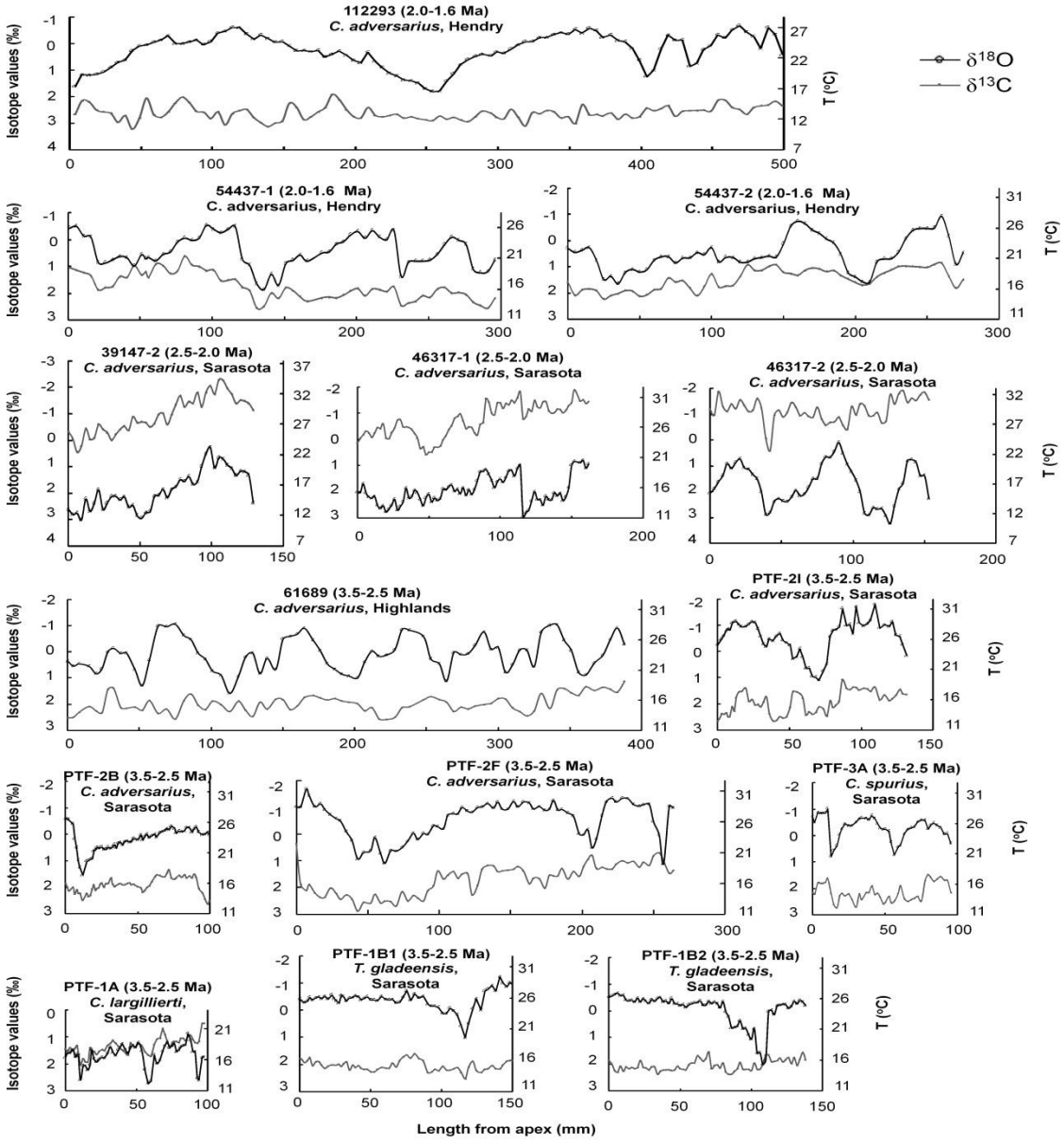

FIGURE 2-2—Oxygen and carbon isotope profiles of 14 gastropod shells collected in the middle Pliocene Pinecrest Beds in Sarasota and Highlands counties and Plio-Pleistocene Caloosahatchee Formation in Hendry County. Isotope values are versus VPDB; paleotemperature calculated after Grossman and Ku (1986) eq. 1, assuming $\delta^{18}O_{sw}$ = 1.02‰ (Williams et al., 2009).

factors that can influence $\delta^{13}C$ values include metabolic changes with ontogeny (e.g., Jones et al., 1983; Lorrain et al., 2004), which are evidenced in the overall decreasing trend in most specimens. The decreasing $\delta^{13}C$ trend is also seen in modern *Conus* specimens (Kobashi and Grossman, 2003; Gentry et al., 2008). According to Klein et al. (1996), rapid growth rate, such as during the gastropod's juvenile stage, correlates with low mantle metabolic activity and lesser influence of ^{13}C-depleted metabolic CO_2 on shell $\delta^{13}C$. As the specimen ages, however, slower growth rate and higher mantle metabolic activity result in greater influence of ^{13}C-depleted metabolic CO_2 and lower shell $\delta^{13}C$. Shell $\delta^{13}C$ values may also reflect the spatial variations in the local seawater $\delta^{13}C$, as discussed later.

TABLE 2-1—$\delta^{18}O$-derived paleotemperatures from mollusks and their $\delta^{18}O$–$\delta^{13}C$ covariance.

Sample ID	species	Formation	$\delta^{18}O_{max}$	$\delta^{18}O_{min}$	$\delta^{18}O_{mean}$	T_{max}	T_{min}	T_{mean}	$\delta^{13}C_{max}$	$\delta^{13}C_{max}$	$\delta^{13}C_{mean}$	O-C Corr	O-C p-value
112293	*C.adversarius*	Caloosa.	1.81	-0.68	0.27	27.1	16.3	23.0	3.22	1.91	2.61	0.12	0.2229
54437-1	*C.adversarius*	Caloosa.	1.86	-0.52	0.44	26.4	16.1	22.2	2.56	0.63	1.75	0.51	<0.0001
54437-2	*C.adversarius*	Caloosa.	1.59	-0.93	0.48	28.2	17.2	22.0	2.23	0.85	1.47	0.64	<0.0001
39147-2	*C.adversarius*	Unit 4	3.02	0.27	1.90	23.0	11.0	15.9	0.46	-2.29	-0.95	0.88	<0.0001
46317-1	*C.adversarius*	Unit 4	2.96	0.79	1.96	20.7	11.3	15.6	0.59	-1.89	-0.71	0.52	<0.0001
46317-2	*C.adversarius*	Unit 4	3.24	0.09	1.70	23.7	10.1	16.7	0.40	-1.92	-1.15	0.10	0.4729
PTF-1A	*C.largillierti*	Unit 7	2.76	0.68	1.67	21.2	12.1	16.9	2.00	0.36	1.29	0.45	0.0005
PTF-1B1	*T.gladeensis*	Unit 7	1.01	-1.23	-0.38	29.5	19.7	25.8	2.52	1.61	2.05	0.43	0.0004
PTF-1B2	*T.gladeensis*	Unit 7	2.01	-0.66	-0.06	27.0	15.4	24.4	2.38	1.54	2.05	0.06	0.6284
PTF-2B	*C.adversarius*	Unit 7	1.54	-0.60	0.21	26.7	17.4	23.2	2.63	1.33	1.91	0.46	<0.0001
PTF-2F	*C.adversarius*	Unit 7	1.11	-1.69	-0.56	31.5	19.3	26.6	2.89	0.37	1.69	0.46	<0.0001
PTF-2I	*C.adversarius*	Unit 7	1.11	-1.80	-0.55	31.9	19.3	26.5	2.65	1.09	1.95	0.42	0.0009
PTF-3A	*C.spurius*	Unit 7	0.80	-1.03	-0.30	28.6	20.7	25.4	2.73	1.48	2.14	0.35	0.0186
61689	*C.adversarius*	Unit 7	1.59	-1.06	0.09	28.7	17.2	23.7	2.58	1.13	1.98	0.10	0.3736

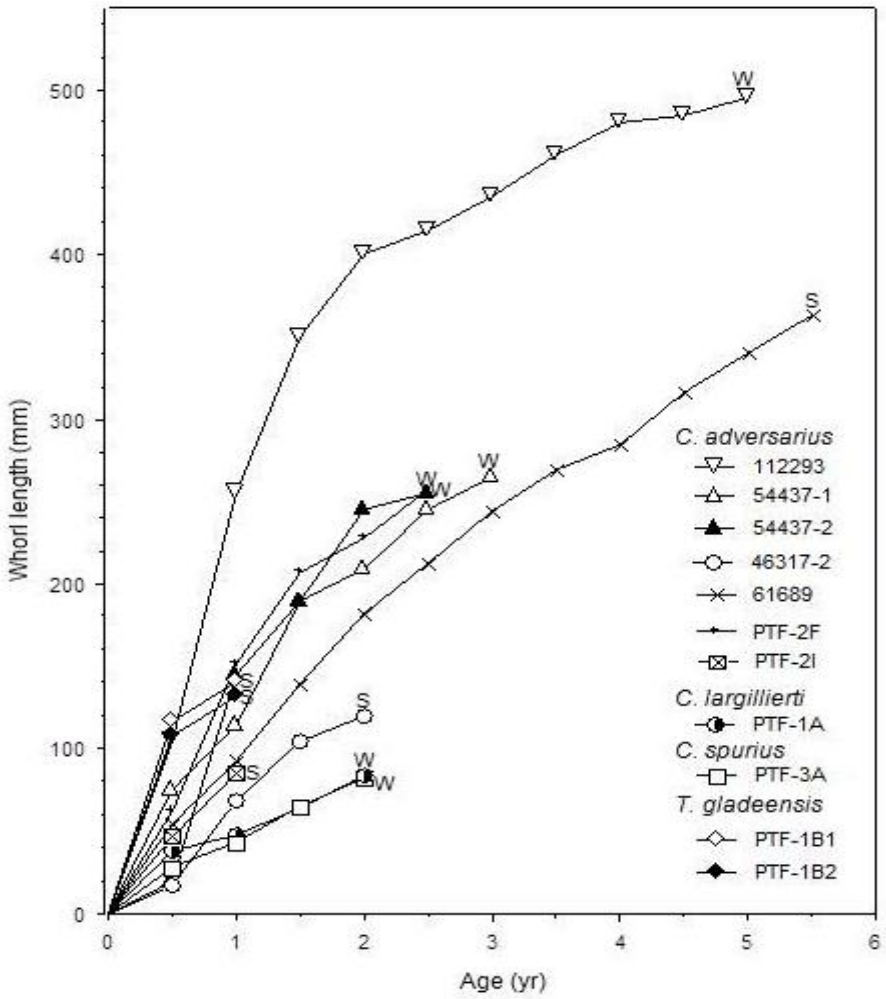

FIGURE 2-3—Growth curves of *Conus* and *Turritella* specimens (whorl length versus age) based on oxygen isotope cyclicity (highest and lowest values represent winter and summer respectively). Growth rates are calculated on semi-annual basis with W (winter) or S (summer) marking their final season of growth.

Sr/Ca Ratios

Eight *Conus* and two *Turritella* shells were selected from the 14 specimens and analyzed for trace elements. These shells provide a range of ages, localities, and taxa. Paired measurements of Sr/Ca and $\delta^{18}O$ are plotted as a function of distance from apex on the spiral (Fig.2- 4). All the *Conus* specimens show significant negative correlation between Sr/Ca and $\delta^{18}O$. These results are similar to those found with modern *Conus*

specimens, which were used along with temperature measurements to define a Sr/Ca paleotemperature relation (Sosdian et al., 2006). The Sr/Ca ratios in the two *Turritella* shells do not correlate with $\delta^{18}O$. This contrasts with results for modern and Paleogene turritellids (Andreasson and Schmitz, 1998; Tripati et al., 2009). Differences in Sr/Ca–$\delta^{18}O$ correlations during juvenile and adult shell portions have been observed in several modern *Conus* specimens (Sosdian et al., 2006; Gentry et al., 2008), which may be caused by changes in habitat, metabolism, and/or diet.

Sr/Ca ratios for *Conus* specimens from Units 7 and 4 have similar ranges, 1.37 to 2.56 and 1.49 to 2.99 mmol/mol, and similar average, 2.04 and 2.11 mmol/mol, respectively (Fig. 2-4, Table 2-2). Caloosahatchee samples have slightly higher Sr/Ca ratios, ranging from 1.79 to 2.57 mmol/mol and averaging 2.17 mmol/mol (excluding one large specimen, 112293 [see later discussion]), respectively. Note that Unit 7 and 4 specimens, while differing in $\delta^{18}O$, do not differ in Sr/Ca ratio.

Among the six *Conus adversarius* specimens, five have accordant Sr/Ca ratios averaging 2.09 ±0.11 (±1σ) mmol/mol, while one (112293) has significantly higher values averaging 2.87 ±0.33 mmol/mol. This abnormally high Sr/Ca ratio may be related to metabolic effects considering the extraordinary size and growth rate of this shell (Fig. 2-3; Klein et al., 1996). Sr/Ca ratios for other *Conus* species in Unit 7, *C. largillierti* (PTF-1A) and *C. spurius* (PTF-3A), are slightly but significantly ($p < 0.05$) lower than those of *C. adversarius* (averaging 1.87 ±0.07 and 1.94 ±0.06 mmol/mol, respectively). These two specimens and species have the slowest growth rates, confirming the relationship between growth rate and Sr/Ca in *Conus*. This relationship suggests the possibility of a

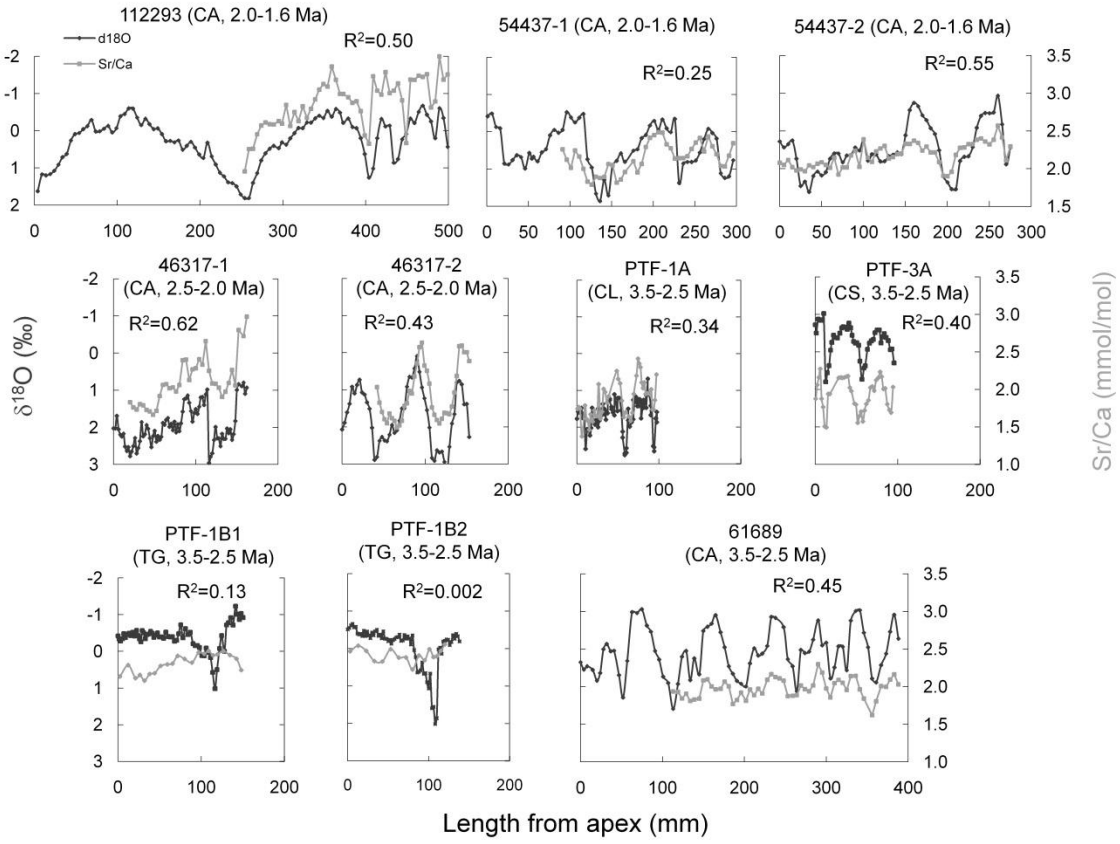

FIGURE 2-4—Sr/Ca ratios and correlation with $\delta^{18}O$ profiles. CA- *Conus adversarius*, CL- *C. largillierti*, CS- *C. spurius*, TG- *Turritella gladeensis*.

growth-rate correction to refine the *Conus* Sr/Ca paleothermometer and its application to extinct species. The two *Turritella gladeensis* shells show Sr/Ca ratios (averaging 2.37 ±0.04 mmol/mol) that are significantly higher than those of the *Conus* specimens, similar to results for Paleogene conids and turritellids (Sosdian et al., submitted).

Other Trace Elements

Other trace elements were analyzed including Mg, Cd, Ba, Mn, P, Fe, and U on select specimens to examine potential proxies for productivity and freshwater input (Table 2-2). P/Ca, in particular, has been used as a proxy for seawater nutrient levels and productivity (Montagna et al., 2006; LaVigne et al., 2008, 2010). Phosphorus may be

derived from upwelling or from freshwater sources. Association of phosphorus with other elements provides clues to the phosphorus source.

Principal component analysis shows that Fe and P have similar factor values (Table 2-3), suggesting that they are responding to the same environmental or metabolic factors. P/Ca ratios in the six *C. adversarius* shells show similar values, with averages ranging from 176 to 261 μmol/mol. Unlike P/Ca ratios, Fe/Ca ratios show inter-species and environmental differences. Unit 7 specimens of *C. adversarius*, *C. spurius* and *T. gladeensis* show a large range (averages of 18, 163, and 13 μmol/mol respectively), while two *C. adversarius* specimens from Unit 4 have low averages (7 and 10 μmol/mol), and three *C. adversarius* specimens from the Caloosahatchee Formation have intermediate averages (37–81 μmol/mol).

U/Ca ratios are only available for four Unit 7 specimens. Two *T. gladeensis* have relatively low average values (170 and 189 nmol/mol) while *C. largillierti* and *C. spurius* have high to very high average values (791 and 10623 nmol/mol, respectively).

Fe/Ca and P/Ca show a positive correlation in four *C. adversarius* specimens (112293, 54437-1, 54437-2, and 61689) but no significant correlations in the other one (46317-1; Fig. 2-5a). Two specimens with both Fe and U data show a correlation between U/Ca and Fe/Ca between specimens and within one specimen (PTF-1B2; Fig. 2-5b, Table 2-2). Although the overall patterns between P, U and Fe are irregular, high P/Ca and U/Ca values are exclusively found with high Fe/Ca values.

TABLE 2-2—Trace element data from ten molluscan specimens including Sr/Ca, P/Ca, Fe/Ca, and U/Ca

			Caloosahatchee Fm			Pinecrest Unit 4		Pinecrest Unit 7				
		TOTAL	112293	54437-1	54437-2	46317-1	46317-2	61689	PTF-1A	PTF-1B1	PTF-1B2	PTF3A
Sr/Ca (mmol /mol)	Mean	2.20	2.87	2.15	2.18	2.12	1.95	1.98	1.87	2.34	2.42	1.94
	SD	0.42	0.33	0.20	0.16	0.32	0.37	0.13	0.25	0.13	0.09	0.21
	Min	1.37	1.95	1.79	1.90	1.67	1.49	1.62	1.37	2.10	2.22	1.50
	Max	3.80	3.50	2.49	2.57	2.99	2.64	2.30	2.43	2.51	2.56	2.28
	Count	420	50	41	56	36	38	53	47	222	16	41
P/Ca (umol/ mol)	Mean	208.9	212.3	191.6	176.4	204.5	198.0	260.9				
	SD	66.6	93.9	76.0	53.3	19.8	22.9	56.2				
	Min	100.9	100.9	103.0	127.5	158.5	165.0	114.7				
	Max	575.6	575.6	498.6	336.3	255.4	303.0	510.7				
	Count	252	43	38	49	36	35	51				
Fe/Ca (umol/ mol)	Mean	50.5	81.5	53.8	36.9	9.7	7.0	17.5			13.0	162.7
	SD	63.8	60.5	33.0	21.5	6.3	2.8	11.2			16.6	93.6
	Min	0.4	7.4	3.9	9.2	2.1	3.6	1.5			0.4	32.5
	Max	355.7	229.5	196.2	115.6	30.0	14.9	49.9			58.5	355.7
	Count	262	48	41	53	33	37	47			16	23
U/Ca (umol/ mol)	Mean	3321							791	170	189	10623
	SD	4831							204	100	73	2869
	Min	37							309	37	111	4630
	Max	16331							1456	468	370	16331
	Count	146							47	22	16	41

TABLE 2-3—Principal component analysis on trace elements of ten molluscan specimens.

	Factor 1	Factor 2	Factor 3	Factor 4
Mg/Ca	0.60	-0.43	-0.33	-0.11
Sr/Ca	0.13	-0.30	0.51	0.75
Cd/Ca	0.31	0.66	-0.44	0.35
Ba/Ca	0.13	-0.68	0.45	-0.19
Mn/Ca	0.59	0.42	0.51	-0.29
P/Ca	0.57	-0.44	-0.30	-0.19
Fe/Ca	0.63	0.60	0.35	-0.12
Al/Ca	0.78	-0.25	-0.18	0.30
U/Ca	N/A	N/A	N/A	N/A

Studies of central Florida's modern freshwater sources help explain observed relations between P, U, and Fe in shells. Central Florida is known to have U-rich phosphate deposits in the Miocene Hawthorn Group (Osmond et al., 1985). Furthermore, Tampa Bay (Florida) waters show local U enrichment attributed to transport across the sediment–water interface by processes such as bioirrigation and submarine groundwater discharge (Swarzenski and Baskaran, 2007). Submarine groundwater input of terrestrial nutrients has been documented for many coastal environments, including coral reefs (Slomp and Van Cappellen, 2004; Paytan et al., 2006; Moore, 2010). High Fe is

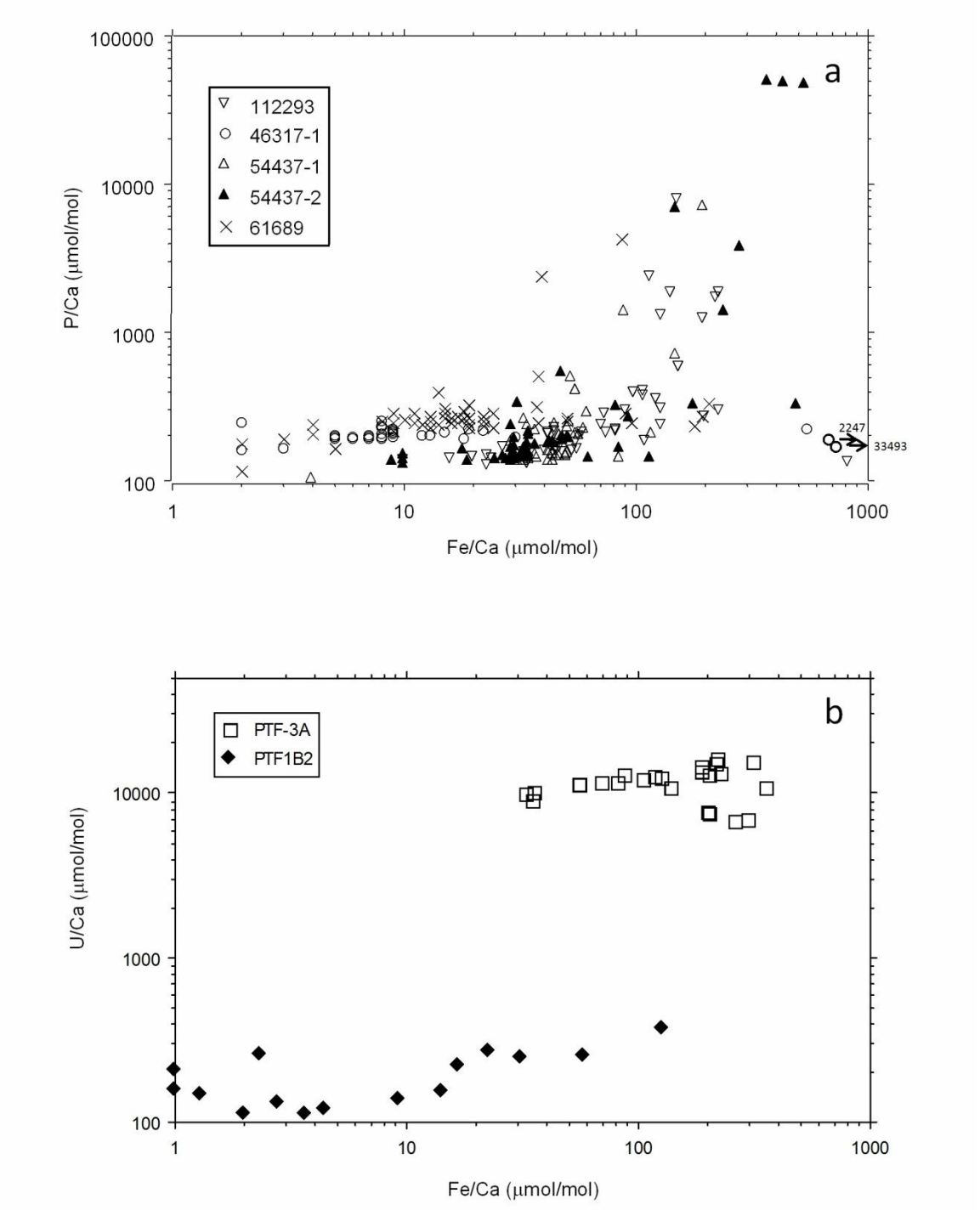

FIGURE 2-5—Trace elements in Plio-Pleistocene *Conus* shells from Florida: a) P/Ca versus Fe/Ca. b) U/Ca versus Fe/Ca.

associated with terrigenous influx in general, but is also delivered with other metals by submarine groundwater discharge (e.g., Windom et al., 2006) and correlates with U in pore waters at depths below the sediment-water interface of more than 25 cm in Tampa Bay (Swarzenski and Baskaran, 2007). At depths above 25 cm, Fe^{2+} oxidation can cause heterogeneous Fe values and a divergence in the U–Fe relationship in pore waters. The heterogeneous distribution of submarine groundwater discharge and bioirrigated sediments can explain the variable nature of P, U, and Fe distribution between and within shells. Overall, these trace element data suggest that the productivity on the Pliocene Florida Platform was enhanced by freshwater input of terrigenous nutrients, including input from submarine groundwater discharge.

Oxygen Isotope and Sr/Ca Paleothermometry

Oxygen isotope paleotemperature determinations require estimation of Pliocene seawater $\delta^{18}O$ on the Florida Platform. The Pliocene Atlantic seawater $\delta^{18}O$ estimate from Williams et al. (2009) was used. This was derived from a coupled ocean-atmosphere general circulation model and follows the formula:

$$\delta^{18}O_{sw} = 0.24 - 0.008\ (P - E),\ r^2 = 0.7$$

where (P - E) is the precipitation minus evaporation estimate given in units of cm/yr. According to Williams et al. (2009), the calculated Pliocene $\delta^{18}O_{sw}$ for this locality is 1.02‰. Such a high local $\delta^{18}O_{sw}$ for the late Pliocene, a time of reduced continental ice volumes, implies highly evaporative waters comparable to modern waters with a $\delta^{18}O$ of 1.7‰ and salinity of ~38 (assuming a global $\delta^{18}O_{sw}$ of 0.7‰ [Lear et al., 2000] and a $\delta^{18}O_{sw}$–salinity slope due to evaporation of 0.35‰ per salinity unit [Railsback et al., 1989]).

Figure 2-6 compares the reconstructed paleotemperatures with other estimates of Pinecrest paleotemperatures (Jones and Allmon, 1995) and with modern SSTs derived from buoy stations in Sarasota Bay area (http://www.ndbc.noaa.gov/maps/Florida.shtml). Statistical *t*-tests show that Unit 7 paleotemperatures (averaging 25.1 ^{o}C excluding PTF-1A) are essentially identical to modern SSTs (averaging 24.5 ^{o}C). The Plio-Pleistocene Caloosahatchee Formation SSTs (averaging 22.5 ^{o}C) are slightly lower than Unit 7 temperatures, which is in agreement with the late Pliocene cooling event (Lisiecki and Raymo, 2005). Paleotemperatures reconstructed from Unit 4 (averaging 16.1 ^{o}C), however, are significantly lower than those of Unit 7 and modern temperatures, and have a minimum of 10.1 ^{o}C, which is inconsistent with the warm water habitat of the species. Thus, the environmental waters during Unit 4 deposition must have been enriched in ^{18}O relative to those during Unit 7 deposition.

Sr/Ca ratios can be used to test whether δ^{18}O variation is due to temperature change or change in the δ^{18}O of ambient water (Sosdian et al., 2006). Sosdian et al. (2006) have produced a Sr/Ca–temperature equation based on modern *Conus ermineus* from Stetson Bank in the Gulf of Mexico. Applying this equation to the Pinecrest samples, using modern seawater Sr/Ca values, yields unrealistic paleotemperatures of 21–49°C. The high *Conus* Sr/Ca ratios cannot be explained by higher temperature and must be caused by either higher seawater Sr/Ca ratios in the Plio-Pleistocene or interspecies differences in distribution coefficient. Since all *Conus* shells in this study (six *C. adversarius*, one *C. spurius*, and one *C. largillierti*) give higher-than-modern Sr/Ca ratios, it is unlikely that a

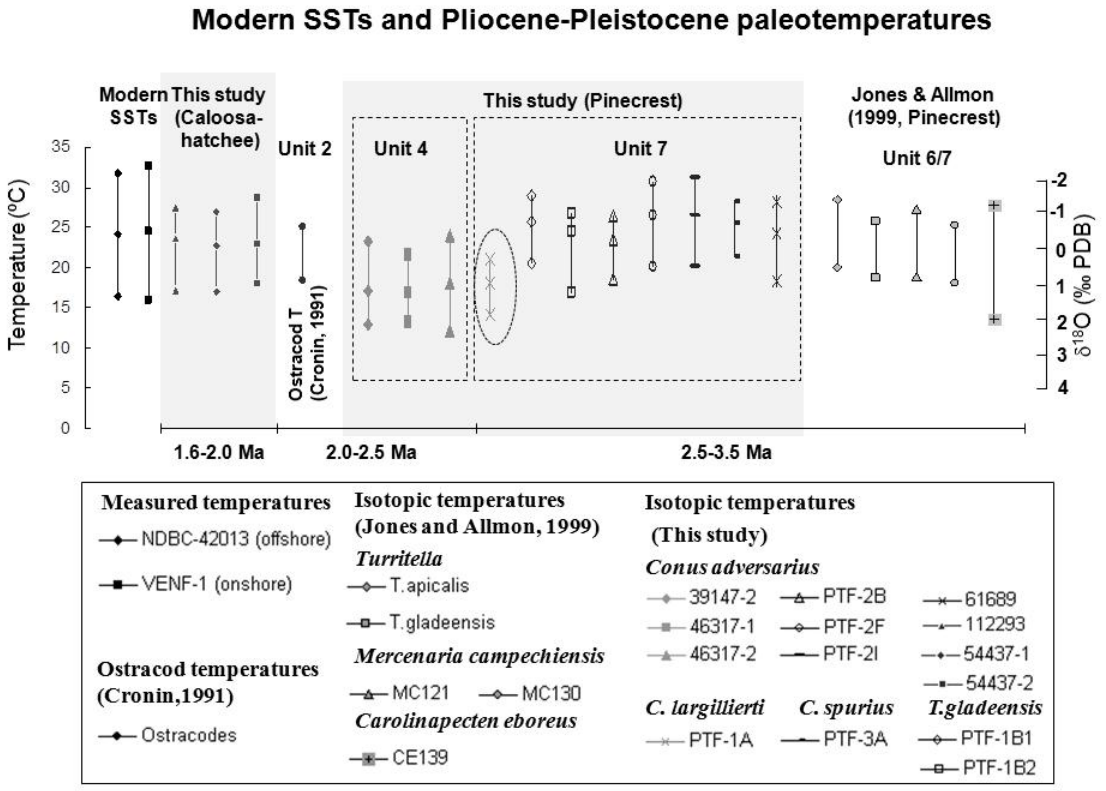

FIGURE 2-6—Modern SSTs from National Data Buoy Center (http://www.ndbc.noaa.gov/maps/Florida.shtml) and middle Pliocene paleotemperatures from Cronin (1991), Jones and Allmon (1995) and this study. Dashed boxes indicate different units in the Pinecrest Beds; elliptical circle indicates the aberrant values of PTF-1A.

difference in distribution coefficient between modern and fossil samples can explain such significant differences in Sr/Ca ratios. Instead, these data along with data from Paleogene *Conus* and turritellids (Sosdian, 2008; Sosdian et al., 2009; Tripati et al., 2009) provide evidence that Cenozoic seawater Sr/Ca ratios were high relative to modern values. Despite the uncertainty of seawater Sr/Ca during the Plio-Pleistocene, *Conus* Sr/Ca ratios still can provide relative paleotemperatures for time intervals.

$\delta^{18}O$-$\delta^{13}C$ Trends and the Florida Bay Model

The paleoenvironmental information provided by oxygen and carbon isotope profiles can determine which nutrient source, nearshore upwelling (Jones and Allmon, 1995) or terrigenous input (Weinlein et al., 2008; Sliko and Herbert, 2009), was primarily responsible for higher Pliocene productivity off western Florida. Upwelling induces low $\delta^{13}C$ and high $\delta^{18}O$, resulting in a negative $\delta^{18}O$–$\delta^{13}C$ correlation. In contrast, input of freshwater runoff during rainy seasons lowers both $\delta^{18}O$ and $\delta^{13}C$, resulting in a positive $\delta^{18}O$–$\delta^{13}C$ correlation. Table 2-1 lists the linear regression $\delta^{18}O$–$\delta^{13}C$ slope and correlation coefficient for all 14 specimens. Ten specimens show a strong positive correlation ($p < 0.05$), four samples show no significant correlation ($p > 0.05$), while none show a negative correlation. This suggests that the salinity-induced factor is evident in the $\delta^{18}O$ and $\delta^{13}C$ while the upwelling-induced factor is minimal. As discussed earlier, Allmon et al. (1996) observed negative covariances between carbon and oxygen isotopes in one *Mercenaria campechiensis* and two *Turritella gladeensis* specimens from older quarries in Pinecrest Unit 6/7. No other gastropod specimens show such a strong negative relationship. Thus, upwelling as a predominant cause for the high productivity in middle Pliocene Pinecrest Beds is questionable. The data presented, however, support the hypothesis that the high productivity was caused by terrigenous nutrient input from freshwater.

Mixing with freshwater typically decreases seawater $\delta^{18}O$; however, Lloyd (1964) observed that excess evaporation caused ^{18}O enrichment in the freshwater along the northern margin of Florida Bay. Lloyd also found that $\delta^{13}C$ values in Florida Bay were lower than those in the open ocean due to the oxidation of organic debris. A study of

modern Florida Bay water (Swart and Price, 2002) shows that the brackish estuarine waters with salinities of 25–30 can have $\delta^{18}O$ values as high as 4‰ (vs. VSMOW), a value higher than open seawater $\delta^{18}O$ (2‰) in this area. Only when salinity becomes lower than 10 do brackish water $\delta^{18}O$ values become significantly lower than open-ocean values. Considering their natural habitat, *Conus* and *Turritella* are unlikely to inhabit environments with such low salinities. If Pinecrest Unit 4 was deposited in a brackish environment similar to modern Florida Bay, it is entirely possible that mollusks recorded higher-than-open-seawater $\delta^{18}O$ values. On the other hand, the middle Pliocene Unit 7 was deposited in a typical offshore environment during a sea level high-stand (Allmon, 1993). Therefore, Unit 7 seawater would be lower in $\delta^{18}O$ than Unit 4 water.

Analyzing modern mollusk shells from Florida Bay, Halley and Roulier (1999) reported a gradient from high $\delta^{18}O$ and low $\delta^{13}C$ in northeastern Florida Bay (more lagoonal) towards normal $\delta^{18}O$ and $\delta^{13}C$ in southwestern Florida Bay (near open water; Fig. 2-7). Using their model, the Unit 4 isotope values fit exactly in the nearshore lagoonal data field (red, orange, and green ellipses) while Unit 7 isotope values fit in the open ocean data field (purple ellipse). Although the sample locations of Units 4 and 7 are on the west coast of Florida instead of Florida Bay, similar environmental conditions and thus a similar isotopic gradient likely existed in the middle-late Pliocene. The outlier

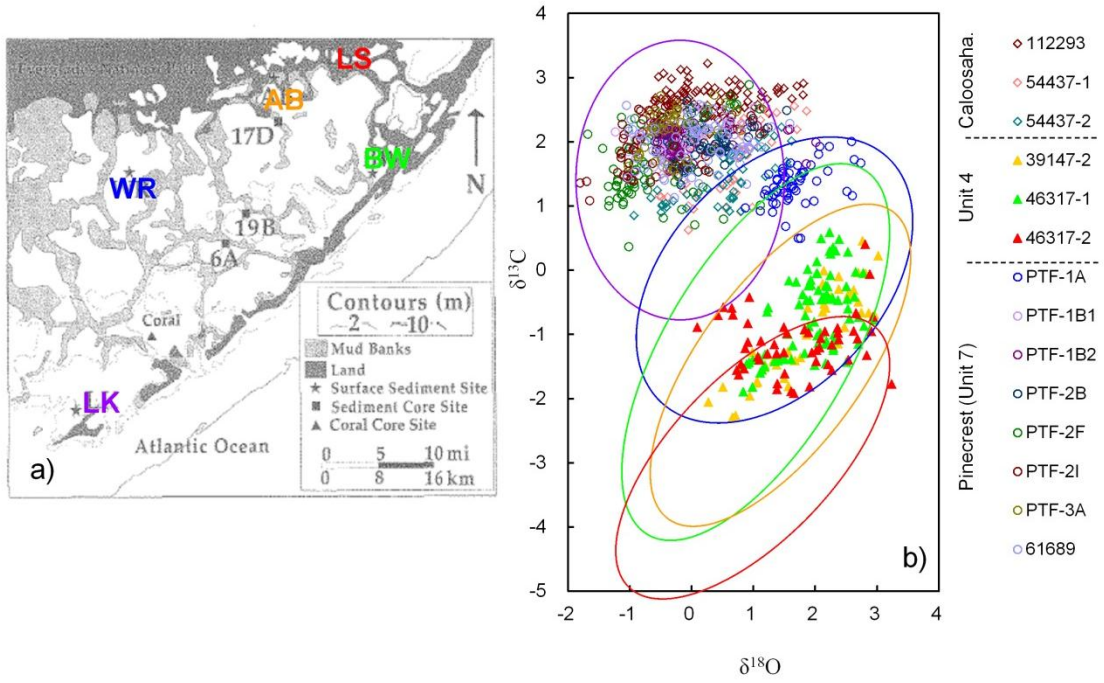

FIGURE 2-7—a) Sample sites in Florida Bay from Halley and Roulier (1999). Red, orange, green, blue and purple colors mark lagoonal to open-sea environments. b) $\delta^{18}O$-$\delta^{13}C$ data from this study projected onto the circles related to the molluscan isotopic values from locations in 7a.

specimen in Unit 7, PTF-1A, which lies in the blue ellipse in the midst of those two extremes, remains a mystery and may represent a brief interval of restriction or drought.

In light of the Florida Bay model, the upwelling signal of *Mercenaria campechiensis* specimen MC 130 analyzed by Jones and Allmon (1995) can be reinterpreted as representing an intermediate environment fluctuating seasonally between restricted (high $\delta^{18}O$, low $\delta^{13}C$) and more open ocean (low $\delta^{18}O$, high $\delta^{13}C$) conditions

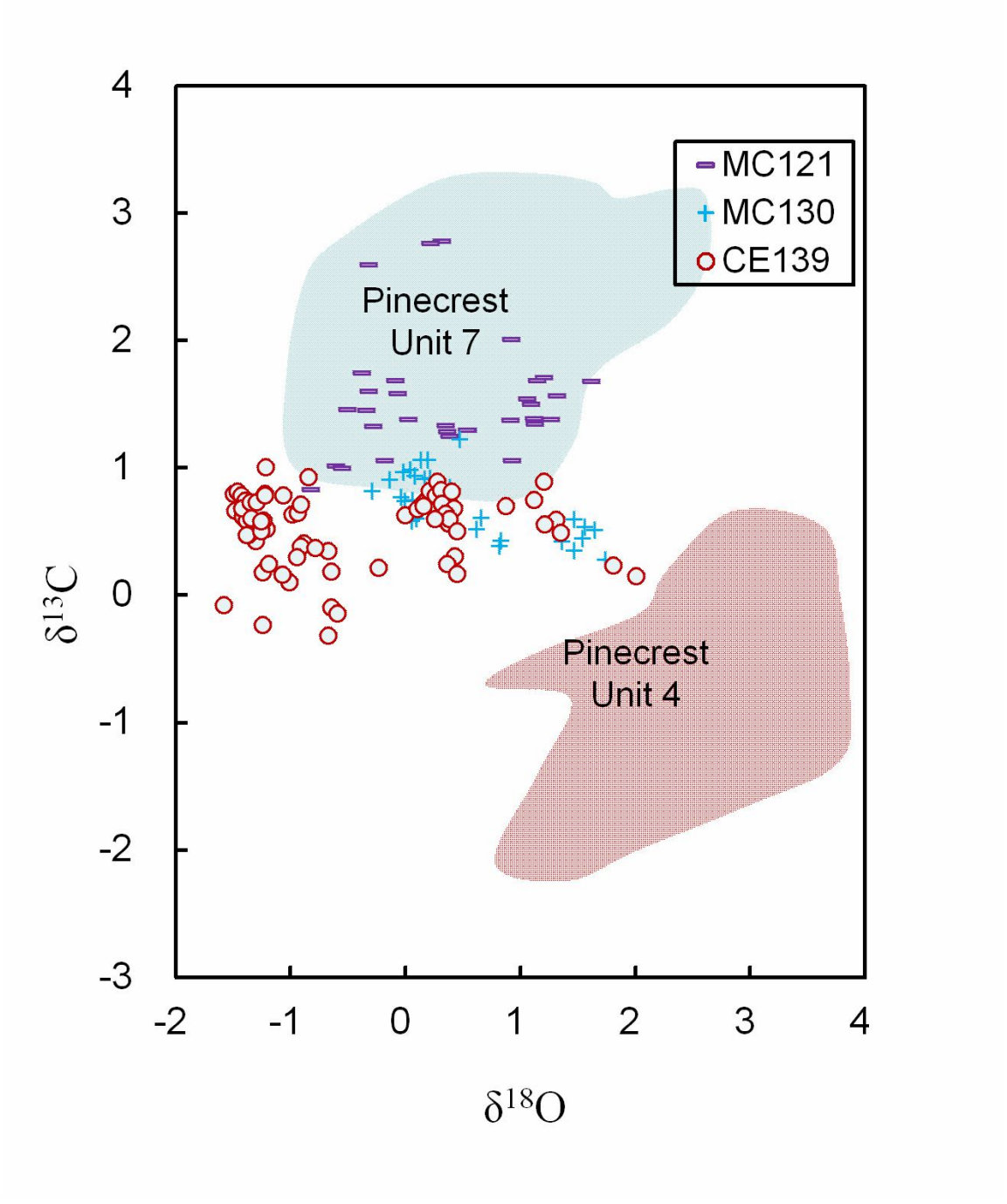

FIGURE 2-8—Oxygen and carbon isotopic data for *Mercenaria campechiensis* (MC121 and MC130) and *Carolinapecten eboreus* (CE139) from Jones and Allmon (1995) compared with data fields for mollusks analyzed in this study.

(Fig. 2-8). The $\delta^{18}O$ values of MC 130 are higher than those of the other *M. campechiensis* in the study (MC 121), consistent with the restricted, lagoonal environment for the former. Furthermore, MC 130 yields lower $\delta^{13}C$ values than MC 121, consistent with this model.

Although oxygen and carbon isotopes in molluscan shells have been used as a paleosalinity index in estuarine environments (Hudson, 1963), caution should be exercised in hydrologically restricted areas like swamps or lagoons (Lloyd, 1964; Swart and Price, 2002). In addition to modern Florida Bay and Unit 4 of the Pinecrest Beds, high $\delta^{18}O$ values have also been found in what appear to be highly-evaporated, brackish lagoons of middle Jurassic Bathonian age in central England and Scotland (Hendry and Kalin, 1997; Holmden and Hudson, 2003). Contrary to Florida Bay and Pinecrest waters, however, the Bathonian lagoon waters are enriched in $\delta^{13}C$, possibly due to *in situ* photosynthesis and enhanced burial of organic carbon (Hendry and Kalin, 1997).

Summary

Stable isotope and trace element analyses of *Conus* and *Turritella* gastropods shells indicate that the dominant cause of high tropical productivity off Florida's west coast (Pinecrest beds) during the middle Pliocene was not upwelling, but rather nutrient input from freshwater sources, including submarine groundwater discharge. This conclusion is based on (1) the lack of an upwelling signature in $\delta^{13}C$ and $\delta^{18}O$, (2) correlations between P/Ca, Fe/Ca, and U/Ca, and (3) $\delta^{18}O$–$\delta^{13}C$ patterns similar to those of Florida Bay mollusks. Unusually high $\delta^{18}O$ values for specimens from Pinecrest Unit 4, believed to be a brackish environment based on faunal assemblage, indicate

evaporative ^{18}O enrichment of brackish seawaters. This interpretation is supported by (1) the similar Sr/Ca values for shells from both units, and (2) the coincidence of the $\delta^{18}O$–$\delta^{13}C$ pattern of the shells and that of mollusks from modern Florida Bay. These results highlight the utility of combining trace elements with stable isotopic analyses to understand complex environments with excess evaporation and submarine groundwater discharge.

CHAPTER III

QUANTIFYING UPWELLING AND FRESHENING IN NEARSHORE TROPICAL ENVIRONMENTS USING STABLE ISOTOPES IN MODERN TROPICAL AMERICAN MOLLUSKS

Overview

Proxies for nutrients delivered by upwelling and freshwater input in ancient marine ecosystems are critically required for understanding tropical origination, extinction, and diversity changes associated with environmental change. In order to identify and quantify differences in upwelling and terrigenous influences in contrasting ecosystems, this study performs stable isotope analyses ($\delta^{13}C$ and $\delta^{18}O$) on 13 serially-sampled modern *Conus* shells collected from southwestern Caribbean (SWC, non-upwelling) and tropical eastern Pacific (TEP) Gulf of Chiriquí (non-upwelling) and Gulf of Panama (upwelling) coastal waters across the Central American Isthmus (CAI). Most shells reveal seasonal variations in temperature and (or) the oxygen isotopic composition of the water, which varies with salinity. Unusually high or low seasonal $\delta^{18}O$ values in the shells measure the intensity of seasonal upwelling or freshwater input respectively. To quantify upwelling and freshening signals and contrast these signals between regions, baseline $\delta^{18}O$ values that are free of seasonal upwelling or freshening influences have been estimated from temperature and salinity data loggers and the World Ocean Atlas 2001 (WOA 2001) database using average temperature during non-upwelling periods and normal (dry-season) salinity. Shell $\delta^{18}O$ values normalized to the baseline reveal little or no upwelling in SWC and Gulf of Chiriquí, and strong upwelling in the Gulf of Panama,

as well as strong freshwater input in most areas. For example, dry-season $\delta^{18}O$ values for Gulf of Panama *Conus* can exceed the baseline by as much as 2‰, which equates to seawater temperatures ~9°C lower than normal. In contrast, rainy-season $\delta^{18}O$ values can be as low as 1.8‰ below the baseline, equivalent to seawater salinities ~7 lower than normal. No shells from the Gulf of Panama had the negative $\delta^{13}C$–$\delta^{18}O$ (δ –δ) correlations that are often associated with upwelling of cool, ^{18}O-enriched, ^{13}C-depleted waters. However, when data from the upwelling seasons (usually January to April) of Gulf of Panama shells are isolated, four of the five shells tested show significant negative δ –δ correlations, indicating that the freshwater signal during the rainy, non-upwelling season masks the expected upwelling profile.

Introduction

Formation of the Central American Isthmus (CAI) isolated the Pacific and Caribbean during the late Neogene and Pleistocene (Coates and Obando, 1996) resulting in major oceanographic and biological change in Tropical America (Fuglister, 1960; Glynn, 1972; Keigwin, 1978; D'Croz et al., 1991). Detailed environmental data from coastal waters during the formation of the Isthmus is lacking (Schmidt, 2007; Farris et al., 2011), hindering our understanding of the evolutionary and ecological origins of the modern Tropical American marine fauna (D'Croz and O'Dea, 2007).

Modern coastal waters around the CAI show extreme hydrologic variability. This is principally caused by the presence of strong seasonal wind-jet driven upwelling in the TEP and the general absence of upwelling in SWC (D'Croz and Robertson, 1997, D'Croz and O'Dea, 2007). Additionally, within each ocean there are substantial environmental

differences particularly in the origins of nutrient-rich waters critical for maintaining productivity.

In this paper we characterize a variety of modern Tropical American coastal environments by performing stable isotope analyses of serially-sampled molluscan shells. In doing so, we provide a reference for interpreting isotopic variations in fossil mollusk shells to characterize the changing environmental conditions associated with the uplift of the CAI.

Modern Tropical American Hydrology

Trade winds blowing across the CAI from late December to late March/April push coastal waters offshore in several areas along the Pacific coast, such as the Gulf of Panama, resulting in strong seasonal upwelling. This contributes to the contrast between the tropical eastern Pacific (TEP) and the southwest Caribbean (SWC). TEP coastal upwelling brings cold, nutrient-rich water to the surface and greatly increases primary productivity (D'Croz and O'Dea, 2007). The TEP is also affected by El Niño events, yet the influence of El Niño on upwelling in the TEP remains unclear (Agujetas and Mitchelson-Jacob, 2008, O'Dea and Jackson, 2002). In contrast, SWC waters generally don't experience seasonal upwelling, although there are three areas in the northern coast of Colombia and Venezuela that experience Eckman-driven upwelling (Reuer et al., 2003). Consequently, the most striking differences across the isthmus is that upwelling in TEP brings nutrients driving a fervent planktonic productive system, whereas in the SWC the productivity is shifted to the benthos because nutrients are considerably lower and supplied by terrigenous runoff (D'Croz et al., 2005, D'Croz and O'Dea, 2007). Trade

winds also lead to Caribbean waters being more saline as evaporation exceeds precipitation (Fuglister, 1960; Glynn, 1972; Keigwin, 1978; D'Croz et al., 1991).

Despite the inter-ocean differences, neither the TEP nor the SWC environments can be so simply characterized. In the TEP, the variation of upwelling is correlated with the altitude of CAI. During the boreal winter the trade winds are built up by the high pressure in the SWC and Gulf of Mexico. Only where the CAI is sufficiently low will the trade winds be able to pass over the cordillera of Central America and be intense enough to push surface water away from the Central American coast, creating room for upwelled deep water (D'Croz and O'Dea, 2007). This wind-driven upwelling occurs in the Gulf of Panama, but not in the Gulf of Chiriquí, where the altitude of CAI is much higher. In the SWC, in addition to the three Eckman-driven upwelling regions, the seasonal surface water run-off pattern also varies along the Caribbean coast resulting from the seasonal movement of the intertropical convergence zone (ITCZ). For example, mean annual rainfall varies along the Caribbean coast and is highest near the canal zone (Lachniet and Patterson, 2002, 2006).

Stable Isotopes as Chronicle of Environmental Conditions

Oxygen and carbon isotopes in serially-sampled mollusks can provide high-resolution seasonal and inter-annual environmental records. Oxygen isotopes in serially-sampled mollusks have been used as a proxy of sea surface temperatures (SSTs) for decades (e.g., Lowenstam and Epstein, 1954; Krantz, 1990; Jones and Allmon, 1995; Kobashi et al., 2003; Surge and Walker, 2006). Carbon isotopes, though influenced by vital effects (e.g., Gillikin et al., 2006), still provide an environmental record of ambient dissolved inorganic carbon (DIC) $\delta^{13}C$ (Mook, 1971; Fritz and Poplawski, 1974; Gentry

et al., 2008; Beirne et al., 2012). The coupling of oxygen and carbon isotopic profiles can be used to detect seasonal upwelling (Killingley and Berger, 1979) and freshwater input (Mook, 1971). In the absence of other influences, shell deposited during upwelling seasons will have higher $\delta^{18}O$ and lower $\delta^{13}C$ than shell deposited during non-upwelling seasons. This is because upwelled waters are cool, ^{18}O-enriched, and ^{13}C-depleted, resulting in a negative $\delta^{18}O$–$\delta^{13}C$ correlation. Conversely, carbonate deposited during freshwater input is generally depleted in both $\delta^{18}O$ and $\delta^{13}C$, a reflection of the ^{18}O-depletion of meteoric waters and ^{13}C depletion of soil CO_2. This results in a positive δ–δ correlation in the isotopic profiles of mollusks.

Previous studies of modern mollusks from the TEP and SWC have successfully used oxygen isotopes to distinguish upwelling and non-upwelling environments (Geary et al., 1992; Bemis and Geary, 1996). Geary et al. (1992) observed a significantly higher $\delta^{18}O$ range for strombid gastropods from Gulf of Panama (4.5‰) versus Caribbean non-upwelling areas (1.5‰). Bemis and Geary (1996) obtained similar results for venerid bivalves, showing large $\delta^{18}O$ ranges in shells from upwelling regions compared with shells from non-upwelling regions. The present study builds upon the previous work by Bemis and Geary (1996), but rather that analyzing slow-growing bivalve shells we analyze fast-growing *Conus* shells to provide high resolution isotopic profiles. Furthermore, the data are used for the first time to quantify upwelling and freshening, both critical factors in nutrient delivery and productivity. These data are then used to develop a method for quantifying upwelling and freshwater influence in ancient tropical environments.

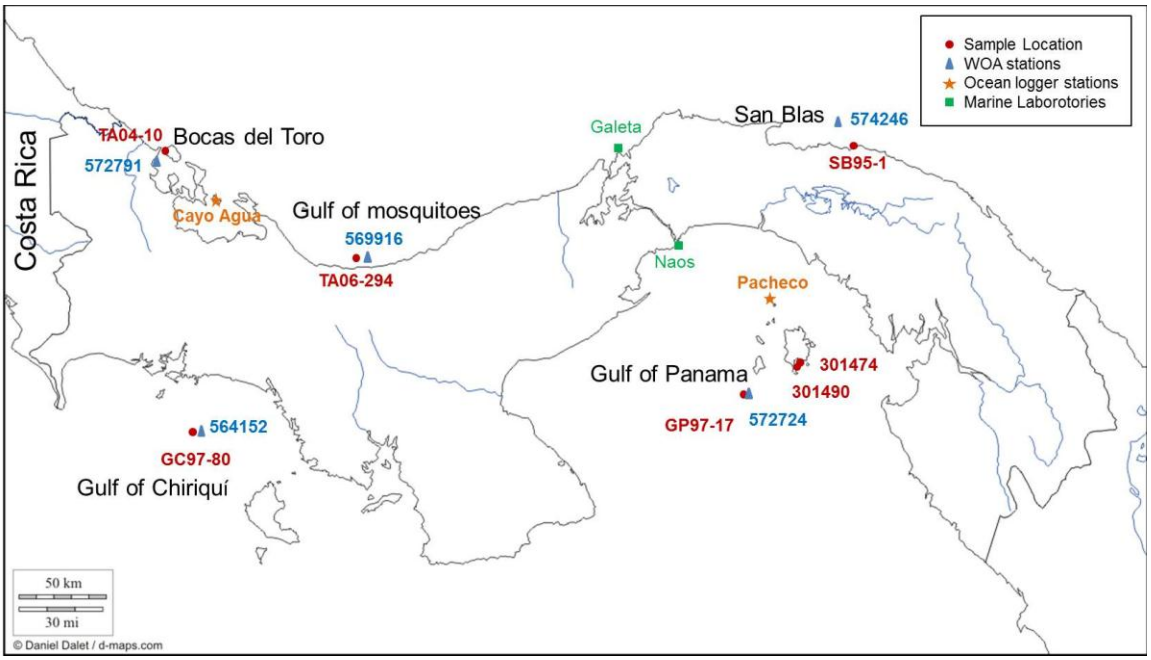

FIGURE 3-1—Map of sample localities and WOA and temperature logger sites.

Study Area

To help isotopically characterize the variability in isthmian waters, we analyzed 13 gastropod shells collected from a variety of environmental settings. Specifically, three non-upwelling areas in the Caribbean (Bocas del Toro, 9.4460°N, 82.3245°W; San Blas Archipelago, 9.4400°N, 78.5850°W; Golfo de los Mosquitos, 8.8355°N, 81.2323°W), and upwelling (Gulf of Panama, 7.9883°N, 79.2500°W) and non-upwelling (Gulf of Chiriquí, 7.8650°N, 82.1800°W) areas on the Pacific coast of Panama (Fig. 3-1). Specimens from the Pacific coast were collected in coarse sands at depths of 10 to 61 m. The Caribbean samples were collected from sediments ranging from muddy to coarse sands at depths of 11 to 41 m (Table 3-1).

Figure 3-2A shows the temperature and salinity profiles for each sample location at different depths through the year 2001 derived from the World Ocean Atlas 2001 (WOA

TABLE 3-1—Specimen taxonomy, location information, collection date, and dimensions.

Sample ID	Species	Location[1]	Collection Date	Latitude	Longitude	Shell length (cm)	Shell width (cm)	Whorl length (cm)	Sediment type[2]
Caribbean									
TA06-294A	*Conus* spp.	GoM	8/20/06	8.84	-81.23	28.5	12.5	76.0	BSS
TA06-294B	*Conus.* spp.	GoM	8/20/06	8.84	-81.23	16.3	8.9	23.5	BSS
SB95-1	*Conus mus*	San Blas	10/14/95	9.44	-78.59	23.4	13.4	57.5	BMT
TA04-10A	*Conus jaspideus*	Isla Colon, BdT	9/30/04	9.45	-82.32	21.3	12.2	52.5	MSC
TA04-10B	*Conus jaspideus*	Isla Colon, BdT	9/30/04	9.45	-82.32	20.5	12.2	53.5	MSC
TA04-10C	*Conus jaspideus*	Isla Colon, BdT	9/30/04	9.45	-82.32	22.3	11.9	52.0	MSC
Pacific									
GP97-17A	*Conus recurvus*	GoP	2/16/97	7.99	-79.25	52.3	23.2	162.4	CS
GP97-17B	*Conus mahogani*	GoP	2/16/97	7.99	-79.25	36.3	16.4	72.7	CS
301474	*Conus patricius*	GoP	3/18/00	8.27	-78.89	46.2	25.9	140.2	
301490A	*Conus ximenes*	GoP	3/15/00	8.27	-78.91	38.3	17.1	123.0	
301490B	*Conus ximenes*	GoP	3/15/00	8.27	-78.91	30.4	12.6	73.8	
GC97-80A	*Conus arcuatus*	GoC	3/21/97	7.87	-82.18	41.9	20.1	123.0	MS
GC97-80B	*Conus arcuatus*	GoC	3/21/97	7.87	-82.18	30.1	13.8	69.0	MS

[1]GoM = Golfo de los Mosquitos, BdT = Bocas del Toro, GoP = Gulf of Panama, GoC = Gulf of Chiriquí.
[2]BSS = brown sediments with many shells, BMT = brown terrigenous mud, MWC = mud with sands and abundant cupuladriids, CS = coarse sand, MS = muddy sand.

2001; Conkright et al., 2002) database. Also shown are the expected shell $\delta^{18}O$ values based on estimates of seawater temperature and salinity in each sample location and

depth (Fig. 3-2B; details for this calculation will be discussed later). Note that both temperature and $\delta^{18}O$ profiles flatten in deep waters (100 m) because of little variation in temperature and salinity below the thermocline (~60 m). Maximal temperature variations

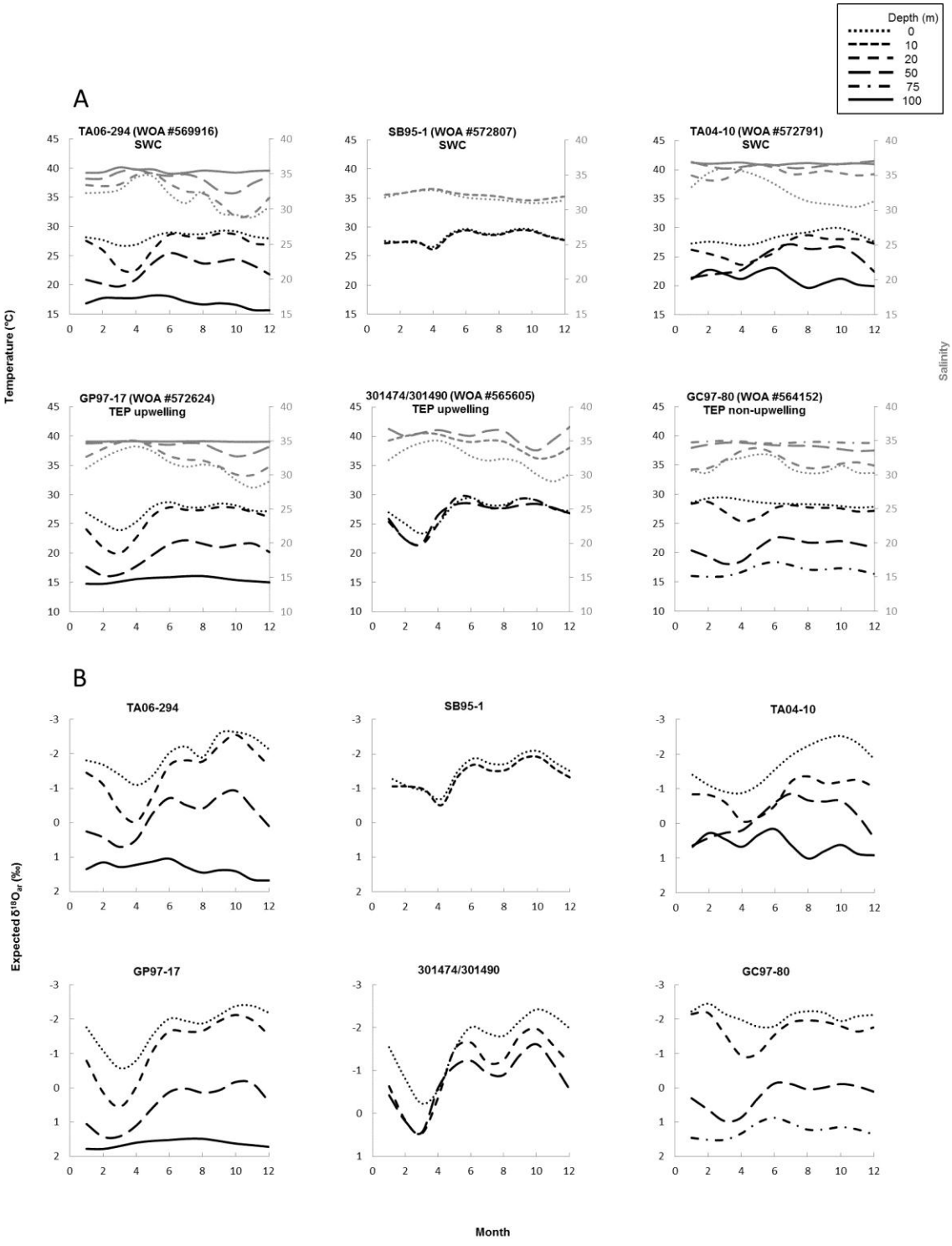

FIGURE 3-2—Temperature and salinity profiles at depths of 0, 10, 20, 50, 75 and 100 m, and the estimated shell $\delta^{18}O$ profiles for each sample locality using Ocean Data View World Atlas 2001 database (Conkright et al., 2002).

are found in water depths of 20–50 m where strong seasonal upwelling occurs. Maximal salinity variations are found in surface waters due to the dominant influence of freshwater runoff in the rainy season. For most of the Panamanian coast, intense rainfall starts in May and lasts until December, while the dry season occurs from January to April. The Gulf of Panama experiences upwelling during the dry season when narrow wind-jets blow across the isthmus causing offshore water movement (D'Croz and Robertson, 1997; D'Croz et al., 2001). Upwelling is absent during the rainy season. This creates a significant contrast between the SWC and TEP seasonal temperature patterns as seen in temperature logger records from Smithsonian Tropical Research Institute (STRI) monitoring stations in Bocas del Toro and Gulf of Panama (Fig. 3-3; http://www.stri.si.edu/sites/esp//mesp/water_quality/water_quality_intro.htm) as well as WOA data (Figure 3-2A, Conkright et al., 2002). In the Gulf of Panama, sea surface temperatures (SSTs) can drop from ~28.5°C during non-upwelling (rainy) periods to as low as 15.5°C during upwelling (dry) intervals. In contrast, at Bocas del Toro the seasonal SST variations typically are within ±1°C (2σ) of the mean (28.6°C) (Kaufmann and Thompson, 2005). Though the Gulf of Chiriquí is characterized as non-upwelling, seasonal shoaling of the thermocline to nearly 30 m does occur in response to seasonal trade winds passing over the isthmus. The higher elevations north of Gulf of Chiriquí, however, preclude the development of wind-jets and strong upwelling (Fig. 3-2; D'Croz and O'Dea, 2007; Liang et al., 2009).

Methods

Prior to sampling for stable isotopic analysis, all gastropod specimens were cleaned, polished and ultrasonicated to remove extraneous materials from surfaces. Serial

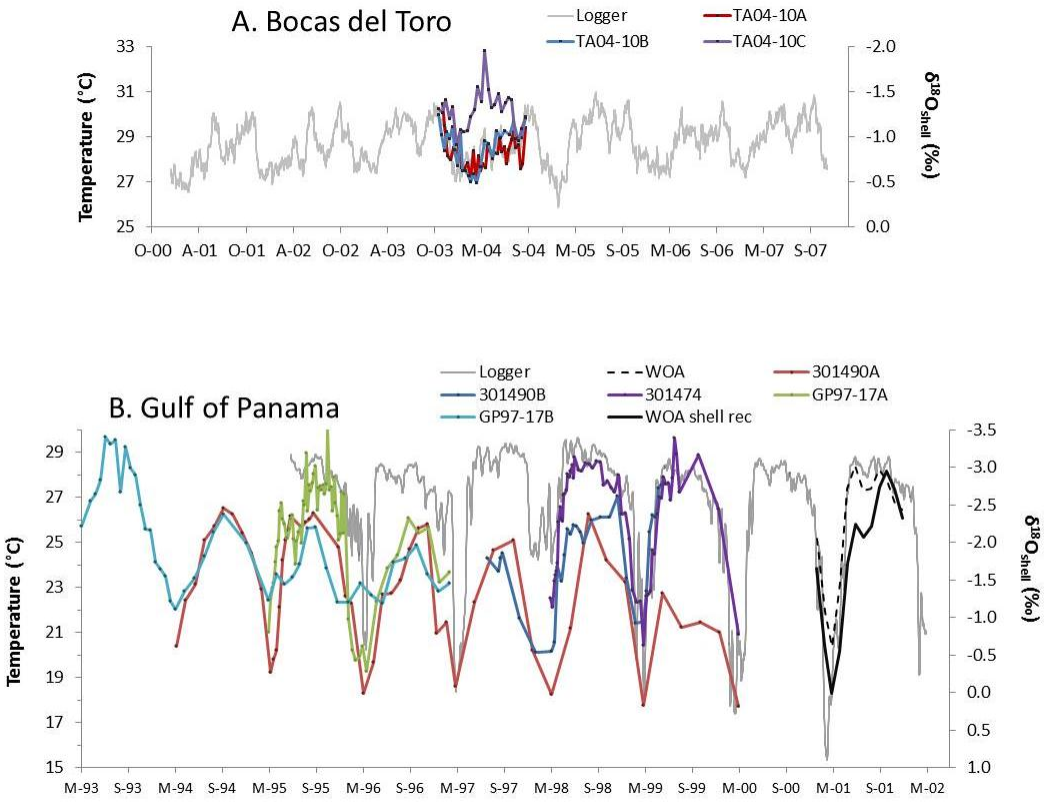

FIGURE 3-3—Temperature records from logger data from 4 m depth at Cayo Agua (Bocas del Toro) and 12 m depth at Pacheco (Gulf of Panama) watch station of Smithsonian Tropical Research Institute (grey curve) compared with WOA temperature data (black curve) and shell $\delta^{18}O$ (color curves).

sampling was applied at 2–3 mm intervals, starting from the apex of the shell spiral, to collect sample powders from shallow grooves perpendicular to growth direction using a 0.5 mm Brasseler carbide dental drill bit. Approximately 300 µg of powder was collected for each sample. For each analysis, about 100–150 µg sample powder was reacted with "100%" phosphoric acid at 70℃ on a GasBench II gas handling system. The CO_2 gas generated was then analyzed on a DeltaPlusXP isotope ratio mass spectrometer. All

results were calibrated to Vienna-PDB using NBS-19 standard. At least every fifth sample was analyzed in replicate to test for quality control.

Shell chronologies were determined using comparisons with expected $\delta^{18}O$ profiles for the appropriate sample location and depth. These profiles were estimated for analyzed specimens using modern temperatures and salinities obtained through Ocean Data View (ODV) software using the WOA 2001 database (Fig. 3-2, Conkright et al., 2002). Data for 2001 were chosen because this year provides the highest spatial (quarter degree) and temporal resolution (monthly) among all the years covered by the WOA database. For each sample location, at least two nearby WOA stations were chosen and averaged. Seawater $\delta^{18}O$ values were calculated from salinity data using relationships derived by Fairbanks et al. (1992) for Pacific and Atlantic waters.

$$\delta^{18}O_{w,\ Pacific} = 0.26S - 8.77 \quad (1)$$

$$\delta^{18}O_{w,\ Atlantic} = 0.19S - 5.97 \quad (2)$$

Currently, surface water samples for isotopic and salinity measurements are being collected twice-weekly at the Galeta Marine Laboratory (SWC, 9.4029 N, 79.8608 W) and Naos Island Marine Laboratory (Gulf of Panama, TEP, 8.9159 N, 79.5322W) of the STRI (Robbins, Morales, Thompson, Grossman, and O'Dea, in prep.). Once a complete year has been sampled, the water sample data will be used to produce a regional $\delta^{18}O_w$–salinity correlation that will be used in place of the general equations of Fairbanks et al. (1992). Preliminary data from March to August 2011 are shown in Fig. 3-4 and yield

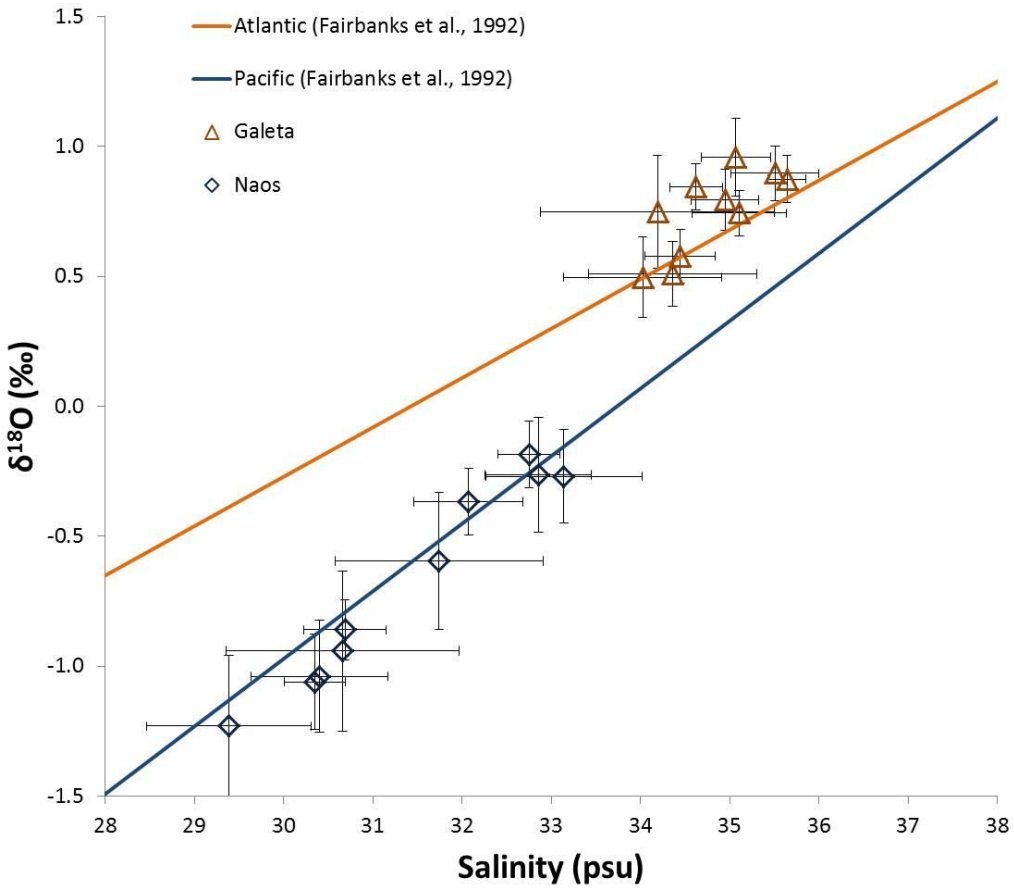

FIGURE 3-4— Average monthly seawater $\delta^{18}O$ versus salinity for water samples collected twice-weekly at the Galeta Marine Laboratory (Caribbean) and Naos Island Marine Laboratory (Pacific) of the Smithsonian Tropical Research Institute compared with the Fairbanks et al. (1992) equations for the Atlantic and the Pacific Oceans (Robbins, Morales, Thompson, Grossman, and O'Dea, in prep).

slopes and y-intercepts that, within the precision, agree with those of Fairbanks et al. (1992). Expected shell $\delta^{18}O$ values were then determined from the temperature and seawater $\delta^{18}O$ using Grossman and Ku (1986, eq. 1 in that paper as modified by Hudson and Anderson, 1989),

$$T(°C) = 19.7 - 4.34\ (\delta^{18}O_{aragonite} - \delta^{18}O_{w}) \quad (3)$$

which can be written as:

$$\delta^{18}O_{TEP\ shell} = (19.7-T) / 4.34 + 0.26S - 8.77 \quad (4)$$

$$\delta^{18}O_{SWC\ shell} = (19.7-T) / 4.34 + 0.19S - 5.97 \quad (5)$$

When temperature logger data were available (e.g., Bocas del Toro and Gulf of Panama, both in daily resolution), chronologies were easily established by comparing the measured $\delta^{18}O$ with the seawater temperature profile (Figs.3- 3A&B). For the remainder of sample locations the relatively low-resolution (monthly) WOA 2001 data were used (Fig. 3-2). The sclerochronologies were established as follows. Firstly, the months with maximum and (or) minimum expected $\delta^{18}O$ were identified as reference points and assigned to the 15th day of that month. For live-collected specimens, collection date was also used as a reference point. Next, the measured maximal, minimal and last growth $\delta^{18}O$ values of each annual cycle were assigned to the appropriate date for that location. Lastly, a constant growth rate was assumed between reference points. Growth curves based on these chronologies are shown in Fig. 3-4; note only one specimen from the SWC (SB95-1 from San Blas) was plotted because most SWC annual cycles are unrecognizable.

Results

Oxygen Isotopes

The averages, ranges, and extreme $\delta^{18}O$ values for modern *Conus* shells from SWC and TEP areas are summarized in Table 3-2. Overall, values of Gulf of Panama (TEP upwelling) shells have larger $\delta^{18}O$ ranges and lower $\delta^{18}O$ averages than SWC shells, while the two deeper specimens (GC97-80A & B, 61 m) from the Gulf of Chiriquí

(TEP, non-upwelling) have ranges between the SWC and Gulf of Panama shells and the highest averages.

Samples from the three nearshore localities in the SWC generally show little seasonal variation and small overall range, thus resulting in relatively flat $\delta^{18}O$ profiles (the figure on page 47 and Table 3-2). Two specimens from Golfo de los Mosquitos (TA06-294A & B) average -0.9‰ and -0.6‰ and have ranges of 0.8‰ and 0.4‰, respectively. The larger shell, 294A, with a whorl length of 76.0 mm, shows one minimum and one maximum in $\delta^{18}O$, which appear to reflect one year of growth. The smaller shell, 294B (whorl length = 23.5 mm), has a shorter record which is likely responsible for the lower seasonality relative to 294A. Three specimens from Bocas del Toro (TA04-10A, B & C) have average $\delta^{18}O$ values of -0.8‰ to -1.3‰ and ranges of 0.7‰ to 1.0‰. The mean values are close to those of the Golfo de los Mosquitos shells but slightly lower. A single specimen from San Blas (SB95-1) shows a significantly lower average $\delta^{18}O$ value of -1.6‰ and a larger annual range of 1.6‰ with recognizable annual cycles.

In contrast to shells that represent SWC non-upwelling waters (TEP upwelling), *Conus* shells from the Gulf of Panama (TEP) have $\delta^{18}O$ profiles that show substantial seasonal variations, revealing 2 to 6 years of growth (the figure on page 47). Importantly, maximal $\delta^{18}O$ values (averaging -0.4‰) exceed those of SWC samples (averaging -0.6‰) despite TEP seawater being lower in $\delta^{18}O$ by 0.3 to 0.6‰ (Table 3-2). Mean $\delta^{18}O$ values fall between -1.4 and -2.1‰ and annual ranges are between 2.3 and 3.2‰. Based on the chronology provided by the $\delta^{18}O$ profiles, most shells show faster growth (greater linear extension rate) during their juvenile years (first one or two years;

Figs. 3-5 and 3-6). This pattern of *Conu*s shell growth has also been observed by Perron (1983), who interpreted

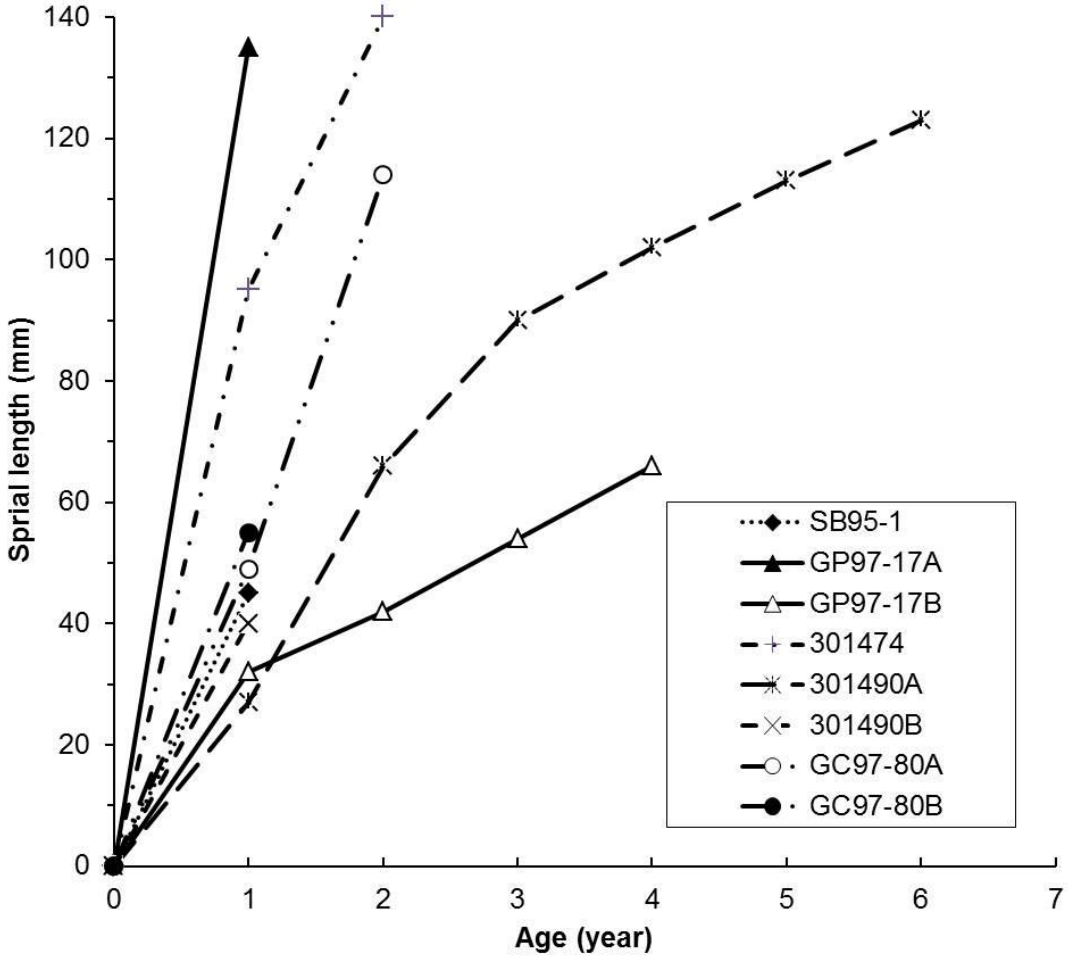

FIGURE 3-5—Growth curves based on chronologies established by shell $\delta^{18}O$ profiles.

Figure 6

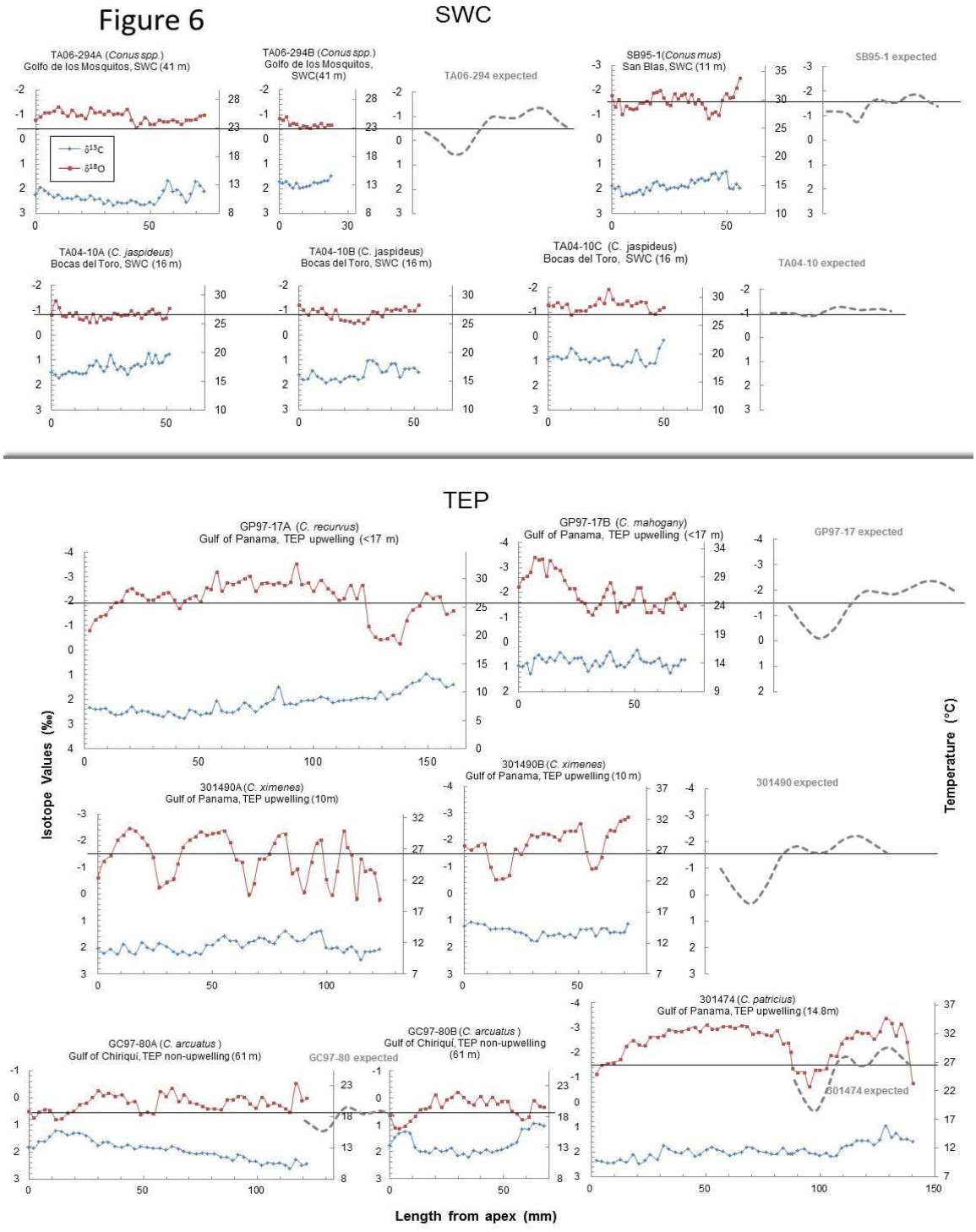

FIGURE 3-6—$\delta^{18}O$ and $\delta^{13}C$ profiles of each specimen, together with the expected shell $\delta^{18}O$ profiles estimated from WOA data.

TABLE 3-2—Specimen information and environment, and stable isotope values and correlations. Blue figures represent values from the dry season only.

Sample ID	Depth (m)	T (°C)	S (psu)	$\delta^{18}O_w$	$\delta^{18}O_{mean}$	sd $\delta^{18}O$	$\delta^{18}O_{expeot}$	$\Delta^{18}O$	$\Delta^{18}O_{expeot}$	$\delta^{13}C_{mean}$	δ-δ corr	δ-δ p-value
TA06-294A	40.7	23.6	33.6	0.41	-0.9	0.2	-0.5	0.8	1.9	2.3	0.06	0.71
TA06-294B	40.7	23.6	33.6	0.41	-0.6	0.1	-0.5	0.4	1.9	1.8	0.22	0.41
SB95-1	11	27.5	35.6	0.79	-1.6	0.3	-1.2	1.6	1.1	1.8	0.01	0.96
TA04-10A	15.9	27.1	35.1	0.7	-0.8	0.2	-1.0	0.9	1.2	1.3	0.06	0.74
TA04-10B	15.9	27.1	35.1	0.7	-0.9	0.2	-1.0	0.7	1.2	1.5	0.28	0.16
TA04-10C	15.9	27.1	35.1	0.7	-1.3	0.2	-1.0	1	1.2	0.9	0.2	0.32
											0.19	0.12
GP97-17A	<17	26.5	31.7	-0.53	-2.1	0.7	-1.5	3.2	2.2	2.2	-0.81	0.05
											0.34	0.02
GP97-17B	<17	26.5	31.7	-0.53	-2	0.7	-1.5	2.3	2.2	0.8	0.59	0.05
											0.42	0.00
301474	14.8	27	34.2	0.12	-2.4	0.7	-1.2	2.9	2.5	2	-0.97	0.00
											0.08	0.57
301490A	10	27.1	33.8	0.02	-1.4	0.8	-1.2	2.6	2.5	1.9	-0.72	0.01
											0.25	0.18
301490B	10	27.1	33.8	0.02	-1.8	0.7	-1.1	2.3	2.5	1.4	-0.69	0.04
GC97-80A	61	18.3	34.6	0.23	0.2	0.3	0.7	1.3	0.9	1.9	0.25	0.09
GC97-80B	61	18.3	34.6	0.23	0.4	0.4	0.7	1.3	0.9	1.7	-0.55	0.00

the change in shell growth pattern as a shift in energy from growth to spawning with maturity. Within each year, growth is mostly faster from maximum to minimum $\delta^{18}O$ (note the reverse scale of isotope values), thus creating an asymmetrical sawtooth pattern suggestive of enhanced spring growth during upwelling (see also Kobashi and Grossman, 2003).

The Gulf of Chiriquí shells (GC97-80A & B), presumably representing TEP non-upwelling conditions, show moderate seasonal variations and annual ranges with subdued cyclicity. The mean $\delta^{18}O$ values of each specimen are 0.2‰ and 0.4‰, respectively and the annual ranges are both 1.3‰. This annual range lies between those of shells growing in the highly-upwelling environments of the Gulf of Panama and shells growing in the non-upwelling SWC environments. The mean $\delta^{18}O$ values are significantly higher ($p <$

0.05) than those for the other two areas, probably due to the greater depth (61 m vs. 10 to 15 m for shells from Gulf of Panama and 11 to 41 m for shells from SWC waters).

Carbon Isotopes

Unlike oxygen isotopes, carbon isotopes show greater differences within each locality rather than between localities (Figs. 3-6 & 3-7). There are no distinct seasonal variations within the shell profiles though a long-term trend is sometimes present in which the $\delta^{13}C$ values decrease with ontogeny (e.g. SB95-1, GP97-17A, and GC97-80A). The mean $\delta^{13}C$ values of both SWC and TEP samples mostly fall between 1.3‰ and 2.3‰, with two exceptions (TA04-10C, 0.9‰, and GP97-17B, 0.8‰).

Discussion

Expected versus Measured Oxygen Isotope Profiles

Nearshore marine environments proximal to freshwater sources can be highly variable, both spatially and temporally, complicating comparisons between shell isotopic profiles and environmental data collected kilometers to tens of kilometers from the shell recovery site. As discussed earlier, environmental temperature and salinity data were available from offshore oceanographic sites (WOA) and, in certain cases, from nearshore temperature logger sites. WOA data from Bocas del Toro (SWC) generally agree with logger data (within ±1°C, Fig. 3-3A). For the Gulf of Panama (TEP) sites, the WOA data agree with high (rainy season) temperatures but do not capture the lowest temperatures during the upwelling season, perhaps because upwelling is patchy and sporadic, resulting in higher average temperatures and reduced annual range (Fig. 3-3B).

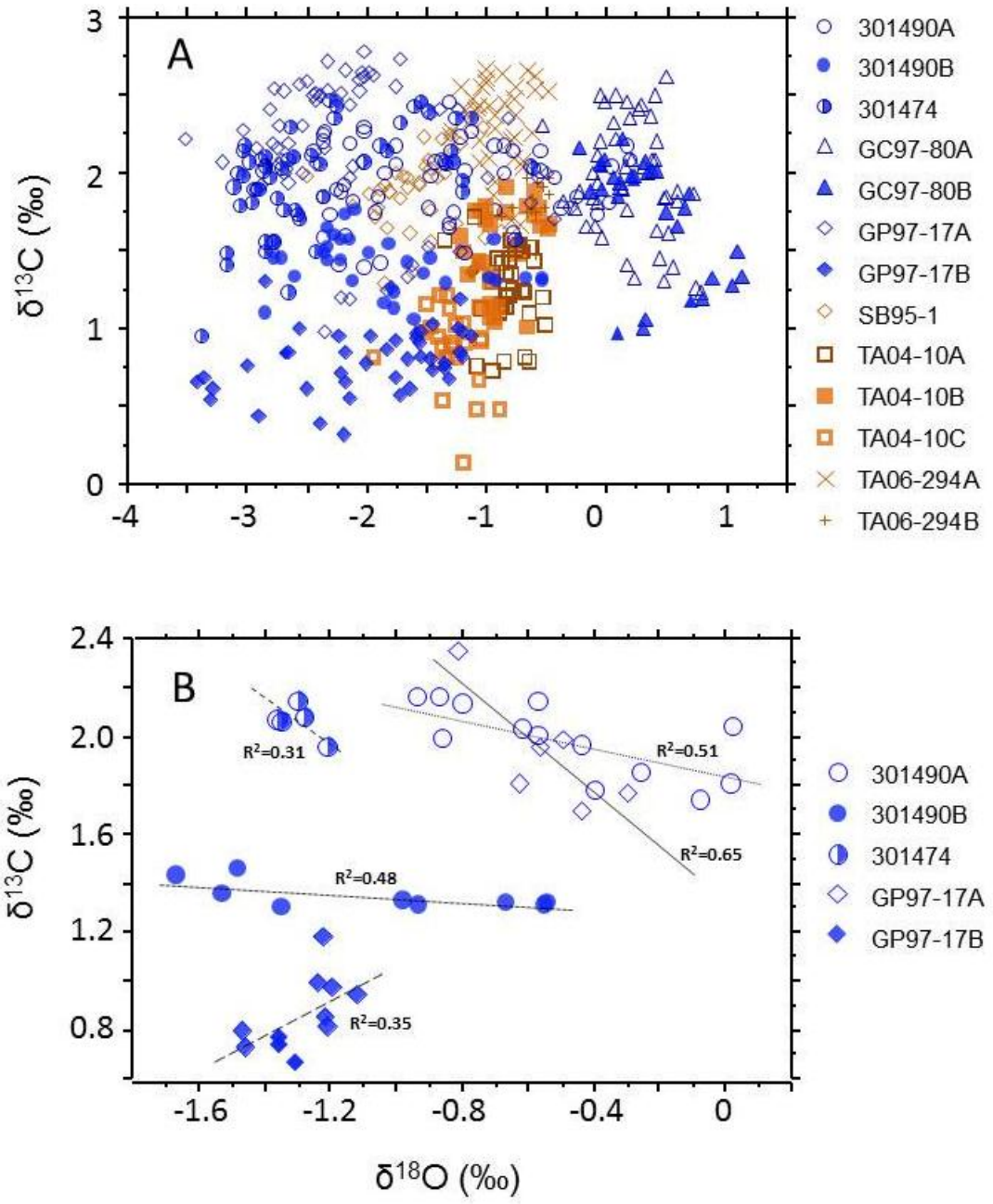

FIGURE 3-7—$\delta^{13}C$ versus $\delta^{18}O$ for all *Conus* shells (A) and for samples in the dry season only (B). Orange and blue symbols represent Caribbean and Pacific specimens respectively.

Most of the measured average SWC $\delta^{18}O$ values are statistically identical to the expected $\delta^{18}O$ values, while the average TEP $\delta^{18}O$ values are significantly (0.2–1.2‰)

lighter (Table 3-2). The ranges of measured $\delta^{18}O$ values from the SWC shells are 0.2–1.4‰ lower than the ranges of expected $\delta^{18}O$ values, except for SB95-1, which is 0.5‰ higher. In contrast, the ranges of measured $\delta^{18}O$ values from the TEP shells are 0.1-1.0‰ higher than the expected $\delta^{18}O$ ranges. For the Bocas del Toro and Gulf of Panama shells, the measured $\delta^{18}O$ profiles match well with the logger temperature profiles (Fig. 3-3), though with slightly lower resolution (weekly to fortnightly for the stable isotopic analyses compared with daily for the logger data) and with time-averaging of three to seven days in each sample hole (calculated using shell chronology). For the Bocas del Toro shells, differences between measured $\delta^{18}O$ values and WOA data may be caused by inter-annual fluctuations (i.e. WOA data for the year 2001 compared with logger and isotopic data for the year 2004). For the Gulf of Panama shells, WOA data do not appear to record the temperature minima during the upwelling season (as mentioned earlier), resulting in higher average temperatures and reduced annual range. This could explain the range difference in the TEP shells mentioned above. However, WOA average temperatures are already higher than logger temperatures, and our $\delta^{18}O$-derived mean temperature are even higher (i.e., $\delta^{18}O$ values lighter [e.g. specimens 301474 and GC97-80B], Fig. 3-6). The likely explanation is that the salinity at the nearshore localities is lower than that estimated from the WOA.

Isotopic Proxies for Upwelling and Freshwater Input

We argue here that oxygen isotope profiles can be used to quantify seasonal upwelling and freshening signals. Baseline shell $\delta^{18}O$ values (no upwelling or freshening) are calculated using average temperature during the non-upwelling season, "normal" seawater $\delta^{18}O$, and the Grossman and Ku (1986) equation. "Normal" seawater $\delta^{18}O$ is

calculated from dry-season salinities from logger or WOA data and the $\delta^{18}O_w$-salinity relationship of Fairbanks et al. (1992). These range from 32 to 36 psu (Table 3-2).

We can assume that shell $\delta^{18}O$ values seasonally greater than the baseline (i.e., plotting below the baseline in Fig. 3-8) can only be caused by cooler temperatures as normal seawater salinity fixes the upper limit of seawater $\delta^{18}O$. Because tropical SSTs are relatively stable when not upwelling, unusually cool temperatures undoubtedly reflect upward water mass transport (Fig. 3-2A). Shell $\delta^{18}O$ values less than the baseline (i.e., plotting above the baseline) no longer represent temperature variations, but salinity variations caused by freshening. Salinities can be derived from Fairbanks et al. (1992) and Grossman and Ku (1986):

$$S_{Pacific} = ((\delta^{18}O_{shell} + 8.77) - (19.7 - T) / 4.34) / 0.26 \quad (6)$$

$$S_{Atlantic} = ((\delta^{18}O_{shell} + 5.97) - (19.7 - T) / 4.34) / 0.19 \quad (7)$$

where -8.88‰ and -4.61‰ are the average freshwater input into the tropical Pacific and Atlantic, respectively. These values are reasonable approximations of runoff on the Pacific and Caribbean sides of Panama (Lachniet and Patterson 2006, Lachniet 2009), and are supported by preliminary data for coastal water on the Pacific and Caribbean sides of the isthmus (Fig. 3-4). Figure 3-8 shows that the Gulf of Panama specimen GP97-17A recorded temperatures of upwelled seawaters as low as 23°C and salinities of freshened seawaters as low as 30.5 psu from a dry-season salinity of 35 psu. The error bar is calculated based on the standard deviations of the environmental data (salinity and temperature) and the error in the Fairbanks equations.

Figure 3-9 plots all the shell $\delta^{18}O$ values normalized to baseline. The gray bars represent $\pm 1\sigma$ error based on determinations of baseline, derived from the uncertainty in

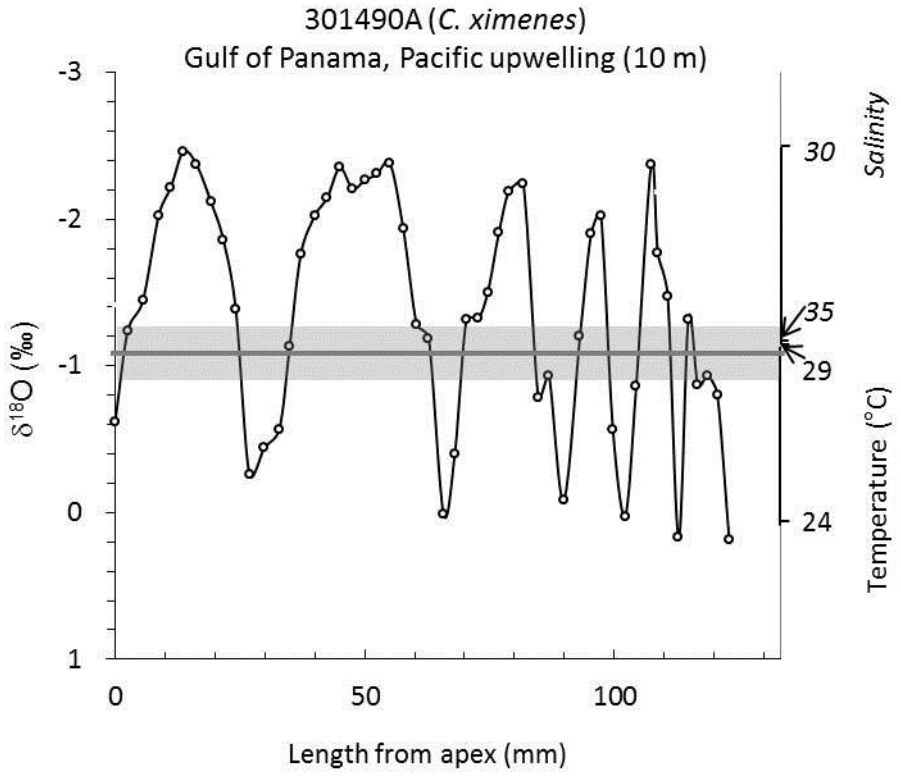

FIGURE 3-8—$\delta^{18}O$ and $\delta^{13}C$ profiles of specimen 301490A with $\delta^{18}O$ baseline. $\delta^{18}O$ values lower than the baseline values are calibrated to salinity change while those higher than the baseline values are calibrated to temperature change.

temperature and salinity within and between each WOA sites and the error in $\delta^{18}O_w$–S relationship, where the T and S errors within each WOA sites are their internal standard deviations, the T and S errors between nearby WOA sites for each sample are their external standard deviations, and the error in the $\delta^{18}O_w$–S relationship is the standard deviation of residuals in the Fairbanks et al. (1992) regression model (Fig. 3-4). Seventy-five percent of the SWC $\delta^{18}O$ values lie below (to the left of) the baselines, with isotopic salinities up to 7 psu below baseline, suggesting strong freshening and little or no upwelling. Thus freshwater input helps drive productivity in this locality. The Gulf of Panama sample profiles (TEP upwelling area) fluctuate across the baseline, suggesting

both freshening and upwelling. Samples 301494A and GP97-17A in this area show the greatest evidence for upwelling, with isotopic temperatures up to 9°C below baseline (Fig. 3-8, 3-9). The Gulf of Chiriquí (TEP non-upwelling) profiles, however, lay largely within the error of the baseline, except for several data points in GP97-80B. This suggests little or no upwelling in the SWC but strong upwelling in the TEP upwelling areas, as predicted above. Temperature and salinity relative to baseline values are calculated using their $\delta^{18}O$ values. The temperatures of TEP upwelled waters are at least 4℃ lower than baseline values, suggesting upward movement of nutrient-rich waters of more than 60 m (D'Croz and O'Dea, 2007). Isotopic profiles document rainy-season salinities as low as 24 psu in the Gulf of Panama.

The upwelling and freshening events can be identified using $\delta^{13}C$–$\delta^{18}O$ covariance within shell isotopic profiles. Upwelling brings cold, saline deep water (^{18}O enriched but ^{13}C-depleted) to the surface, resulting in ^{18}O enrichment and ^{13}C depletion in shell carbonate (e.g., Killingley and Berger 1979, Jones and Allmon 1995). In contrast, freshwater input decreases both $\delta^{18}O$ and $\delta^{13}C$ values, resulting in a positive correlation (e.g., Mook 1971). Surprisingly, with minor exception these relationships are not apparent in the Panama samples. Table 3-2 lists the slopes, correlation coefficients, and *p*-values of δ–δ correlations of all the specimens (also seen in Figure 3-7A). Only three out of 13 specimens show significant correlations ($p < 0.05$). However, among those three specimens, two from TEP upwelling area (GP97-17B and 301474) actually have positive

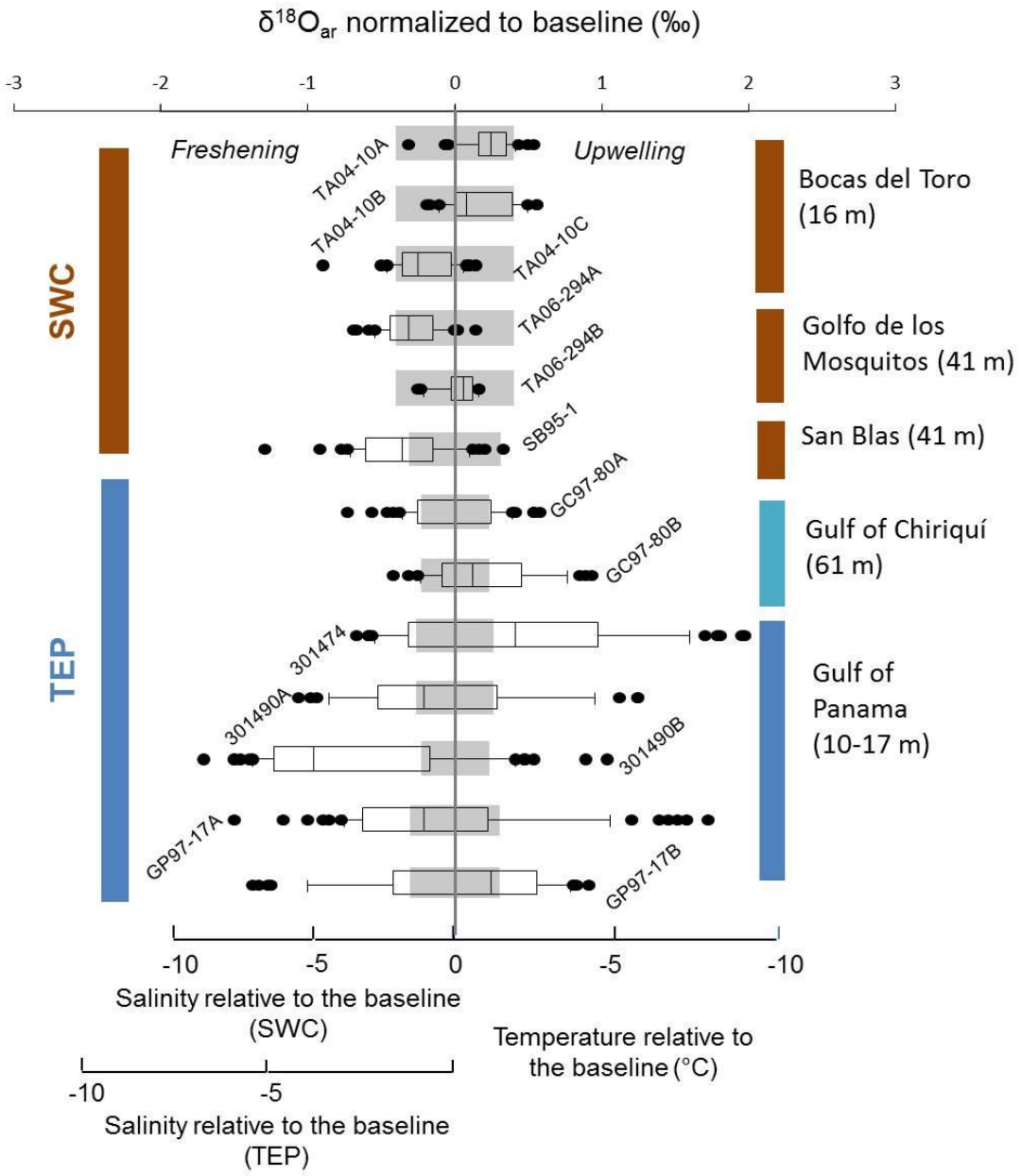

FIGURE 3-9—Box and whisker plot of shell $\delta^{18}O$ values normalized to baseline values for all specimens. Gray bars represent analytical error (1σ) for each sample location. $\delta^{18}O$ values lower than the baseline values are calibrated to salinity change (note that TEP and SWC samples have different scale) while those higher than the baseline values are calibrated to temperature change.

$\delta^{18}O$–$\delta^{13}C$ correlations. No inverse correlation between $\delta^{18}O$ and $\delta^{13}C$ was found in the bivalve and gastropod shells from the TEP upwelling areas studied by Geary et al. (1992) and Bemis and Geary (1996). Geary et al. (1992) proposed that the absence of negative

δ–δ correlations in this upwelling area may be caused by intense freshwater input during the rainy season, which mitigates the upwelling signal during the dry season. Similar to upwelling, freshwater input during the rainy season introduces ^{13}C- depleted DIC into marine waters, masking the effect of ^{13}C depletion during upwelling. Because of this effect, Matthews et al. (2008) found no significant difference in marine $\delta^{13}C$ between upwelling and non-upwelling times in the Gulf of Panama. Confirming this, a closer examination by isolating dry season data (according to the shell chronology) from the remaining shell growth reveals significant correlations ($p < 0.05$) in four of the five Gulf of Panama specimens (Table 3-2, Fig. 3-7B). In Bemis and Geary's data (1992), only two of seven Pacific upwelling area shells show significant negative correlations by isolating the dry-seasons. This likely reflects the greater influence of vital effect (e.g., incorporation of metabolic CO_2) in the $\delta^{13}C$ of bivalve shells compared with that of gastropod shells, as indicated by the ~2.5‰ lower mean $\delta^{13}C$ of the Bemis and Geary's bivalves compared with the *Conus* shells used in this study. The "upwelling" signals detected in GC97-80B from both baseline and correlation methods results from the previously-discussed seasonal shoaling of the thermocline, rather than upwelled deep water.

Freshwater and Upwelling as Sources of Nutrient Delivery

As discussed above, Caribbean and Gulf of Chiriquí samples show little upwelling signal but strong freshwater signal while the Gulf of Panama samples shows both strong upwelling signal during the dry season and significant freshwater signal during the rainy season. In the former case, the nutrient source primarily comes from freshwater input as suggested by a study of the distribution of dissolved inorganic

nutrients and plankton in the Caribbean coast of Panama (D'Croz et al., 2005). In their study, high nutrient (nitrate, phosphate, and silicate) levels, chlorophyll a, and zooplankton biomass all correlate with the rainy season. Significant negative correlations between nutrient level and salinity also confirm the contribution of freshwater runoff. In the Gulf of Panama, there are two nutrient sources, upwelling and freshwater input. According to D'Croz and O'Dea (2007), the nutrient levels in this area are low in the rainy season, but high in the dry season, suggesting that the upwelling is the dominant contributor to the nutrient delivery.

Neogene Application of Isotopic Proxies for Upwelling and Freshwater Input

Application of isotopic proxies for upwelling and freshening to quantifying paleoenvironments depends on our ability to accurately define baseline values. These values can be determined from (1) invariant molluscan $\delta^{18}O$ profiles which represent a lack of seasonal upwelling or rainfall, and (2) planktonic foraminiferal $\delta^{18}O$ and Mg/Ca data, for the paleo-depths of interest. Obtaining data from both materials provides a check on the determination. To correct for cross-isthmian temperature and especially salinity differences, these baseline data should be collected for samples on the Caribbean and Pacific sides of the Isthmus. This application will be the subject of future papers.

Summary

The shell $\delta^{18}O$ profiles generally follow the pattern of the expected $\delta^{18}O$ values estimated from temperature and salinity, making possible the determination of shell chronologies based on seasonal variations in upwelling and rainfall when present. Positive and negative deviations from baseline $\delta^{18}O$ values, representing periods of non-upwelling and normal salinity, are used to identify and quantify upwelling and freshwater

input respectively in modern TEP and SWC waters. Shell profiles reveal little upwelling in SWC and Gulf of Chiriquí, but strong upwelling in the Gulf of Pacific, consistent with observations. Temperatures of upwelled waters that are at least 9°C lower than baseline values are observed, suggesting upward movement of nutrient-rich waters of more than 60 m. Isotopic profiles document rainy-season salinities as low as 24 in the Gulf of Panama. Surprisingly, none of the shells in the upwelling region show a negative covariance between $\delta^{13}C$ and $\delta^{18}O$ expected with upwelling. However, four out of five specimens show strong negative $\delta^{13}C$–$\delta^{18}O$ correlation when the upwelling dry season data are isolated, suggesting freshwater input during the non-upwelling seasons masks the upwelling signals. Our findings demonstrate that for tropical environments, seasonally deviations from baseline $\delta^{18}O$ values can be used to quantify upwelling and freshening and consequently nutrient delivery and productivity.

CHAPTER IV

SEASONAL ENVIRONMENTAL VARIATIONS DURING THE LATE NEOGENE: STABLE ISOTOPIC RECORDS IN MOLLUSKS FROM THE CENTRAL AMERICAN ISTHMUS

Overview

The late Neogene marine environment has undergone significant changes due to the formation of Central American Isthmus (CAI). The modern contrasts such as temperature, salinity, nutrient level, and stable isotope composition between tropical east Pacific (TEP) and southwestern Caribbean (SWC) seawaters are not seen prior to the final closure of CAI around 3.5 Ma. To quantify the Neogene seasonal marine environmental variations, 16 Neogene *Conus* shells collected from three major Caribbean sedimentary basins and the Pacific coast in Panama and Costa Rica were analyzed for oxygen and carbon isotopes in this study. Two different approaches, $\delta^{18}O$-$\delta^{13}C$ correlation and $\delta^{18}O$ baseline method, were used to identify and quantify upwelling and freshening signals. The records reveal significant upwelling in the late Miocene and mid Pliocene TEP waters, significant to moderate freshening in the SWC waters between 2.2–5.7 Ma, and minimal seasonal upwelling and (or) freshening variations in the Plio-Pleistocene SWC waters. The reconstructed sea-surface temperatures (SSTs) agree with the global cooling trend through late Miocene, but lack evidence for the warming event in the middle Pliocene or the late Neogene global cooling trend.

Introduction

The formation of Central American Isthmus (CAI) had a dominant impact on late Neogene climate. At present, there are significant differences between tropical east Pacific (TEP) and southwestern Caribbean (SWC) waters across the isthmus, which include differences in mean annual temperature (MAT), salinity, nutrient concentrations, primary productivity, and the stable isotopic composition of the water. The modern Caribbean-Pacific contrast of surface water MAT of 2°C and salinity of 1–1.5‰ was established by about 4.2 Ma (Keigwin, 1982; Haug et al., 2001), resulting largely from (1) strong seasonal upwelling of nutrient-rich waters in the Pacific that reduces temperature and increases productivity, and (2) high evaporation in the Caribbean and net Caribbean-Pacific vapor flux that increases salinity in the Caribbean and reduces salinity in the Pacific (Maier-Reimer et al., 1990; D'Croz et al., 1991; D'Croz and O'Dea, 2007). Prior to the isthmian uplift, when the seaway was still open, these contrasts were minimal.

Previous studies have suggested that a broad marine connection was present before the middle Miocene (Coates et al., 1992; Collins et al., 1996). Since the middle Miocene, the CAI was gradually formed by the growth of volcanic arcs and the collision of the Costa Rica-Panama microplate with South America. The CAI reached its first complete closure in the middle Pliocene (ca. 3.5–3.1 Ma) and reopened during 3.1–2.8 Ma owing to high sea level as a negative feedback from enhanced heat transport from tropical areas to high latitudes that reduced Antarctic ice. The CAI again closed during 2.4–2.0 Ma (Cronin et al., 1994).

During the period of CAI formation, global climate underwent a long-term cooling trend through the late Miocene to early Pliocene and a short interval of global warming during the middle Pliocene (Zachos et al., 2001). Studies of ostracode assemblages from the west coast of Florida and planktonic foraminifera from the western Caribbean Sea and North Atlantic (middle to high latitude) suggest that southwest North Atlantic water temperatures increased when the CAI closed (Cronin and Dowsett, 1996). However, the tropical sea-surface temperature (SST) changes may differ from the global trend that is largely derived from high-latitudes. Recently, there has been a debate regarding low-latitude climate change during the late Miocene cooling. A study of planktonic foraminiferal $\delta^{18}O$-derived SSTs from 33 late Miocene (7.2–5.6 Ma) Ocean Drilling Project (ODP) and Deep Sea Drilling Project (DSDP) sites suggests markedly cool low-latitude temperatures, in some cases more than 9°C lower than modern SSTs (e.g. DSDP 216 and 709C, Williams et al., 2005). SST estimates from Mg/Ca analyses of planktonic foraminifera in the western Caribbean (ODP 999) suggest cool tropical temperatures that are about 2℃ lower than modern (Groeneveld, 2005). However, SST estimates from alkenone unsaturation analyses from ODP site 958, northeastern Atlantic (23.9990°N, 20.0008°W), suggest subtropical SSTs that were warmer by 2–4°C (Herbert and Schuffert, 1998). Discrepancies such as these have lead scientists to question the accuracy of the $\delta^{18}O$-derived paleotemperatures from calcitic planktonic foraminifers, citing the potential influences of dissolution and diagenesis, vital effect, and changes in seawater $\delta^{18}O$ (Pearson et al., 2001; Williams et al., 2005).

These hypotheses can be tested by measuring additional SST proxies, such as $\delta^{18}O$ of molluscan (especially gastropods) shells (e.g., Kobashi et al., 2001). In isotopic

studies, mollusks provide a strong complement to planktonic foraminifera for reconstructing ancient climates in that: 1) their long life span provides records of both seasonal and interannual temperature variations which are unavailable from foraminifera; 2) their aragonitic mineralogy makes it easier to assess chemical preservation; 3) their shallow benthic habitat ensures that they do not sink below the carbonate compensation depth (CCD) and are thus less likely to be dissolved.

These advantages have raised interest in using mollusks to complement the use of planktonic foraminifera in isotopic studies of paleoclimate (Krantz et al., 1990; Teranes et al., 1996;Andreasson and Schmitz, 2000; Kobashi et al., 2001; Latal et al., 2004). However, isotope records from the mollusks have their own limitations resulting from uncertain global and local salinity variation. Previous studies of modern mollusk shells from the CAI have demonstrated the utility of oxygen isotope analyses of serially-sampled bivalve and gastropod shells as paleothermometers and upwelling indicators (Geary et al., 1992; Bemis and Geary, 1996). Geary et al. (1992) observed that a strombid gastropod from the Pacific shelf of Panama showed a large $\delta^{18}O$ range ($\Delta^{18}O$), indicative of large temperature and salinity variation. In contrast, a Caribbean strombid showed a narrow range indicating low variability in temperature and salinity. Bemis and Geary (1996) confirmed these findings with venerid bivalves. Pacific and Caribbean specimens from upwelling areas showed a large $\Delta^{18}O$ whereas shells from non-upwelling areas showed a reduced range. Our data for modern *Conus* shells from the CAI parallel the results of Geary et al. (1992) and Bemis and Geary (1996), with lower $\Delta^{18}O$ for SWC specimens from non-upwelling areas and higher $\Delta^{18}O$ for TEP specimens (Tao et al., in prep.). In addition, by comparing oxygen isotopic values to baseline $\delta^{18}O$ for "normal"

temperatures and salinities, we were able to use $\delta^{18}O$ profiles to quantify both upwelling and freshening. These interpretations were confirmed by $\delta^{18}O$-$\delta^{13}C$ correlations.

Only one study has examined the isotopic profiles of Neogene mollusk shells from the CAI. Teranes et al. (1996) analyzed serially-sampled specimens of venerid bivalves from the Caribbean ($n = 9$) and the Pacific ($n = 4$). While the data suggest a Caribbean-Pacific difference in seasonality since at least 3.5 Ma, changes in Caribbean seasonality between late Miocene ($n = 2$) and the Plio-Pleistocene and modern ($n = 8$) are not clear cut. Furthermore, no effort is made to distinguish between $\delta^{18}O$ range reflecting upwelling and freshwater impact. This paper reports on data for serially-sampled fossil *Conus* shells to examine changes in mean annual temperature (MAT), mean annual range in temperature (MART), upwelling, and freshwater input in the coastal CAI associated with the closing of the isthmus and the development of north hemisphere glaciation. Our results show that SWC samples generally show strong upwelling signals prior to 8 Ma and moderate to weak freshening signals since 5.7 Ma, while the TEP samples show strong upwelling signals in the middle Pliocene (3.5 Ma) as they do today.

Study Area and Samples

A total of 16 fossil *Conus* shells collected from three major Neogene Caribbean sedimentary basins (Panama Canal Basin, Bocas del Toro Basin, and Limón Basin) and the Pacific coast were analyzed. *Conus* shells were chosen because of their relatively large sizes, long life-span, and shallow-dwelling habitat. Of the 16 specimens, six were collected in 2009 by Kai Tao and Ethan Grossman at three sites in the Panama Gatun

Formation in the Panama Canal Basin (Sabanitas, Gatun lock, and Payardi Refinery), and ten were collected in 2006 by Aaron O'Dea and Jill Leonard-Pingel at Neogene outcrops in Panamanian and Costa Rican coastal regions (Burica Peninsula, Bocas del Toro Basin, and Limón Basin). The sample locations, stratigraphy, and sample information are summarized in Figures 4-1 and 4-2 and Table 4-1.

The Gatun Formation in central Panama, exposed on the north side of Lake Gatun and cut by the Panama Canal, is most often considered to be late Miocene in age, 12.0-8.0 Ma (Coates et al., 1992). The richness of molluscan fauna in the Gatun Formation suggests a shallow nearshore environment of approximately 15–40 m water depth (Collins et al., 1996). The first site is located in a quarry in Sabanitas (GFS series) in the Lower Gatun Formation (12.0–11.0 Ma). It contains about 20 m of dark grey muddy to sandy deposits with abundant molluscan shells of varying size and concentration. Condensed shell beds, consisting mostly of turritellids and bivalves, are found in the upper sections (GFS-2 and GFS-3). Large whole cone shells and large concretions are found in-situ only in the upper sections, whereas in the lower section (GFS-1) most fossils are fragmented and small. The second site, also in the Lower Gatun Formation, is located on the roadside near the gate of Payardi Refinery (GPR). This site features a 5 m fossiliferous outcrop with large turritellids and other molluscan shells, and is covered by weathered, iron-stained soil. The base of the outcrop is completely weathered with fewer fossils. The third site is beside the Panama Canal near the Gatun Lock (GFG series), in the upper Gatun Formation (ca. 8 Ma). This site contains grey soft sandstone with abundant bivalve and gastropod fragments. Most large shells, for example cone shells,

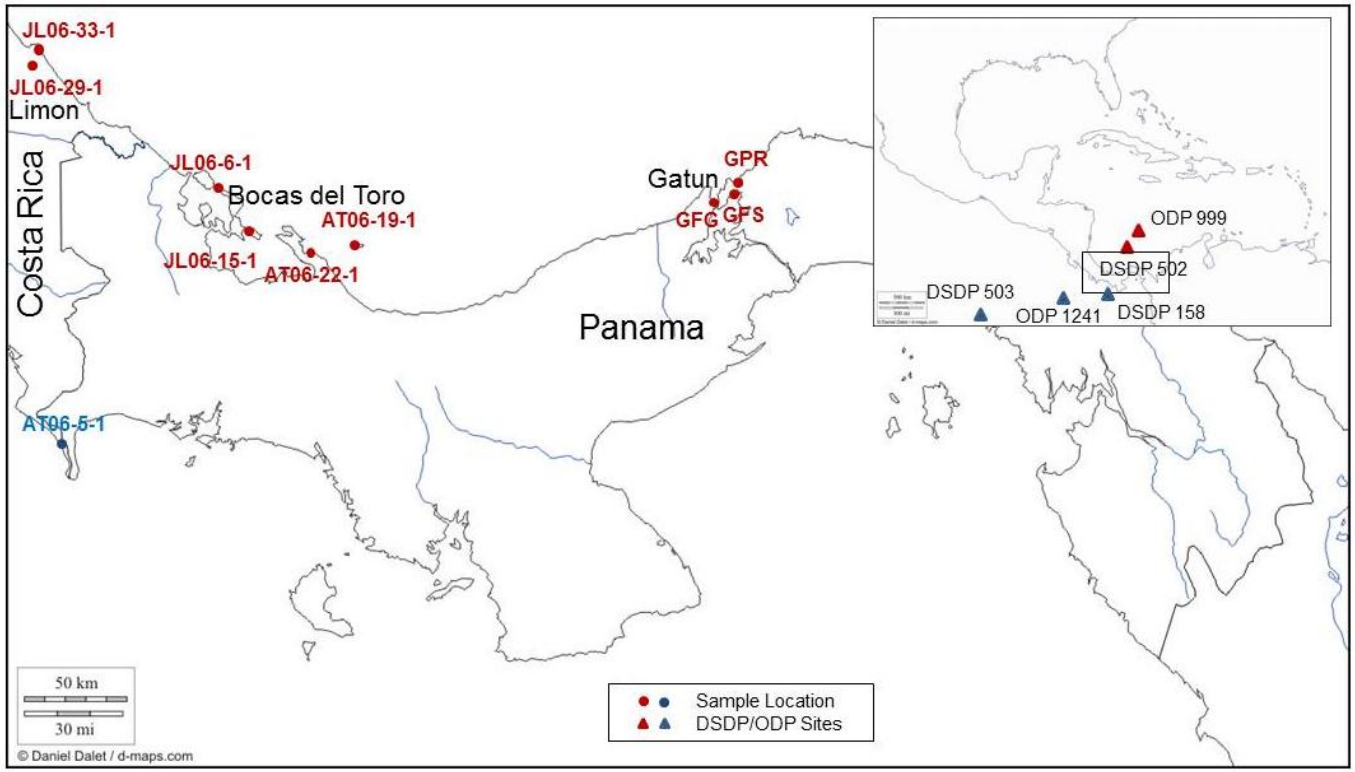

FIGURE 4-1—Map of sample localities and DSDP and ODP sites.

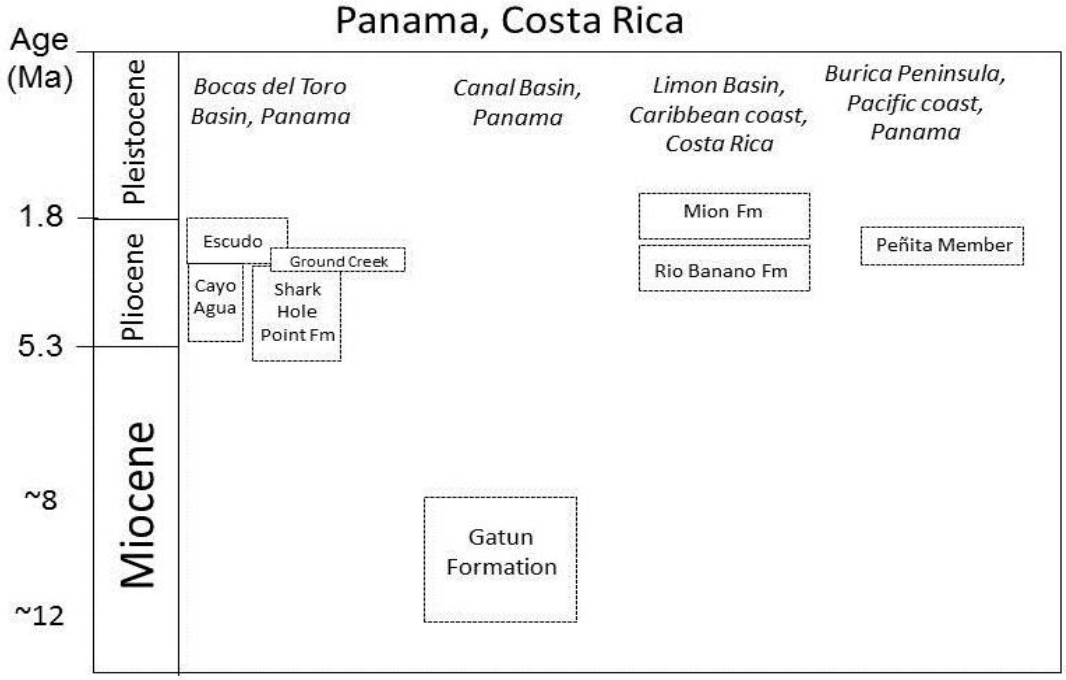

FIGURE 4-2—Stratigraphy for the studied sections based on Coates et al. (1992, 2005).

are weathered, leaving only interior molds. Only small cone shells can be found in their original state. Also found at this site are some float coquinas derived from the overlying Chagres Formation.

TABLE 4-1— Specimen taxonomy, location, age, paleodepth, and dimensions.

Sample ID	Species	Location	Lat. (°)	Long. (°)	Age/ Fm	Age (Ma)	Paleo-depth (m)	Shell length (cm)	Shell width (cm)	Whorl length (cm)
Caribbean										
JL06-33-1C	*Conus spp.*[1]	Limon, Costa Rica	9.996	-83.040	Mion	1.5-1.7	50-100	31.5	17.3	86.6
JL06-33-1F	*Conus spp.*	Limon, Costa Rica	9.996	-83.040	Mion	1.5-1.7	50-100	N/A	16.3	78.0
JL06-6-1	*Conus spp.*[2]	Wild Cane Key, Panama	9.351	-82.169	Ground Creek	1.9-2.2	~30	35.6	20.0	83.3
JL06-29-1A	*Conus spp.*	South of Limon, Costa Rica	9.913	-83.067	Rio Banano	2.9-3.2	20-40	38.1	19.5	97.3
JL06-29-1B	*Conus spp.*	South of Limon, Costa Rica	9.913	-83.067	Rio Banano	2.9-3.2	20-40	31.5	17.3	84.0
AT06-19-1	*Conus spp.*[3]	Escudo de Veraguas	9.090	-81.540	Escudo	3.5-3.6	100-150	32.9	15.5	78.3
JL06-15-1	*Conus spp.*[4]	Cayo Agua	9.175	-82.042	Cayo Agua	3.5-5.0	40-80	65.1	39.6	179.8
AT06-22-1A	*Conus spp.*	Shark Hole Point	9.065	-81.782	Shark Hole Point	5.6-5.7	150-200	43.6	18.5	67.7
GFG-A	*Conus spp.*	Gatun lock, east bank	9.295	-79.921	Gatun	8	15-40	47.8	24.2	127.3
GPR-A	*Conus spp.*	Peyardi Refinery, float on top	9.383	-79.821	Gatun	11-12	15-40	36.5	21.7	108.6
GFS-2A	*Conus spp.*	Sabanitas, 2 m above T-bed	9.354	-79.838	Gatun	11-12	15-40	38.8	22.1	100.5
GFS-3A	*Conus spp.*	Sabanitas, T-bed	9.353	-79.837	Gatun	11-12	15-40	30.5	15.0	67.8
GFS-3B	*Conus spp.*	Sabanitas, 7 m below T-bed	9.353	-79.837	Gatun	11-12	15-40	31.0	19.6	84.8
GFS-3F	*Conus spp.*	Sabanitas, 14 m below T-bed	9.353	-79.837	Gatun	11-12	15-40	36.2	21.9	87.1
Pacific										
AT06-5-1A	*Conus spp.*	Punta La Peña	8.214	-82.947	Peñita	3.5	<50	63.0	31.9	241.3
AT06-5-1B	*Conus spp.*	Punta La Peña	8.214	-82.947	Peñita	3.5	<50	N/A	13.5	88.0

[1] *Jaspidiconus pfluegeri*?
[2] *C. jaspideus*?
[3] *C. austini*?
[4] *C. Spurius*?
N/A = Not available

The Bocas del Toro Basin can be divided into the southern region containing early Miocene to Pliocene deposits, and the northern region with late Plio-Pleistocene shallow-water sediments (Coates et al., 2005). The Bocas del Toro Group in the southern regions comprises five major late Neogene formations: Tobabe Formation (7.2–5.3 Ma), Nancy Point Formation (7.2–5.3 Ma), Shark Hole Point Formation (5.6–3.5 Ma), Cayo Agua Formation (5.0–3.5 Ma), and Escudo de Veraguas Formation (3.5–1.8 Ma). Samples from the last three formations are used in this study. The Shark Hole Point Formation (AT06-22-1A) consists of bioturbated micaceous, clayey siltstone with abundant, thin shell beds in the uppermost part (Coates et al, 2005). Benthic foraminifera

indicate a paleobathymetry of 150-200 m (Collins, 1993). The Cayo Agua Formation (JL06-15-1) consists of muddy, silty sandstone with abundant mollusks and corals. Shallow-water coral and benthic foraminiferal taxa indicate a paleobathymetry of 40–80 m for these deposits (Collins, 1999). The Escudo de Veraguas Formation (AT06-19-1) consists of bioturbated siltstone and claystone, with frequent concretions and scattered molluscan shells and corals in the upper part (ca. 1.8 Ma) and densely-packed cemented burrow concretions, scattered corals, and abundant mollusks in the lower part (ca. 3.5 Ma). The paleodepth of this unit is approximately 100–150 m (Collins, 1999). The geology of Colon and Bastimentos Islands in the northern region of the Bocas del Toro archipelago differ from that of the southern region, which is still being studied. Although the formal lithostratigraphic units and ages are not finalized, this sequence is generally believed to be younger than that of the southern regions except for the Escudo de Veraguas Formation, with the oldest units around 3.5 Ma (Coates et al., 2005). In this study, one specimen (JL06-6-1) was collected from Wild Cane Cay in the west side of Bastimentos Island. This unit was named Ground Creek (2.2–1.9 Ma, O'Dea et al., 2007), and consists of extensive shelly coral-bearing bioclastic carbonate and volcaniclastic sandstone and siltstone, with abundant molluscan shells. The coral taxa indicate a depth of ~30 m.

The Neogene stratigraphy of the Limón Basin (Costa Rica) is represented by the Limón Group, which comprises the Uscari Formation (8.3–5.6 Ma), Rio Banano Formation (3.6–2.8 Ma), Quebrada Chocolate Formation (3.2–3.0 Ma), and Moin Formation (1.9–1.5 Ma). In this study two specimens were collected from the upper Rio Banano Formation (JL06-29-1A, B), which consists of blue-gray clayey siltstone with

abundant mollusks and bryozoans. The depositional environment of this formation is inner neritic, about 20-40 m deep (Jackson et al., 1999). Another two specimens (JL06-33-1C, F) were collected in the Upper Lomas del Mar member of the Moin Formation, which consists of blue-gray clayey siltstone and calcarenite with small, diverse mollusks, corals, and bryozoans. These sediments represent coral reef deposits which are about 50-100 m deep (Collins, 1999).

Two specimens (AT06-5-1A, B) were collected on the Burica Peninsula on the Pacific side. The unit sampled, the lower Pliocene Peñita Member of the Charco Azul Formation, consists of volcaniclastic sandstone, conglomerate, and cemented concretions at the base and a massive green muddy siltstone with abundant gastropods in the upper section. The shallow-water benthic foraminiferal fauna suggest an outer-forearc environment (Corrigan et al., 1990).

Methods

Each specimen was cleaned and ultrasonicated to remove all extraneous material from shell surfaces. X-ray diffraction analyses were performed to detect diagenesis. Only specimens with >99% aragonite were used for isotopic analyses. Using a dental drill with a 0.5 mm bur, sample powders were drilled along shallow grooves on growth lines in ontogenetic sequence on the spire of the gastropod shells. The sampling interval was determined by shell size and growth rate. Previous study of shells from the middle Miocene Pinecrest Beds in Florida (Tao and Grossman, 2010) established that good seasonal resolution was provided by a 2–5 mm sampling interval. Roughly 0.4–0.5 mg of sample powder were collected for stable isotopic and trace elemental analyses (trace

element data will be reported elsewhere). For isotopic analysis, sample powder was acidified with "100%" phosphoric acid at 75ºC. Evolved CO_2 gas was analyzed on a Thermo Scientific MAT 253 isotope ratio mass spectrometer coupled with Kiel IV carbonate device for carbon and oxygen isotope analyses. All results were calibrated to VPDB using NBS-19 standards. Precisions for carbon and oxygen isotopes are 0.08‰ and 0.10‰, respectively. Stable isotope paleotemperatures were calculated according to Grossman and Ku (1986, eq.1).

Results

Oxygen Isotopes

The averages, ranges, and extreme $\delta^{18}O$ values from *Conus* shells tested here from the Neogene Panama and Costa Rica coastal areas are summarized in Table 4-2 and Figs. 4-3 and 4-4. Specimens from the two lower Gatun Formation sites (Payardi Refinery and Sabanitas, 12–11 Ma) show significantly lower average annual $\delta^{18}O$ values (-1.0 to -1.3‰) than the specimen from the upper Gatun Formation (Gatun Lock, -0.6‰, ~8 Ma). Similarly, within the lower Gatun Formation, the average shell $\delta^{18}O$ values increase slightly from old to young sections. The GPR samples at the top of Lower Gatun Formation average -1.0‰, while the GFS samples from 50 m, 52 m, 57 m, and 66 m below the top average -1.1, -1.1, -1.2, and -1.3‰, respectively. All the Gatun samples show middle-high seasonal $\delta^{18}O$ variations (e.g., $\Delta^{18}O$ = 1 to 2‰ to >2‰). Most samples show an annual $\delta^{18}O$ range of 0.9 to 1.3‰ except GFS-3B, which has a range of 1.8‰.

The specimen from the latest Miocene Shark Hole Point Formation (AT06-22-1A) shows a significantly high average $\delta^{18}O$ value of 0.1‰, which is 0.7‰ higher than

TABLE 4-2— Sample information and descriptive statistics for stable isotope values and $\delta^{18}O$-$\delta^{13}C$ correlations.

Sample ID	Age/ Fm	Age (Ma)	Depth (m)	$\delta^{18}O_{min}$	$\delta^{18}O_{max}$	$\delta^{18}O_{avg}$	SD $\delta^{18}O$	$\Delta^{18}O$	$\delta^{13}C_{mean}$	$\delta^{18}O$-$\delta^{13}C$ slope	$\delta^{18}O$-$\delta^{13}C$ p-value
Caribbean											
JL06-33-1C	Mion	1.5-1.7	50-100	-0.4	0.5	0.0	0.2	0.9	2.1	0.16	0.18
JL06-33-1F	Mion	1.5-1.7	50-100	-0.5	0.6	0.0	0.3	1.1	1.7	0.36	0.00
JL06-6-1	Ground Creek	1.9-2.2	<50	-0.7	0.4	-0.1	0.2	1.1	1.1	-0.40	0.03
JL06-29-1A	Rio Banano	2.9-3.2	20-40	-1.4	-0.1	-0.9	0.2	1.3	1.5	-0.33	0.19
JL06-29-1B	Rio Banano	2.9-3.2	20-40	-1.7	-0.5	-0.8	0.2	1.2	1.3	0.29	0.37
AT06-19-1	Escudo de Veraguas	3.5-3.6	100-150	0.0	1.4	0.7	0.3	1.3	2.2	2.08	0.06
JL06-15-1	Cayo Agua	3.5-5.0	40-80	-1.3	-0.2	-0.7	0.2	1.1	0.2	0.84	0.03
AT06-22-1A	Shark Hole Point	5.6-5.7	150-200	-0.2	0.3	0.1	0.1	0.6	2.1	1.41	0.00
GFG-A	Gatun	8	15-40	-1.2	0.1	-0.6	0.2	1.3	2.0	-0.12	0.38
GPR-A	Gatun	11.0-12.0	15-40	-1.7	-0.6	-1.0	0.2	1.1	2.1	-0.26	0.04
GFS-2A	Gatun	11.0-12.0	15-40	-1.8	-0.6	-1.1	0.4	1.1	2.7	-0.38	0.05
GFS-3A	Gatun	11.0-12.0	15-40	-2.0	-0.2	-1.1	0.3	1.8	2.1	-0.16	0.02
GFS-3B	Gatun	11.0-12.0	15-40	-1.7	-0.8	-1.2	0.3	0.9	2.6	-0.36	0.03
GFS-3F	Gatun	11.0-12.0	15-40	-1.9	-0.7	-1.3	0.3	1.2	2.4	-0.51	0.01
Pacific											
AT06-5-1A	Peñita	3.5	<50	-1.9	0.1	-0.8	0.4	2.0	2.3	-0.25	0.01
AT06-5-1B	Peñita	3.5	<50	-1.3	0.2	-0.4	0.4	1.5	2.7	0.17	0.04

the mean Gatun Lock $\delta^{18}O$ value. This sample also shows a very small seasonal variation (0.6‰). The high average value and small annual range are consistent with the estimated paleodepth of 150–200 m (Collins, 1993).

The early Pliocene specimen from the Cayo Agua Formation (JL06-15-1) shows an annual range similar to that of the Gatun Formation specimens, suggesting no significant change in the shallow water seasonality from late Miocene to early Pliocene. Although the average $\delta^{18}O$ value is similar to that of the Upper Gatun Formation specimen, the greater paleodepth of the Cayo Agua Formation specimen (40–80 m vs. <50 m) suggests, for this limited sampling, a higher SST in the early Pliocene. The middle Pliocene specimen from Escudo de Veraguas Formation (AT06-19-1) shows a significant increase in average $\delta^{18}O$ (1.4‰) relative to the Cayo Agua sample. This can be attributed to its 100–150 m paleodepth. However, the $\delta^{18}O$ range of this sample, 1.3‰, is identical to those of the shallow water specimens. The reason for this large $\delta^{18}O$ range is unknown. The profile shows an increasing $\delta^{18}O$ trend that, based on average growth

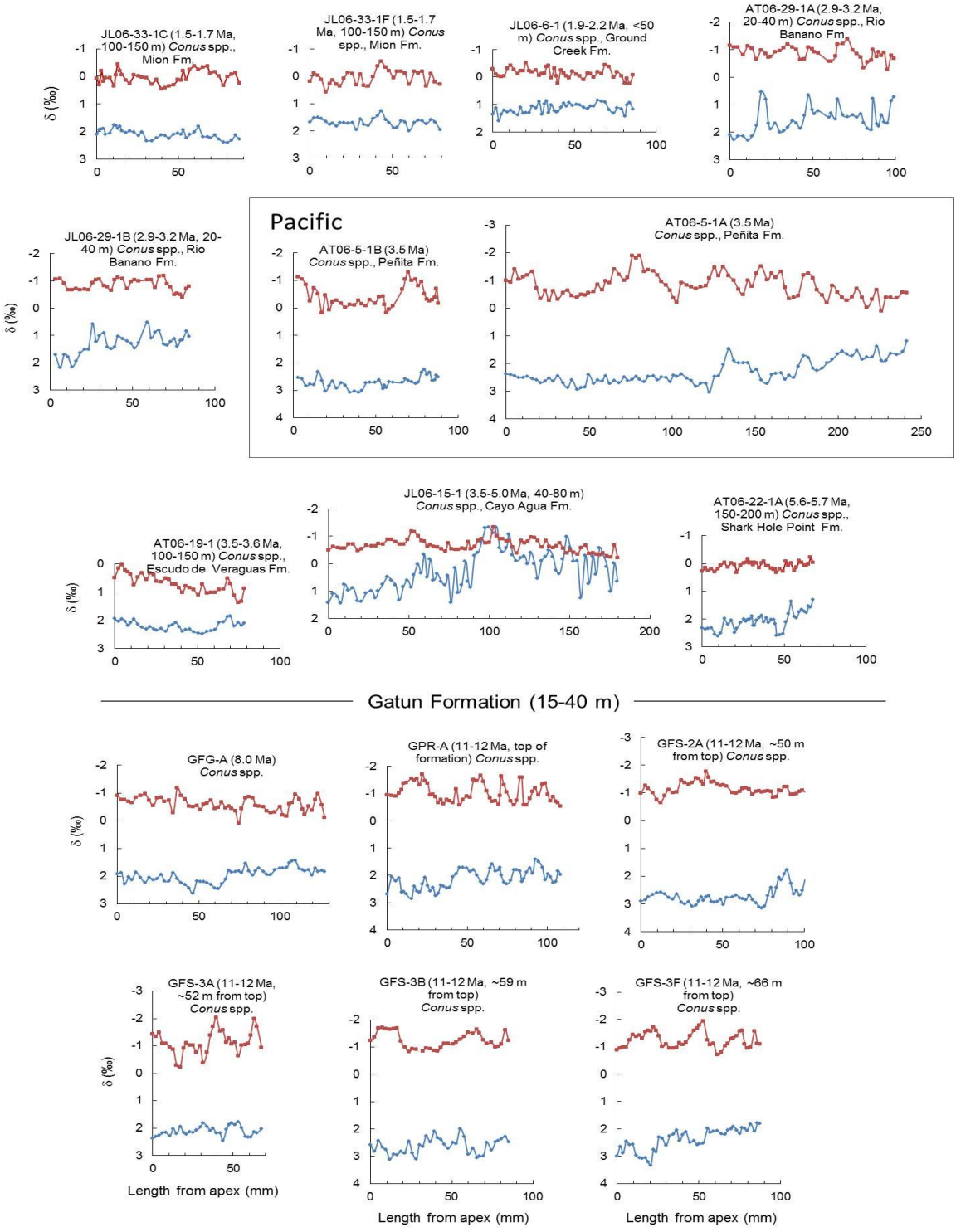

FIGURE 4-3—$\delta^{18}O$ (red) and $\delta^{13}C$ (blue) profiles for *Conus* specimens. All profiles are for the Caribbean side of Panama except the AT06-5-1 specimens from the Pacific side (enclosed in box).

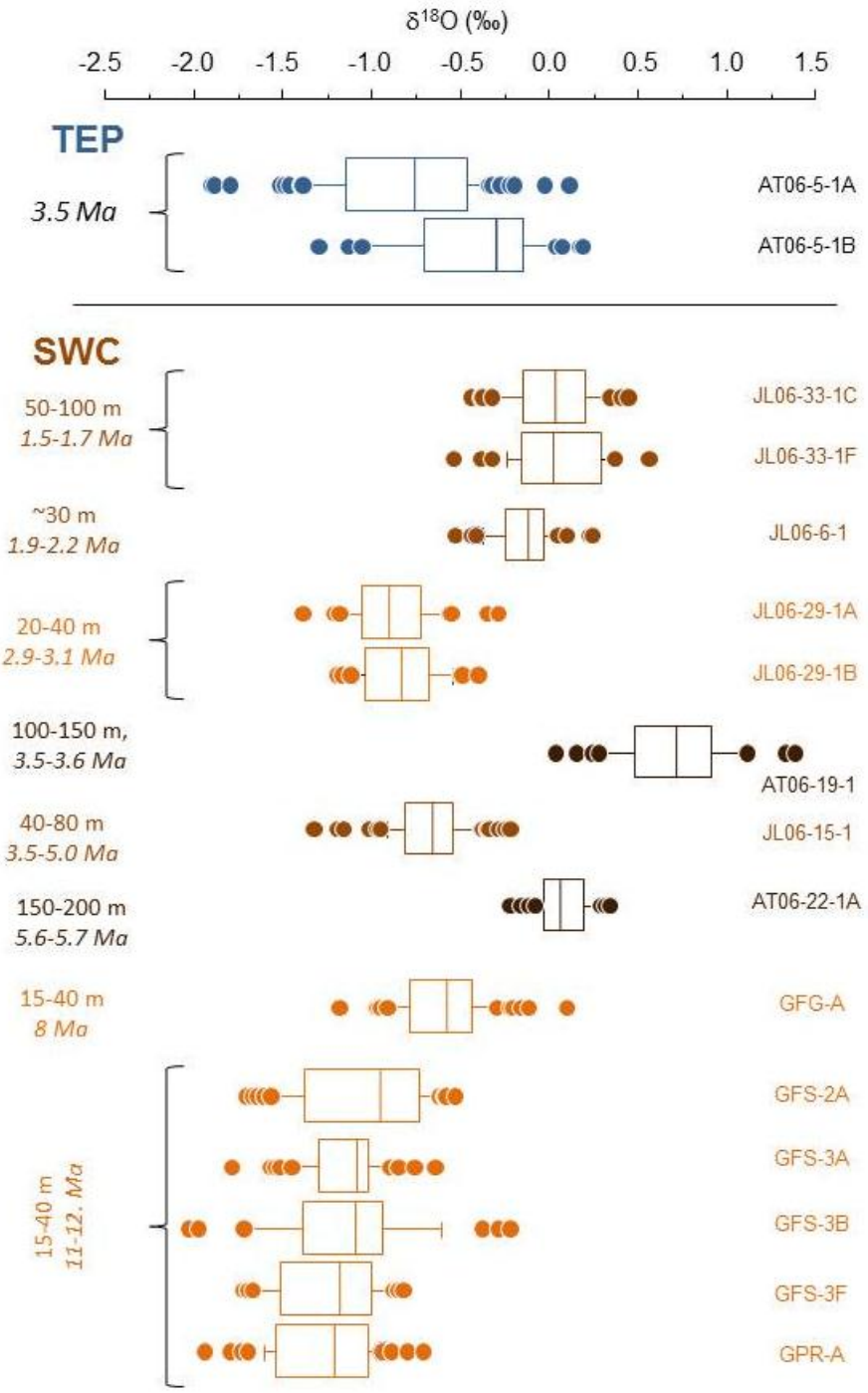

FIGURE 4-4—Box and whisker plot of sample $\delta^{18}O$ values.

rates of Caribbean *Conus* shells, is unlikely to represent a single summer-winter transition. This trend may represent migration and transport from shallower depths or environmental change.

The two middle Pliocene specimens from the Pacific area (AT06-5-1A&B) show small but significant differences in average value (-0.8 vs. -0.4‰) and range (2.0 vs. 1.5‰). Specimen B is much smaller than specimen A and based on the $\delta^{18}O$ profile has a life span of a little more than one year whereas specimen A has a life span of more than six years. The range of specimen B is relatively less than those of modern specimens from Gulf of Panama (2.3-3.2‰, Tao et al., in prep.). Thus, it is highly possible that the small specimen did not capture the same annual range as the large one and the average values were biased. This small specimen has a larger annual range than Caribbean specimens of similar age (<1.3‰), suggesting a significant difference in seasonality between Caribbean and Pacific waters at 3.5 Ma.

The two middle Pliocene specimens from the Rio Banano Formation (JL06-29-1A, B) show slightly lower average $\delta^{18}O$ values and similar annual range relative to the early Pliocene Cayo Agua specimens, which is insignificant considering the depth difference (20–40 m vs. 40–80 m). The three specimens from the Plio-Pleistocene Moin and Ground Creek Formations (JL06-33-1C, F; JL06-6-1) average 1.0‰ higher than the middle Pliocene shallow-water Caribbean specimens, which is also insignificant due to the depth contrast (50–100 m vs. ~30 m).

Carbon Isotopes

Carbon isotopic profiles are more complicated to interpret than oxygen isotopic profiles. Seasonal variations are seen in some of the specimens (e.g., JL06-33-1F, GPR-

A) but are often difficult to identify. Some of the carbon isotope profiles tend to show long-term declines rather than seasonal variations (e.g., GFS-3F). The mean $\delta^{13}C$ values of both SWC and TEP samples mostly fluctuate between 1.1 and 2.7‰, with one exception (JL06-15-1, 0.2‰).

Discussion

Constraining Seawater Isotopic Composition

The main factors controlling $\delta^{18}O$ values in gastropod shells are seawater temperature and $\delta^{18}O$, the latter being primarily dependent on global ice volume on timescales of thousands to millions of years (Shackleton and Opdyke, 1973; Zachos et al., 2001) and local salinity (e.g., freshwater flux) on seasonal timescales (e.g., Bice et al., 2000). During periods of large ice-sheet volume, global seawater $\delta^{18}O$ values are high as ice-sheets store large quantities of ^{16}O-enriched water. In the nearshore marine environment, the mixing of less saline, ^{18}O-depleted freshwater lowers local seawater $\delta^{18}O$. During times of ice-free conditions, such as the Cretaceous and Early Cenozoic, the mean seawater $\delta^{18}O$ is estimated to be -1.0‰ vs. SMOW (Shackleton and Kennett, 1975). This estimated value is unsuitable for the Neogene, as there is evidence of continental ice-sheet accumulation (Raymo et al., 2011). Lear et al. (2000) has compiled a curve of global seawater $\delta^{18}O$ composition using Mg/Ca paleotemperatures and benthic foraminiferal $\delta^{18}O$ data. However, their seawater estimate is not the best for this study because a global estimate is not be applicable to a local area such as the Panama region. In this study we estimated the paleo-seawater $\delta^{18}O$ values following the method used in Lear et al. (2000) but with some modifications: 1) we choose the nearest ODP and DSDP

sites (DSDP site 503 and ODP site 1241 for TEP and DSDP site 502 and ODP sites 999 for SWC; Keigwin, 1982; Groeneveld, 2005; Groeneveld et al., 2008); 2) we use planktonic foraminiferal $\delta^{18}O$ data and Mg/Ca SSTs instead of benthic data because all the samples come from nearshore environments; 3) for the calculation of seawater $\delta^{18}O$ we use the Hays and Grossman (1991) quadratic approximation of the O'Neil et al. (1969) calcite-water fractionation relation:

$$T\ (°C) = 15.7 - 4.36\ (\delta^{18}O_{cl} - \delta^{18}O_w) + 0.12\ (\delta^{18}O_{cl} - \delta^{18}O_w)^2 \qquad (1)$$

where $\delta^{18}O_{cl}$ and $\delta^{18}O_w$ are the oxygen isotopic compositions of calcite (vs. PDB) and water (vs. SMOW), respectively. The calculated seawater $\delta^{18}O$ values are summarized in Table 4-2, as well as seawater $\delta^{18}O$ values from Lear et al. (2000) corrected for latitudinal differences based on Zachos et al. (1994).

Neogene Paleotemperatures

Late Miocene to Plio-Pleistocene paleotemperatures were reconstructed using the oxygen isotope profiles of the *Conus* shells, the seawater $\delta^{18}O$ values derived above, and the aragonite $\delta^{18}O$-temperature equation (Grossman and Ku, 1986). To provide comparisons with proxy data for sea surface temperatures (SSTs) based on foraminiferal $\delta^{18}O$ and Mg/Ca, molluscan $\delta^{18}O$, and alkenone unsaturation, these paleotemperatures were corrected for paleo-depth using the modern temperature-depth profiles (WOD 2009; Table 4-2, see Appendix for more details). Fig. 4-5 compares the SSTs from this study (also seen in Table 4-3) with those from other studies, as well as modern samples. For the late Miocene, one shell from Caribbean Shark Hole Point Formation (AT06-22-1A, 5.7–5.6 Ma) shows a mean annual temperature (MAT) of 31.8 ± 2.2°C, which is 3°C higher than the modern Bocas del Toro MAT of 28.6 ± 0.8°C. This paleo-SST agrees with the

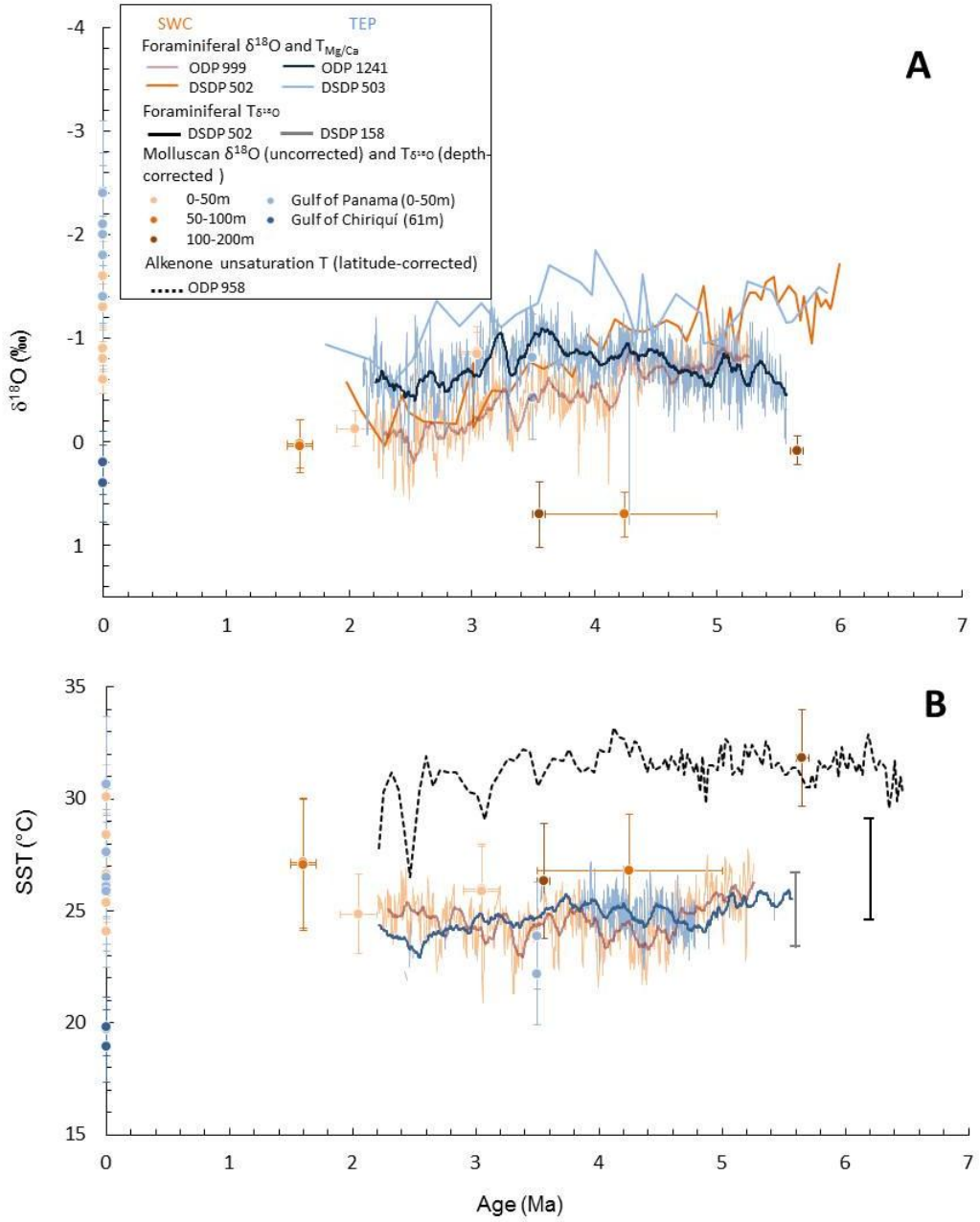

FIGURE 4-5—A) Neogene and modern $\delta^{18}O$ values for planktonic foraminifera (*Globigerinoides sacculifer*) from ODP 999 (Groeneveld, 2005), adjusted for aragonite-calcite fractionation (+0.8‰), and mollusk $\delta^{18}O$ averages; B) reconstructed molluscan $\delta^{18}O$-derived SSTs (DSDP 158 and DSDP 502A, Williams et al., 2005), and Mg/Ca-derived SSTs (ODP 999, Groeneveld, 2005).

alkenone-derived SST from the Canary Basin (Herbert and Schuffert, 1998, corrected for latitudinal difference based on Williams et al., 2005), but about 5–8°C higher than the

planktonic foraminiferal $\delta^{18}O$-derived paleo-SST of this study compared with alkenone-derived SSTs (ODP 958A, Herbert and Schuffert, 1998), planktonic foraminiferal $\delta^{18}O$-derived SSTs from ODP 502 and DSDP 158 (Williams et al., 2005) and Mg/Ca-derived SST from ODP 999 (Groeneveld, 2005). The specimen from the Early Pliocene Caribbean Cayo Agua Formation (JL06-15-1, 5.0–3.5 Ma) shows a cooler MAT of 26.8 ± 2.5°C, which is about 2°C lower than modern, but 2°C higher than the Ma/Ca SST from ODP 999. In the mid Pliocene, one shell from Caribbean Escudo de Veraguas Formation (3.6–3.5 Ma) shows an MAT of 26.3 ± 2.5°C, two shells from the Caribbean Rio Banano Formation (3.2–2.9 Ma) both show a MAT of 26.0 ± 2.0°C, which are slightly (1.5–1.8°C) lower than the modern MAT. The TEP paleo-SSTs, however, are significantly (3.7–5.4°C) lower than modern ones (22.2–23.9°C vs. 27.6℃). These SSTs are not supportive of the global warming event suggested by Cronin and Dowsett (1996). Such no-warmer-than-modern SSTs were also observed in the $\delta^{18}O$ of gastropod shells from the mid-Pliocene Pinecrest Beds in Florida (Tao and Grossman, 2010). In the Plio-Pleistocene, one shell from the Caribbean Ground Creek Formation (2.2–1.9 Ma) shows an MAT of 24.9 ± 1.8°C, while both shells from Caribbean Moin Formation (1.7–1.5 Ma) show identical MATs of 27.1 ± 2.9°C, which is inconsistent with a late Pliocene global cooling trend from previous studies(e.g., Raymo, 1994; Lear et al., 2003).

Upwelling and Freshwater Input

Two stable isotope approaches can be used to identify upwelling and freshwater input. First, seasonal upwelling and freshening can be definitively identified from oxygen isotope profiles referenced to non-upwelling, non-freshwater baseline $\delta^{18}O$ values

calculated using "normal" temperatures and salinities (See Appendix for methods). Though coastal surface waters in the tropics can have highly variable salinities, upwelled water should have relatively invariant salinities representative of normal, open ocean seawater because low-density freshwater will be restricted to the shallow mixed layer (Mignot et al., 2007). Furthermore, the upwelling season coincides with the dry season when salinities are less variable (D'Croz and O'Dea, 2007). Thus, shell $\delta^{18}O$ values that are significantly higher than the baseline value can only be explained by cooler temperatures associated with upwelling events. In contrast, shell $\delta^{18}O$ values that are significantly lower than the baseline cannot be explained by seasonal warming because, outside of upwelling events, tropical SSTs are relatively invariant. For example, temperatures at Bocas del Toro on the Caribbean coast of Panama show a consistent value of 28.6 ± 0.8°C. Thus, $\delta^{18}O$ data below the baseline values represent low salinities caused by freshwater input. Once the baseline is determined using open ocean data from planktonic foraminifera, we can quantify the magnitude of upwelling from seasonal cooling, and the degree of freshening from $\delta^{18}O$-derived salinity. The baseline values and sample $\delta^{18}O$ values normalized to baseline are summarized in Table 4-3.

Fig. 4-6 shows a box-and-whisker plot of shell $\delta^{18}O$ values normalized to baseline values determined for each locality. Based on this method, the mid Pliocene TEP samples show strong upwelling signals. Late Miocene-mid Pliocene SWC samples show moderate to strong freshening signals while the Plio-Pleistocene samples show little

TABLE 4-3—Baseline $\delta^{18}O$ values, sample $\delta^{18}O$ values normalized to baseline, and paleo-SSTs. Subscripts: cl = foraminiferal calcite, w = water, bl = baseline, max = maximum, min = minimum, dep = depth, and dep-corr = depth corrected.

Sample ID	Age/ Fm	Age (Ma)	Depth (m)	$T_{Mg/Ca}$	$\delta^{18}O_{cl}$	$\delta^{18}O_w$	$\delta^{18}O_w$ (Lear, lat-corrected)	$\delta^{18}O_{bl}$	$\delta^{18}O_{dep}$	$\delta^{18}O_{dep\text{-}corr}$	T - $\delta^{18}O$	T-$\delta^{18}O$ (Lear)	SD $T_{Mg/Ca}$	SD $\delta^{18}O_{cl}$	SD $\delta^{18}O_{bl}$	SD $\delta^{18}O_{dep}$	SD T-$\delta^{18}O$	SD $\delta^{18}O_{norm}$
Caribbean																		
JL06-33-1C	Mion	1.5-1.7	50-100	25.8	-1.2	0.99	1.03	-0.42	-0.7	-0.7	27.1	27.2	1.06	0.22	0.46	0.58	4.50	1.0
JL06-33-1F	Mion	1.5-1.7	50-100	25.8	-1.2	0.99	1.03	-0.42	-0.7	-0.7	27.0	27.2	1.06	0.22	0.46	0.58	4.61	1.0
JL06-6-1	Ground Creek	1.9-2.2	<50	25.2	-1	1.06	0.82	-0.21	0.0	-0.1	24.9	23.8	1.06	0.22	0.46	0.30	3.01	0.8
JL06-29-1A	Rio Banano	2.9-3.2	20-40	24.2	-1.1	0.78	0.43	-0.26	0.2	-0.7	26.0	24.5	0.90	0.19	0.40	0.36	3.41	0.8
JL06-29-1B	Rio Banano	2.9-3.2	20-40	24.2	-1.1	0.78	0.43	-0.26	0.2	-0.6	25.9	24.4	0.90	0.19	0.40	0.36	3.31	0.8
AT06-19-1	Escudo de Veraguas	3.5-3.6	100-150	24.8	-1.3	0.66	0.32	-0.51	-1.5	-0.8	25.9	24.4	0.48	0.17	0.28	0.42	3.97	0.7
JL06-15-1	Cayo Agua	3.5-5.0	40-80	24.5	-1.4	0.52	0.12	-0.59	-0.4	-1.1	26.7	25.0	1.06	0.22	0.46	0.50	4.06	1.0
AT06-22-1A	Shark Hole Point	5.6-5.7	150-200	27.2	-1.7	0.77	0.22	-0.96	-1.7	-1.6	29.8	27.5	1.06	0.22	0.46	0.30	2.85	0.8
GFG-A	Gatun	8	15-40						0.0	-0.6								
GPR-A	Gatun	11.0-12.0	15-40						0.0	-1.0								
GFS-2A	Gatun	11.0-12.0	15-40						0.0	-1.1								
GFS-3A	Gatun	11.0-12.0	15-40						0.0	-1.1								
GFS-3B	Gatun	11.0-12.0	15-40						0.0	-1.2								
GFS-3F	Gatun	11.0-12.0	15-40						0.0	-1.3								
Pacific																		
AT06-5-1A	Peñita	3.5	<50	24.8	-1.8	0.15	0.31	-1.03	0.0	-0.8	23.9	24.6	0.76	0.18	0.36	0.30	3.92	0.7
AT06-5-1B	Peñita	3.5	<50	24.8	-1.8	0.15	0.31	-1.03	0.0	-0.4	22.2	22.9	0.76	0.18	0.36	0.30	3.78	0.7

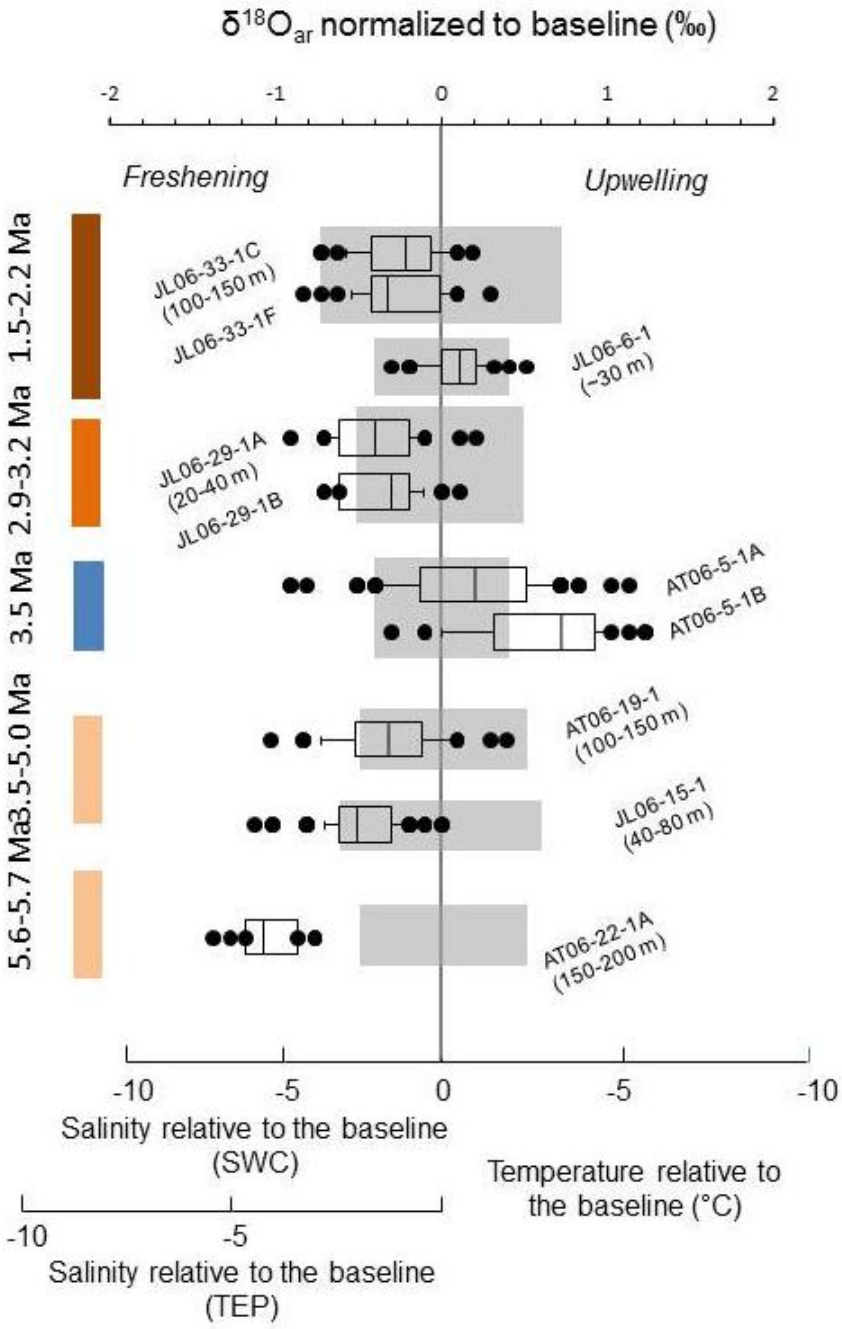

FIGURE 4-6—Box and whisker plot of shell $\delta^{18}O$ values normalized to baseline values for all Neogene specimens. Gray bars represent analytical error (±1σ) for each sample location. $\delta^{18}O$ values lower than the baseline values are calibrated to salinity change while those higher than the baseline values are calibrated to temperature change.

seasonal variations. Normally shallow samples show more freshening signals. However, the strongest freshening signals are detected in the specimen AT06-22-1A, which has an estimated paleo-depth of 150–200 m. The reconstructed SST from this specimen is much higher than the foraminiferal Mg/Ca and $\delta^{18}O$ derived SSTs. This discrepancy may be caused by the overestimate of paleo-depth (i.e. the specimen may have lived at a shallower depth and have migrated downslope before or after death), difference in the $\delta^{18}O$-depth profile between the modern and late Miocene, overestimation of the baseline $\delta^{18}O$ value (due to the lack of data in 5.7–5.6 Ma, the $T_{Mg/Ca}$ and $\delta^{18}O_{cl}$ are both estimated from a younger age of ~5.2 Ma), and/or other environmental variations.

The second approach for identifying upwelling and freshwater input is $\delta^{13}C$-$\delta^{18}O$ correlations. Upwelling of deep water (cold, ^{18}O-enriched, and ^{13}C-depleted) results in a negative correlation (Killingley and Berger, 1979; Jones and Allmon, 1995) while ^{18}O- and ^{13}C-depleted freshwater input results in a positive $\delta^{13}C$–$\delta^{18}O$ correlation in seawater and consequently in serially-sampled mollusk shells (e.g., Mook, 1971; Surge et al., 2003). Table 4-2 summarizes all the correlation coefficients of this study. Five of six late Miocene Gatun Formation shells (12–8.0 Ma) show significant upwelling signals ($p<0.05$); all three late Miocene-mid Pliocene SWC Bocas del Toro shells show significant freshening signals; one middle Pliocene TEP sample shows upwelling and the other one shows freshening; and three of five Plio-Pleistocene SWC samples show no significant correlations.

Fig. 4-7 shows the model of $\delta^{13}C$–$\delta^{18}O$ (δ–δ) correlation versus *Conus* $\delta^{18}O$ range ($\Delta^{18}O$) and modern and Neogene isotopic data from Tao et al. (in prep) and this

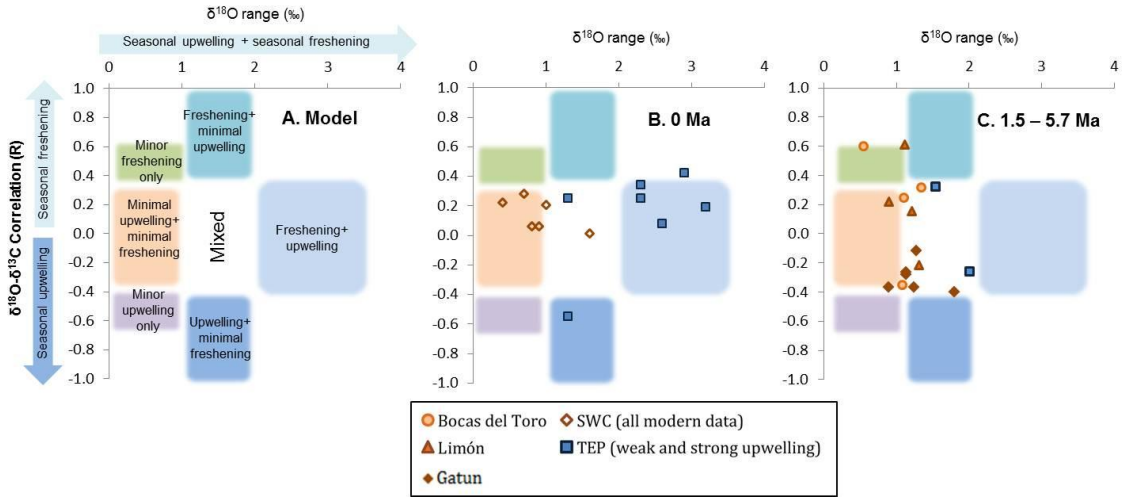

FIGURE 4-7— $\delta^{18}O$–$\delta^{13}C$ correlation vs. $\delta^{18}O$ range. A) Model of environments representing different data fields, B) data for modern *Conus* specimens (Tao et al., in prep.), and C) data for Neogene *Conus* specimens.

study. A minimal upwelling and minimal freshening environment, like that of Golfo de los Mosquitos, Panama (Tao et al., in prep.) will yield data with a $\Delta^{18}O$ of < 1‰ and no significant δ-δ correlation. In some small areas, minor freshening or upwelling may occur but without much variation in $\Delta^{18}O$ (< 1‰). Environments characterized by freshwater input and minimal upwelling, such as some modern Bocas del Toro localities, are identified by moderate $\Delta^{18}O$ (1–2‰) and a significant positive δ-δ correlation. Specimens growing in areas with upwelling and minimal freshening will show a moderate $\Delta^{18}O$ range (1–2‰) and a significant negative δ-δ correlation. Lastly, isotopic data for serially-sampled mollusks living in areas with upwelling and freshwater input, like the Gulf of Panama, will have a large $\Delta^{18}O$ range (2–3‰) and no significant δ-δ correlation.

Most modern SWC specimens fall into the area of minimal upwelling and minimal or slight freshening and most TEP specimens fall into the area of strong

upwelling and freshening (Fig. 4-7B), both agreeable with logger records. However, most Neogene specimens, including both SWC and TEP, fall into the mixed area (Fig. 4-7C). The Late Miocene Gatun Formation specimens and one of the two TEP specimens are closer to the upwelling and minimal freshening area while the SWC specimens and the other TEP specimen are closer to the freshening and minimal upwelling area.

In most cases the above two approaches agree with each other. Both identify minimal upwelling and minimal freshening signals in Plio-Pleistocene SWC specimens and strong-moderate freshening signals in late Miocene-mid Pliocene SWC specimens, especially AT06-22-1A. However, the apparent freshening signals based on positive δ-δ correlations in AT06-5-1B do not replicate in the baseline plot, which shows strong upwelling signals instead. Unfortunately, the baseline approach cannot be applied to the Gatun Formation specimens due to the lack of paleo-SSTs in 12–8 Ma.

The above stable isotopic examinations help to generate a picture of late Neogene seasonal patterns. Prior to the final closure of CAI in the late Miocene (12–8.0 Ma), there was significant seasonal upwelling in the area that is presently the SWC (Gatun Formation), similar to modern Gulf of Panama conditions. In the late Miocene-mid Pliocene (5.7–3.5 Ma), due to the gradual closure of CAI and separation of Pacific and Caribbean waters, seasonal upwelling declined in the SWC, but due to high precipitation during the rainy season, freshwater influx played an important role in the nearshore marine environment. At the time of final closure of the CAI (3.5 Ma), both upwelling and freshening occurred in the TEP area, similar to modern conditions. After the final closure of the CAI, in the late Pliocene to early Pleistocene (3.2–1.5 Ma), no significant upwelling or freshwater signals were recorded in the SWC samples.

Comparison with Other Studies

Teranes et al. (1996) provided isotopic profiles from modern and fossil venerid bivalve shells from the SWC and TEP areas. Their study suggested that: (1) late Miocene SWC environmental variability (e.g. seasonal temperature and salinity change), as indicated by $\Delta^{18}O$ values, was much higher than that of the modern environment; (2) the SWC and TEP environmental patterns started to differentiate around 3.5 Ma, as the SWC seasonality decreased and the TEP seasonality increased. These environmental changes were closely connected to the uplift and final closure of CAI. Results from this study confirm the observations of Teranes et al. (1996), but show some differences: (1) the gastropod *Conus* oxygen isotopic ranges ($\Delta^{18}O$) analyzed in this study are generally smaller than the bivalve values, which may be caused by species or habitat differences; (2) significant positive or negative carbon-oxygen correlations are found in most TEP and SWC samples prior to 3.5 Ma in this study, which can be used to identify nutrient sources.

Summary

This study uses stable isotopes in serially-sampled *Conus* shells to produce paleo-SSTs and seasonal environmental records from both sides of the CAI through the late Neogene. Stable isotopic records reveal a significant upwelling signal in late Miocene SWC and mid Pliocene TEP waters, significant to moderate freshwater signals in the SWC waters after 5.7 Ma, and little seasonal variations in the Plio-Pleistocene SWCs. The reconstructed Miocene SSTs are higher than the modern SSTs with a decreasing trend with time. The middle Pliocene SSTs are slightly lower than modern SSTs, with

little variation from late Miocene to middle Pliocene, which is inconsistent with the middle Pliocene warm event. The Plio-Pleistocene SSTs are similar to modern.

CHAPTER V

CONCLUSIONS

Stable isotope and trace element analyses of *Conus* and *Turritella* gastropod shells reveal that the dominant cause of high productivity off Florida's west coast (Pinecrest Beds) during the middle Pliocene was not upwelling or temperature increase, but nutrient input from freshwater sources including surface runoff and (or) submarine groundwater discharge. This conclusion is based on (1) the lack of an upwelling signature in $\delta^{13}C$ and $\delta^{18}O$, (2) correlations between P/Ca, Fe/Ca, and U/Ca, and (3) $\delta^{18}O$-$\delta^{13}C$ patterns similar to those of Florida Bay mollusks. Unusually high $\delta^{18}O$ values for specimens from Pinecrest Unit 4, believed to be a brackish environment based on faunal assemblage, indicate evaporative ^{18}O enrichment of brackish seawaters. This interpretation is supported by (1) the similar Sr/Ca values for shells from both units, and (2) the coincidence of the $\delta^{18}O$-$\delta^{13}C$ pattern of the shells and that of mollusks from modern Florida Bay. The reconstructed open-ocean paleo-SSTs during the middle Pliocene are no higher than modern ones, which is inconsistent with the "global" warm event. The subsequent Plio-Pleistocene paleo-SSTs are slightly but significantly (2°C) lower than the middle Pliocene ones, which is consistent with the late Neogene cooling trend after the final closure of CAI.

The modern TEP and SWC shell $\delta^{18}O$ profiles are agreeable with the expected pattern estimated from environmental temperature and salinity data, facilitating the determination of shell chronology based on seasonal variations in upwelling and freshening events. Positive and negative deviations from baseline $\delta^{18}O$ values, representing periods of non-upwelling and normal salinity, are used to identify and

quantify upwelling and freshwater input respectively in modern TEP and SWC waters. Shell profiles reveal little upwelling in SWC and Gulf of Chiriquí, but strong upwelling in the Gulf of Pacific, consistent with observations. Temperatures of upwelled waters that are at least 9°C lower than baseline values are observed, suggesting upward movement of nutrient-rich waters of more than 60 m. Isotopic profiles document rainy-season salinities as low as 24 in the Gulf of Panama. Surprisingly, none of the shells in the upwelling region show a negative covariance between $\delta^{13}C$ and $\delta^{18}O$ expected with upwelling. However, four out of five specimens show strong negative $\delta^{13}C$– $\delta^{18}O$ correlation when the upwelling dry season data are isolated, suggesting freshwater input during the non-upwelling seasons masks the upwelling signals. This finding demonstrates that for tropical environments, seasonally deviations from baseline $\delta^{18}O$ values can be used to quantify upwelling and freshening and consequently nutrient delivery and productivity.

The Neogene study uses stable isotopes in serially-sampled *Conus* shells to produce paleo-SSTs and seasonal environmental variation from both sides of the CAI. Stable isotopic records reveal a significant upwelling signal in late Miocene SWC and mid Pliocene TEP waters, significant to moderate freshwater signals in the SWC waters after 5.7 Ma, and little seasonal variations in the Plio-Pleistocene SWCs. The reconstructed Miocene SSTs are higher than the modern SSTs with a decreasing trend with time. The middle Pliocene SSTs are slightly lower than modern SSTs, with little variation from late Miocene to middle Pliocene, which is also inconsistent with the middle Pliocene warm event. The Plio-Pleistocene SSTs are similar to modern.

REFERENCES

AGUJETAS, J. and MITCHELSON-JACOB, G., 2008, The seasonal upwelling and primary production of the Gulf of Panama: ENSO implications: Eastern boundary upwelling ecosystems. Las Palmas, Spain.

ALLMON, W.D., 1988, Ecology of Recent turritelline gastropods (Prosobranchia, Turritellidae): Current knowledge and paleontological implications: Palaios, v. 3, p. 259–284.

ALLMON, W.D., 1993, Age, environment and mode of deposition of the densely fossiliferous Pinecrest Sand (Pliocene of Florida): Implications for the role of biological productivity in shell bed formation: Palaios, v. 8, p. 183–201.

ALLMON, W.D., EMSLIE, S.D., JONES, D.S., and MORGAN, G.S., 1996, Late Neogene oceanographic change along Florida's west coast: evidence and mechanisms: The Journal of Geology, v. 104, p. 143–162.

ANDREASEN, D. H., SOSDIAN, S., PERRON-CASHMAN, C., LEAR, C., DEGARIDEL-THORON, T., FIELD, P., and ROSENTHAL, Y., 2006, Fidelity of radially viewed ICP-OES and magnetic-sector ICP-MS measurement of Mg/Ca and Sr/Ca ratios in marine biogenic carbonates: Are they trustworthy together?: Geochemistry Geophysics Geosystem, v. 7, Q10P18, doi: 10.1029/2005GC001124.

ANDREASSON, F.P., and SCHMITZ, B., 1998, Tropical Atlantic seasonal dynamics in the early middle Eocene from stable oxygen and carbon isotope profiles of mollusk shells: Paleoceanography, v. 13, p. 183–192.

ANDREASSON, F.P., and SCHMITZ, B., 2000, Temperature seasonality in the early middle Eocene North Atlantic region: Evidence from stable isotope profiles of marine gastropod shells: Geological Society of America Bulletin, v. 112. p. 628–641

BEIRNE, E.C., WANAMAKER, A.D., and FEINDEL, S.C., 2012, Experimental validation of environmental controls on the $\delta^{13}C$ of *Arctica islandica* (ocean quahog) shell carbonate: Geochimica et Cosmochimica Acta, v. 84, p. 395–409.

BEMIS, B.E. and GEARY, D.H., 1996, The usefulness of bivalve stable isotope profiles as environmental indicators: Data from the Eastern Pacific Ocean and the southwestern Caribbean sea: Palaios, v. 11, p. 328–339.

BICE, K.L., SCOTESE, C.R., SEIDOV, D., and BARRON, E.J., 2000, Quantifying the role of geographic change in Cenozoic ocean heat transport using uncoupled atmosphere and ocean models: Palaeogeography Palaeoclimatology Palaeoecology, v. 161, p. 295–310.

BILLUPS, K., RAVELO, A.C., AND ZACHOS, J.C., 1998, Early Pliocene deep water circulation in the western equatorial Atlantic: Implications for high-latitude climate change: Paleoceanography, v. 13, p. 84–95.

COATES, A.G., JACKSON, J.B.C., COLLINS, L.S., CRONIN, T.M., DOWSETT, H.J., et al., 1992, Closure of the Isthmus of Panama – The near-shore marine record of Costa Rica and western Panama: Geological Society of America bulletin, v. 104, p. 814–828.

COATES, A.G., MCNEILL, D.F., AUBRY, M.P. BERGGREN, W.A., and COLLINS, L.S., 2005, An introduction to the geology of the Bocas del Toro archipelago, Panama: Caribbean Journal of Science, v. 41, p. 374–391.

COATES, A.G. and OBANDO, J.A., 1996. The geologic evolution of the Central American isthmus. Pages: 21–56 *in* J.B.C. Jackson, A.F. Budd , and A.G. Coates, eds. Evolution and environment in tropical America, ed., University of Chicago Press, Chicago.

COLLINS, L.S., 1993, Neogene paleoenvironments of the Bocas del Toro Basin, Panama: Journal of Paleontology, v. 67, p. 699–709.

COLLINS, L.S., 1999, The Miocene to Recent diversity of Caribbean benthic foraminifera from the Central American Isthmus. *in*: A paleobiotic survey of Caribbean faunas from the Neogene of the Isthmus of Panama, eds. Collins, L.S. and Coates, A.G., Allen Press, Lawrence, pp. 91–108.

COLLINS L.S., BUDD, A.F., and COATES, A.G., 1996, Earliest evolution associated with closure of the Tropical American Seaway, Proceedings of the National Academy of Sciences of the United States of America, v. 93, p. 6069–6072.

CONKRIGHT, M.E., R.A. LOCARNINI, H.E. GARCIA, T.D. O'BRIEN, T.P. BOYER, C. STEPHENS, and J.I. ANTONOV. 2002. World Ocean Atlas 2001: Objective analyses, data statistics, and figures, CD-ROM documentation, National Oceanographic Data Center, Silver Spring, MD. 17 p.

CORRIGAN, J., MANN, P. and INGLE, JR., J. C., 1990, Forearc response to subduction of the Cocos Ridge, Panamá-Costa Rica: Geological Society of America Bulletin, v. 102, p. 628–652.

CRONIN, T.M., 1991, Pliocene shallow-water paleoceanography of the north-Atlantic ocean based on marine ostracodes: Quaternary Science Reviews, v. 10, p. 175–188.

CRONIN, T.M., and DOWSETT, H.J., 1993, Prism warm climates of the Pliocene. Geotimes, v. 38, p. 17–19.

CRONIN, T. and DOWSETT, H., 1996, Biotic and oceanographic response to the Pliocene closing of the Central American Isthmus, in Jackson, J.B.C., Budd, A.F., and Coates, A.G., eds., Evolution and environment in tropical America: Chicago, The University of Chicago Press, p. 76-104.

CRONIN, T.M., KITAMURA, A., IKEYA, N., et al., 1994, Late Pliocene climate-change 3.4–2.3 Ma - paleoceanographic record from the Yabuta formation, sea of Japan. p. 437–455.

D'CROZ, L., DEL ROSARIO, J.B., and GOMEZ, J.A., 1991, Upwelling and phytoplankton in the Bay of Panama: Revista de Biologia Tropical. v. 39, p. 233–241.

D'CROZ, L., DEL ROSARIO, J.B., and GONDOLA, P., 2005, The effect of fresh water runoff on the distribution of dissolved inorganic nutrients and plankton in the Bocas del Toro Archipelago, Caribbean Panama: Caribbean Journal of Science, v. 41(3), p. 414–429.

D'CROZ, L., J.L. MATE, and J.E. OKE, 2001, Responses to elevated sea water temperature and UV radiation in the coral *Porites lobata* from upwelling and non-upwelling environments on the Pacific coast of Panama: Bulletin of Marine Sciences, v. 69, p. 203–214.

D'CROZ, L., and O'DEA, A., 2007, Variability in upwelling along the Pacific shelf of Panama and implications for the distribution of nutrients and chlorophyll. Estuarine, Coastal and Shelf Science. v. 73, p. 325–340.

D'CROZ, L., and ROBERTSON, D.R., 1997, Coastal oceanographic conditions affecting coral reefs on both sides of the Isthmus of Panama: Proceedings of 8th International Coral Reef Symposium, v. 2, p. 2053–2058.

DOWSETT, H., BARRON, J., and POORE, R., 1996, Middle Pliocene sea surface temperatures: A global reconstruction: Marine Micropaleontology, v. 27, p. 13 Upwelling and phytoplankton in the Bay of Panama 25.

DOWSETT, H.J., and LOUBERE, P., 1992, High-resolution late Pliocene sea-surface temperature record from the northeast Atlantic-ocean: Marine Micropaleontology, v. 20, p. 91–105.

FAIRBANKS, R.G., CHARLES, C.D., and WRIGHT, J.D., 1992, Origin of global melt-water pulses. *In*: R.E. Taylor et al. eds. Radiocarbon after four decades. Springer-Verlag, New York. p. 473–500.

FARRIS, D.W., C. JARAMILLO, G. BAYONA, et al., 2011, Fracturing of the Panamanian Isthmus during initial collision with South America: Geology, v. 39, p. 1007–1010.

FRITZ, P. and POPLAWSKI, S., 1974, ^{18}O and ^{13}C in shells of freshwater molluscs and their environments: Earth Planetary Science Letters, v. 24, p. 91–98.

FUGLISTER, F.C. 1960. Atlantic Ocean atlas of temperature and salinity profiles and data from the international geophysical year of 1957–1958. Woods Hole, Massachusetts, Woods Hole Oceanographic Institution.

GEARY, D.H., BRIESKE, T.A., and BEMIS, B.E., 1992, The influence and interaction of temperature, salinity and upwelling on the stable isotope profiles of strombid gastropod shells: Palaios, v. 7, p. 77–85.

GENTRY, D.K., SOSDIAN, S., GROSSMAN, E.L., ROSENTHAL, Y., HICKS, D., and LEAR, C.H., 2008, Stable isotope and Sr/Ca profiles from the marine gastropod Conus ermineus: testing a multiproxy approach for inferring paleotemperature and paleosalinity: Palaios, v. 23, p. 195–209.

GILLIKIN, D. P., LORRAIN, A., BOUILLON, S., WILLENZ, P., and DEHAIRS, F., 2006, Stable carbon isotopic composition of *Mytilus edulis* shells: relation to metabolism, salinity, $\delta^{13}C_{DIC}$ and phytoplankton. Organic Geochemistry, v. 37, p. 1371–1382.

GLYNN, P.W., 1972, Observations of the ecology of the Caribbean and Pacific coasts of Panama: Bulletins of Biology Society Washington, v. 2, p. 13–30.

GROSSMAN, E.L. and KU, T.L., 1986, Oxygen and carbon isotopic fractionation in biogenic aragonite: temperature effects: Chemical Geology, v. 59, p. 59–74.

HALLEY, R.B. and ROULIER, L.M., 1999, Reconstructing the history of eastern and central Florida Bay using mollusk-shell isotope records: Estuaries, v. 22, p. 358–368.

HAQ, B.U., HARDENBOL, J., AND VAIL, P.R., 1987, Chronology of fluctuating sea levels since the Triassic. Science, v. 235, p. 1156–1167.

HAUG, G.H., TIEDEMANN, R., ZAHN, R. AND RAVELO, A.C., 2001, Role of Panama uplift on oceanic freshwater balance: Geology, v. 29, p. 207–210.

HAYS, P.D. AND GROSSMAN, E.L., 1991, Oxygen isotopes in meteoric calcite cements as indicators of continental paleoclimate: Geology, v. 19, p. 441–444.

HENDRY, J.P., and KALIN, R.M., 1997, Are oxygen and carbon isotopes of mollusc shells reliable palaeosalinity indicators in marginal marine environments? A case study from the Middle Jurassic of England: Journal of the Geological Society, London, v. 154, p. 321–333.

HERBERT T.D. AND SCHUFFERT, J.D., 1998, Alkenone unsaturation estimates of late Miocene through late Pliocene sea-surface temperatures at site 958: Proceedings of the Ocean Drilling Program, Scientific Results, v. 159T, p. 17–21.

HOLMDEN, C., and HUDSON, J.D., 2003, $^{87}Sr/^{86}Sr$ and Sr/Ca investigation of Jurassic mollusks from Scotland: Implications for paleosalinities and the Sr/Ca ratio of seawater: Geological Society of America Bulletin, v. 115, p. 1249–1264.

HUDSON, J.D., 1963, The recognition of salinity controlled mollusk assemblages in the Great Estuarine Series (Middle Jurassic) of Inner Hebrides: Palaeontology, v. 6, p. 318–326.

HUDSON, J. D., and ANDERSON, T. F. , 1989, Ocean temperatures and isotopic compositions through time: Transactions of the Royal Society of Edinburgh: Earth Science, v. 80, p. 183–192.

JACKSON, J.B.C, and D'CROZ, L., 1997, The ocean divided. In: Central America: A natural and cultural history. ed. A.G. Coates, Yale University Press, New Haven, p. 38-71.

JACKSON, J.B.C., TODD, J.A., FORTUNATO, H., AND JUNG,P., 1999, Diversity and assemblages of Neogene Caribbean Mollusca of lower Central America: in: A paleobiotic survey of Caribbean faunas from the Neogene of the Isthmus of Panama, eds. Collins, L.S. and Coates, A.G., Allen Press, Lawrence, pp. 193–231.

JONES, D.S. and ALLMON, W.D., 1995, Records of upwelling, seasonality and growth in stable-isotope profiles of Pliocene mollusk shells from Florida: Lethaia, v. 28, p. 61–74.

JONES, D.S., MACFADDEN, B.J., WEBB, S.D., MUELLER, P.A., HODELL, D.A. and CRONIN, T.M, 1991, Integrated geochronology of a classic Pliocene fossil site in Florida: linking marine and terrestrial biochronologies: Journal of Geology, v. 99, p. 637–648.

JONES, D.S., WILLIAMS, D.F., and ARTHUR, M.A., 1983, Growth history and ecology of the Atlantic surf clam, *Spisula solidissima* (Dillwyn) as revealed by stable isotopes and annual shell increments: Journal of Experimental Marine Biology and Ecology, v. 73, p. 225–242.

KAUFMANN, K.W. and THOMPSON, R.C., 2005, Water temperature variation and the meteorological and hydrographic environment of Bocas del Toro, Panama: Caribbean Journal of Geology, v. 41, p. 392–413.

KEIGWIN, L.D., JR., 1978, Pliocene closing of the Isthmus of Panama, based on bio stratigraphic evidence from nearby Pacific Ocean and Caribbean Sea cores: Geology, v.6, p. 630–634.

KEIGWIN, L.D, JR., 1982, Stable isotope stratigraphy and paleoceanography of sites 502 and 503: in W.L. Prell, J.V. Gardner et al. eds., Initial Reports of the Deep Sea Drilling Project, 68, U.S. Government Printing Office, Washington, D.C (1982), pp. 445–453.

KLEIN, R.T., LOHMANN, K.C., and THAYER, C.W., 1996, Sr/Ca and $^{13}C/^{12}C$ ratios in skeletal calcite of *Mytilus trossulus*: Covariation with metabolic rate, salinity, and carbon isotopic composition of seawater: Geochimica et Cosmochimica Acta, v. 60, p. 4207–4221.

KILLINGLEY, J.S. AND BERGER, W.H., 1979, Stable isotopes in a mollusk shell: detection of upwelling events: Science, v. 205, p. 186–188.

KOBASHI, T., and GROSSMAN, E.L., 2003, The oxygen isotopic record of seasonality in *Conus* shells and its application to understanding Late Middle Eocene (38 Ma) climate: Paleontological Research, v. 7, no. 4, p. 343–355.

KOBASHI, T., GROSSMAN, E.L., YANCEY, T.E., and DOCKERY, D.T., 2001, Reevaluation of conflicting Eocene tropical temperature estimates: Molluskan oxygen isotope evidence for warm low latitudes: Geology, v. 29, p. 983-986.

KRANTZ, D.F., 1990, Mollusk-isotope records of Plio-Pleistocene marine paleoclimate, U.S. middle Atlantic coastal plain: Palaios, v. 5, p. 317–335.

LACHNIET, M. S. and PATTERSON, W. P., 2006, Use of correlation and stepwise regression to evaluate physical controls on the stable isotope values of Panamanian rain and surface waters: Journal of Hydrology, v. 324, p. 115–140.

LACHNIET, M. S., 2009, Sea surface temperature control on the stable isotopic composition of rainfall in Panama: Geophysical Research Letters, v. 36, L03701. doi:10.1029/2008GL036625

LATAL, C., PILLER, W.E., AND HARZHAUSER, M., 2004, Palaeoenvironmental reconstructions by stable isotopes of Middle Miocene gastropods of the Central Paratethys: Palaeogeography Palaeoclimatology Palaeoecology, v. 211, p. 157–169.

LAVIGNE, M., FIELD, M.P., ANAGNOSTOU, E., GROTTOLI, A.G., WELLINGTON, G.M., and SHERRELL, R.M., 2008, Skeletal P/Ca tracks upwelling in Gulf of Panama coral:

Evidence for a new seawater phosphate proxy: Geophysical Research Letters, v. 35. doi: L0560410.1029/2007gl031926.

LAVIGNE, M., MATTHEWS, K.A., GROTTOLI, A.G., COBB, K.M., ANAGNOSTOU, E., CABIOCH, G., and SHERRELL, R.M., 2010, Coral skeleton P/Ca proxy for seawater phosphate: Multi-colony calibration with a contemporaneous seawater phosphate record: Geochimica et Cosmochimica Acta, v. 74, p. 1282–1293.

LEAR, C.H., ELDERFIELD, H. and WILSON, P.A., 2000, Cenozoic deep-sea temperatures and global ice volumes from Mg/Ca in benthic foraminiferal calcite, Science, v. 287, p. 269–272.

LEAR, C.H., ROSENTHAL, Y., And WRIGHT, J.D., 2003, The closing of a seaway: ocean water masses and global climate change: Earth and Planetary Science Letters, v. 210, p. 425–436.

LIANG, J., MCWILLIAMS, J.C., and GRUBER, N., 2009, High- frequency response of the ocean to mountain gap winds in the northeastern tropical Pacific: Journal of Geophysical Research, v. 114, C12005, doi:10.1029/2009JC005370.

LISIECKI, L.E. and RAYMO, M.E., 2005, A Pliocene-Pleistocene stack of 57 globally distributed benthic ^{18}O records: Paleoceanography, v. 20(1), PA1003, doi:10.1029/2004PA001071.

LLOYD, R.M., 1964, Variations in the oxygen and carbon isotope ratios of Florida Bay mollusks and their environmental significance: The Journal of Geology, v. 72, p. 84–111.

LORRAIN, A., PAULET, Y.M., CHAUVAUD, L., DUNBAR, R., MUCCIARONE, D., and FONTUGNE, M., 2004, ^{13}C variation in scallop shells: Increasing metabolic carbon contribution with body size?: Geochimica et Cosmochimica Acta, v. 68, p. 3509–-3519.

LOWENSTAM, H.A. and EPSTEIN, S., 1954, Paleotemperatures of the post-Aptian Cretaceous as determined by the oxygen isotope method: The Journal of Geology, v. 62, p. 207–248.

LYONS, W.G., 1990, A Caloosahatchee-Age Fauna at APAC Mine, Sarasota County, Florida, In: Allmon, W.D. and Scott, T.M (eds.), Plio-Pleistocene Stratigraphy and Paleontology of South Florida: Southeastern Geological Society Annual 1990 Fieldtrip Guidebook.

MAIER-REIMER, E., MIKOLAJEWICZ, U., and CROWLEY, T., 1990, Ocean GCM sensitivity experiment with an open Central American Isthmus: Paleoceanography, v. 5, p. 349-366.

MATTHEWS, K.A., GROTTOLI, A.G. , MCDONOUGH, W.F. , and PALARDY, J.E., 2008, Upwelling, species, and depth effects on coral skeletal cadmium-to-calcium ratios (Cd/Ca): Geochimica et Cosmochimia Acta, v. 72, p. 4537–4550.

MIGNOT, J., MONTEGUT, C.D.B., LAZAR, A., AND CRAVATTE, S., 2007, Control of sanlinity on the mixed layer depth in the world ocean: 2. Tropical areas: Journal of Geophysical Research, v. 112, C10010, doi: 10.1029/2006JC003954.

MONTAGNA, P., MCCULLOCH, M., TAVIANI, M., MAZZOLI, C., and VENDRELL, B., 2006, Phosphorus in cold-water corals as a proxy for seawater nutrient chemistry: Science, v. 312, p. 1788-1791, doi: 10.1126/science.1125781.

MOOK, W.G., 1971, Paleotemperatures and chlorinities from stable carbon and oxygen isotopes in shell carbonate: Palaeogeography, Palaeoclimatology, Palaeoecology, v. 9, p. 245–263.

MOORE, W.S., 2010, The effect of submarine groundwater discharge on the ocean: Annual Review of Marine Science, v. 2, p. 59–88.

O'DEA, A., and JACKSON, J.B.C., 2002, Bryozoan growth mirrors contrasting seasonal regimes across the Isthmus of Panama: Palaeogeography Palaeoclimatology. Palaeoecology, v. 185, p. 77–94.

O'DEA, A., RODRIGUEZ, F., And ROMERO, T., 2007, Response of zooid size in *Cupuladria exfragminis* (Bryozoa) to simulated upwelling temperatures: Marine Ecology, v. 28, p. 315–323.

O'Neil, J.R., Clayton, R.N. And Mayeda, T. K. 1969, Oxygen isotope fractionation in divalent metal carbonates: Journal of Chemical Physics, v. 51, p. 5547–5558.

OSMOND, J.K., COWART, J.B., HUMPHREYS, C.L., and WAGNER, B.E., 1985, Radioelement migration in natural and mined phosphate terrains: Florida Institute of Phosphate Research, Bartow, 131 p.

PAYTAN, A., SHELLENBARGER, G.G., STREET, J.H., GONNEEA, M.E., DAVIS, K., YOUNG, M.B., and MOORE, W.S., 2006, Submarine groundwater discharge: An important source of new inorganic nitrogen to coral reef ecosystems: Limnology and Oceanography, v. 51, p. 343–348.

PEARSON, P.N., DITCHFIELD, P.W., SINGANO, J. et al., 2001, Warm tropical sea surface temperatures in the Late Cretaceous and Eocene epochs: Nature, v.413, p. 481–487.

PERRON, F.E., 1983, Growth, fecundity, and mortality of *Conus pennaceus* in Hawaii :Ecology, v. 64, p. 53–62.

PETUCH, E.J., 1982, Notes on the molluscan paleoecology of the Pinecrest Beds at Sarasota, Florida with the description of *Pyruella*, a stratigraphically important new genus (*Gastropoda: Melongenidae*): Proceedings of the Academy of Natural Sciences of Philadelphia, v. 134, p. 12–30.

RAILSBACK, L.B., ANDERSON, T.F., ACKERLY, S.C., and CISNE, J.L., 1989, Paleoceanographic modeling of temperature-salinity profiles from stable isotopic data: Paleoceanography, v. 4, p. 585–591.

RAYMO, M.E., 1994, The initiation of northern hemisphere glaciation: Annual Reviews of Earth and Planetary Sciences, v. 22, p. 353–383.

RAYMO, M. E., MITROVICA, J. X., O'LEARY, M. J. et al., 2011, Departures from eustasy in Pliocene sea-level records: Nature Geoscience, v. 4, p. 328–332.

REUER, M.K., BOYLE, E.A. , and COLE, J.E., 2003, A mid-twentieth century reduction in tropical upwelling inferred from coralline trace element proxies: Earth and Planetary Science Letters, v. 210, p. 437–452.

SCHMIDT, D. 2007. The closure history of the Central American Seaway: evidence from isotopes and fossils to models and molecules. *In:* Williams, M., A.M. Haywood, F.J. Gregory and D.N. Schmidt. Deep-time perspectives on climate change: marrying the signal from computer models and biological proxies. Micropaleontological Society Special Publ., The Geological Society Publishing House, Bath. p. 427–442.

SCHMIDT, G.A., BIGG, G.R. AND ORHLING, E.J., 1999, "Global Seawater Oxygen-18 Database – v1.21" http://data.giss.nasa.gov/o18data/

SHACKLETON, N.J. and KENNETT, J.P. 1975. Paleotemperature history of the Cenozoic and the initiation of Antarctic glaciation: oxygen and carbon isotope analyses in DSDP Sites 277, 279, and 281. p. 743–755. In: Kennett, J.P., Houtz, R.E, et al. (eds), Initial Reports. DSDP, 29. U.S. Government Printing Office, Washington.

SHACKLETON, N.J, and OPDYKE, N.D., 1973, Oxygen isotope and paleomagnetic stratigraphy of equatorial Pacific Core V28-238: oxygen isotope temperatures and ice volume on a 105 year and 106 year scale: Quaternary Research, v. 3, p. 39–55, doi:10.1016/0033-5894(73)90052-5

SLIKO, J. and HERBERT, G., 2009, Nutrient decline, rainfall patterns, and the end-Pliocene regional mass extinction in Florida: Geological Society of America Abstracts with Programs, v. 41, p. 160.

SLOMP, C.P., and VAN CAPPELLEN, P., 2004, Nutrient inputs to the coastal ocean through submarine groundwater discharge: controls and potential impact: Journal of Hydrology, v. 295, p. 64–86.

SOSDIAN, S., 2008, Climate transitions across the Cenozoic: Insight from elemental ratios in benthic foraminifera and marine gastropods: Ph.D., Rutgers University, New Brunswick, 232 p.

SOSDIAN, S., GENTRY, D.K., LEAR C.H., GROSSMAN, E.L., HICKS, D., and ROSENTHAL, Y., 2006, Strontium to calcium ratios in the marine gastropod *Conus ermineus*: Growth rate effects and temperature calibration: Geochemistry Geophysics Geosystems, v.7, Q11023, doi:10.1029/2005GC001233.

SOSDIAN, S., LEAR, C., TAO, K., GROSSMAN, E.L., and ROSENTHAL, Y., Cenozoic Seawater Sr/Ca ratios: Implications for coral reef development through ocean de-acidification: Geology (submitted).

STANLEY, S.M., 1986, Anatomy of a regional mass extinction: Plio-Pleistocene decimation of the western Atlantic bivalve fauna: Palaios, v. 1, p. 7–36.

STEPH, S., TIEDEMANN, R., PRANGE, M., GROENEVELD, J., SCHULZ, M., TIMMERMANN, A., NÜRNBERG, D., RÜHLEMANN, C., SAUKEL, C., AND HAUG, G.H., 2010, Early Pliocene increase in thermohaline overturning: A precondition for the development of the modern equatorial Pacific cold tongue: Paleoceanography, v. 25, PA2202, doi:10.1029/2008PA001645.

SURGE, D.M., LOHMANN, K.C. and GOODFRIEND, G.A., 2003. Reconstructing estuarine conditions: oyster shells as recorders of environmental change, Southwest Florida: Estuarine, Coastal and Shelf Science, v. 57, p. 737–756.

SURGE, D. and WALKER, K.J., 2006. Geochemical variations in microstructural shell layers of the southern quahog (*Mercenaria campechiensis*): implications for reconstructing seasonality: Palaeogeography Palaeoclimatology Palaeoecology, v. 237, p. 182–190.

SWART, P.K., and PRICE, R., 2002, Origin of salinity variations in Florida Bay: Limnology and Oceanography, v. 47, p. 1234–1241.

SWARZENSKI, P.W., and BASKARAN, M., 2007, Uranium distribution in the coastal waters and pore waters of Tampa Bay, Florida: Marine Chemistry, v. 104, p. 43–57.

TAO, K. and GROSSMAN, E.L., 2010, Origin of high productivity in the Pliocene of the Florida platform: evidence from stable isotopes and trace elements: Palaios, v. 25, p. 796–806.

TAO, K., ROBBINS, J.A., GROSSMAN, E.L. AND O'DEA, A., Quantifying upwelling and freshening in nearshore tropical environments using stable isotopes in modern mollusks from the Central American Isthmus. To be submitted to Bulletin of Marine Science.

TERANES, J. L., GEARY, D. H. , and BEMIS, B. E., 1996, The oxygen isotopic record of seasonality in Neogene bivalves from the Central American Isthmus, p. 105-129. In J. B. C. Jackson, A. F. Budd, and A. G. Coates (eds.), Evolution and Environment in Tropical America. The University of Chicago Press, Chicago

TRIPATI, A.K., ALLMON, W.D. and SAMPSON, D.E., 2009. Possible evidence for a large decrease in seawater strontium/calcium ratios and strontium concentrations during the Cenozoic: Earth and Planetary Science Letters, v. 282(1-4), p. 122–130.

TRIPATI, A., and ZACHOS, J., 2000, Environmental controls on Sr/Ca and Mg/Ca ratios in aragonitic shells of turritellid gastropods: Geological Society of America Abstracts with Programs, v. 32, p. A298.

WEINLEIN, W., KASPRAK, A., SLIKO, J., HARRIES, P.J., HERBERT, G.S., OCHES, E.A., PORTELL, R.W., and COE, M.C., 2008, The role of trace-metal proxies as upwelling indicators on the Florida Platform during the Plio-Pleistocene: Geological Society of America Abstracts with Programs, v. 40, p. 72.

WILLIAMS, M., HAYWOOD, A.M., HARPER, E.M., JOHNSON, A.L.A., KNOWLES, T., LENG, M.J., LUNT, D.J., OKAMURA, B., TAYLOR, P.D., and ZALASIEWICZ, J., 2009, Pliocene

climate and seasonality in North Atlantic shelf seas: Philosophical Transactions of the Royal Society a-Mathematical Physical and Engineering Sciences, v. 367, p. 85-108, doi: 10.1098/rsta.2008.0224.

WILLIAMS, M., HAYWOOD, A.M., TAYLOR, S.P. et al., 2005, Evaluating the efficacy of planktonic foraminifer calcite ^{18}O data for sea surface temperature reconstruction for the Late Miocene: Geobios, v. 38, p. 843–863.

WINDOM, H.L., MOORE, W.S., NIENCHESKI, L.F.H., and JAHRIKE, R.A., 2006, Submarine groundwater discharge: A large, previously unrecognized source of dissolved iron to the South Atlantic Ocean: Marine Chemistry, v. 102, p. 252–266.

ZACHOS, J., PAGANI, M., SLOAN, L., THOMAS, E. and BILLUPS, K., 2001. Trends, rhythms, and aberrations in global climate 65 Ma to present: Science, v. 292(5517), p. 686-693.

ZACHOS, J.C., STOTT, L.D., AND LOHMANN, K.C., 1994, Evolution of early Cenozoic marine temperatures. Paleoceanography, v. 9, p. 353–387.

APPENDIX 1

STABLE ISOTOPE AND TRACE ELEMENT MEASUREMENTS OF FLORIDA PINECREST BEDS AND COLOOSAHATCHEE FORMATION SAMPLES

Length from apex (mm)	$\delta^{13}C$ (‰)	$\delta^{18}O$ (‰)	Sr/Ca (mmol/mol)	P/Ca (umol/mol)	Fe/Ca (umol/mol)	U/Ca (umol/mol)
4	2.67	1.62				
9	2.14	1.17				
14	2.21	1.20				
19	2.51	1.16				
24	2.58	1.07				
29	2.63	0.91				
34	2.96	0.71				
39	2.71	0.62				
44	3.22	0.26				
49	2.79	0.09				
54	2.06	0.06				
59	2.68	-0.04				
64	2.78	-0.13				
69	2.58	-0.30				
74	2.24	0.02				
79	2.02	0.01				
84	2.23	-0.06				
89	2.56	-0.13				
94	2.58	0.04				
99	2.81	-0.07				
104	2.58	-0.39				
109	3.07	-0.45				
114	2.63	-0.60				
119	2.53	-0.60				
124	2.48	-0.36				
129	2.79	-0.16				
134	2.98	-0.32				
139	3.12	-0.18				
144	3.00	-0.04				
149	2.92	-0.06				
154	2.24	0.09				
159	2.40	0.28				
164	2.86	0.27				
169	2.76	0.31				
174	2.57	0.26				
179	2.41	0.51				
184	1.91	0.41				
189	2.12	0.29				
194	2.49	0.45				
199	2.75	0.64				
204	2.80	0.73				
209	2.40	0.32				
214	2.70	0.69				
219	2.76	0.90				
224	2.71	1.13				
229	2.66	1.22				

Length from apex (mm)	$\delta^{13}C$ (‰)	$\delta^{18}O$ (‰)	Sr/Ca (mmol/mol)	P/Ca (umol/mol)	Fe/Ca (umol/mol)	U/Ca (umol/mol)
239	2.76	1.40				
244	2.83	1.49				
249	2.87	1.71				
254	2.91	1.81	2.0	157	41	
259	2.73	1.81	2.3	207	42	
264	2.84	1.40	2.3	195	57	
269	2.78	1.14	2.5	154	33	
274	2.88	0.80	2.6	161	35	
279	2.94	0.61	2.6	161	35	
284	2.76	0.48	2.6	141	20	
289	2.54	0.40	2.6	235	72	
295	2.62	0.47	2.6	364	108	
299	2.77	0.31	2.6	137	16	
304	2.84	0.37	2.8	208	75	
309	2.47	0.20	2.6	101	7	
314	2.77	0.06	2.8	129	34	
319	3.10	-0.08	2.6	135	10	
324	2.59	-0.07	2.8	125	23	
329	2.65	-0.22	2.7	132	826	
334	2.52	-0.22	2.8	165	27	
339	2.56	-0.33	2.9	401	108	
344	2.80	-0.41	3.1	1228	196	
349	2.75	-0.34	3.1	1712	222	
354	3.01	-0.54	3.1	2342	115	
359	2.30	-0.38	3.4	1845	229	
364	2.68	-0.59	3.2	212	82	
369	2.67	-0.49	3.0	140	30	
373	2.72	-0.22	3.0	208	59	
379	2.61	-0.33	3.0	161	56	
384	2.85	-0.10	2.9	135	35	
389	2.66	-0.07	2.9	225	45	
394	2.80	0.20	2.8	156	54	
399	2.75	0.63	2.4	1274	130	
404	2.44	1.26	2.3	299	130	
409	2.53	1.01	3.2	232	129	
414	2.45	0.20	3.0	295	91	
419	2.35	-0.32	3.0	159	46	
424	2.74	-0.12	3.3	144	23	
429	2.55	-0.14	3.0	137	24	
434	2.53	0.86	3.0	268	199	
439	2.52	0.76	3.1	180	55	
444	2.51	0.23	2.9	351	124	
449	2.55	0.08	2.3	202	42	
454	2.13	-0.33	3.2	7819	151	
459	2.13	-0.21	3.2	576	155	
464	2.41	-0.51	3.2	390	98	
469	2.48	-0.68	3.2	217	83	
474	2.66	-0.43	3.3	1839	142	
479	2.41	-0.25	2.8	214	45	
484	2.35	0.20	2.9	181	110	
489	2.31	-0.61	3.5	282	74	
494	2.17	-0.34	3.2	165	47	
499	2.35	0.43	3.3	291	229	
1	1.04	-0.42				

Length from apex (mm)	$\delta^{13}C$ (‰)	$\delta^{18}O$ (‰)	Sr/Ca (mmol/mol)	P/Ca (umol/mol)	Fe/Ca (umol/mol)	U/Ca (umol/mol)
11	1.23	-0.13				
16	1.35	-0.09				
21	1.87	0.85				
26	1.80	0.88				
31	1.75	0.76				
36	1.37	0.63				
41	1.41	0.68				
46	0.98	0.99				
51	1.32	0.57				
54	1.21	0.72				
56	1.40	0.67				
61	0.91	0.79				
66	0.97	0.55				
71	1.27	0.47				
76	1.17	0.09				
81	0.63	-0.05				
86	0.95	0.03				
91	1.00	-0.05	2.3	236	34	
96	1.15	-0.52	2.1	152	51	
101	1.14	-0.38	2.0	222	60	
106	1.53	-0.25	2.2	1372	89	
111	1.52	-0.38	2.2	202	57	
116	1.49	-0.48	2.0	242	45	
121	1.77	0.74	1.8	204	47	
126	1.91	0.96	1.8	229	51	
131	2.56	1.66	1.9	103	4	
136	2.48	1.86	1.9	7112	196	
141	1.99	1.29	1.9	218	37	
146	2.19	1.71	2.1	176	49	
151	1.80	0.90	2.1	183	43	
156	1.90	0.78	1.8	283	62	
161	2.14	0.58	1.9	183	29	
166	2.30	0.81	2.0	140	35	
176	2.17	0.50	2.1	134	33	
181	2.14	0.47	2.0	702	150	
186	2.17	0.17	2.1	193	48	
191	2.08	0.08	2.3	156	44	
196	1.92	-0.17	2.4	148	34	
201	1.83	-0.29	2.5	499	53	
206	2.10	-0.05	2.5	141	85	
211	1.84	-0.33	2.5	148	50	
216	1.87	-0.09	2.3	245	52	
221	1.94	0.01	2.3	136	31	
226	1.76	-0.34	2.1	134	42	
231	2.45	1.37	2.1	209	118	
236	2.36	0.85	2.1	151	37	
241	2.30	0.81	2.2	144	46	
246	2.09	0.81	2.3	146	47	
251	2.15	0.77	2.4	135	44	
256	1.85	0.56	2.4	148	44	
261	1.78	0.20	2.2	147	50	
266	1.99	-0.08	2.4	262	33	
271	1.98	0.03	2.3	148	37	
276	2.05	0.18	2.2	142	38	

Length from apex (mm)	$\delta^{13}C$ (‰)	$\delta^{18}O$ (‰)	Sr/Ca (mmol/mol)	P/Ca (umol/mol)	Fe/Ca (umol/mol)	U/Ca (umol/mol)
286	2.46	1.24	2.0	158	42	
291	2.56	1.20	2.2	209	55	
296	2.18	0.76	2.3	406	55	
0	1.56	0.27	2.1	539	48	
5	2.07	0.43	2.1	214	35	
10	1.87	0.35	2.1	179	34	
15	1.84	0.25	2.0	155	34	
20	1.91	0.73	2.0	129	10	
25	2.23	1.46	2.0	178	42	
30	2.09	1.34	2.0	197	51	
35	2.01	1.62	2.0	199	49	
40	1.90	1.19	2.0	184	44	
45	1.91	1.07	2.1	194	30	
50	2.11	1.18	2.1	185	49	
55	2.07	1.09	2.1	190	52	
60	1.87	0.73	2.0	325	178	
65	1.82	0.60	2.1	46802	536	
70	1.42	0.60	1.9	48511	433	
75	1.57	0.83	2.0	164	85	
80	1.52	0.65	2.0	177	44	
85	1.81	0.64	2.2	49565	370	
90	2.10	0.44	2.2	1379	242	
95	1.75	0.51	2.0	318	83	
100	1.27	0.25	2.4	6795	148	
105	1.76	0.79	2.1	160	34	
110	1.72	0.62	2.1	265	94	
115	1.70	0.62	2.2	151	10	
120	1.35	0.81	2.3	203	35	
125	0.92	0.80	2.3	323	494	
130	1.13	0.67	2.1	143	116	
135	1.12	0.63	2.2	170	30	
140	0.98	0.57	2.2	153	30	
145	0.92	0.61	2.2	159	18	
150	1.20	0.11	2.3	3765	282	
155	1.25	-0.55	2.3	183	43	
160	1.32	-0.75	2.4	148	35	
165	1.12	-0.66	2.3	149	32	
170	1.04	-0.42	2.2	143	32	
175	1.08	-0.29	2.3	336	31	
180	1.18	-0.07	2.2	237	29	
185	1.13	0.08	2.2	163	29	
190	1.33	0.51	2.1	165	33	
195	1.46	1.20	1.9	154	30	
200	1.59	1.36	1.9	139	10	
205	1.69	1.54	2.0	140	25	
210	1.63	1.54	2.2	128	10	
215	1.37	0.80	2.3	134	29	
220	1.22	0.68	2.3	127	10	
225	1.12	0.67	2.3	134	19	
230	0.98	0.43	2.3	143	63	
235	0.97	-0.08	2.4	134	9	
240	0.98	-0.40	2.4	138	30	
245	1.00	-0.48	2.4	140	28	
250	1.02	-0.47	2.3	146	29	

Length from apex (mm)	$\delta^{13}C$ (‰)	$\delta^{18}O$ (‰)	Sr/Ca (mmol/mol)	P/Ca (umol/mol)	Fe/Ca (umol/mol)	U/Ca (umol/mol)
260	0.85	-0.93	2.6	147	33	
265	1.35	-0.18	2.4	143	35	
270	1.81	0.88	2.1	175	37	
275	1.47	0.44	2.3	145	27	
0	-0.31	2.62				
3	-0.05	2.82				
6	0.46	2.77				
9	0.22	3.02				
12	-0.43	2.23				
15	-0.04	2.70				
18	-0.10	2.38				
21	-0.59	1.88				
24	-0.41	2.63				
27	-0.30	2.38				
30	-0.01	2.14				
33	-0.21	2.12				
36	-0.42	2.26				
39	-0.52	2.15				
42	-0.38	2.54				
45	-0.89	2.48				
48	-0.67	2.87				
51	-0.69	2.96				
54	-0.66	2.75				
57	-0.50	2.70				
60	-0.65	2.12				
63	-0.98	2.09				
66	-1.01	1.86				
69	-0.59	2.17				
72	-0.98	1.86				
75	-1.36	1.76				
78	-1.69	1.50				
81	-1.27	1.56				
84	-1.47	1.38				
87	-1.41	1.67				
90	-1.81	1.57				
93	-1.28	0.99				
96	-1.82	0.51				
99	-2.06	0.27				
102	-1.75	1.05				
105	-2.29	0.66				
108	-2.26	0.71				
111	-1.96	0.94				
114	-1.74	1.06				
117	-1.39	1.34				
120	-1.52	1.18				
123	-1.48	1.19				
126	-1.39	1.33				
129	-1.15	2.37				
0	0.14	2.03				
2	-0.04	2.03				
4	-0.18	1.69				
6	-0.32	2.05				
8	-0.25	2.20				
10	-0.08	2.25				

Length from apex (mm)	$\delta^{13}C$ (‰)	$\delta^{18}O$ (‰)	Sr/Ca (mmol/mol)	P/Ca (umol/mol)	Fe/Ca (umol/mol)	U/Ca (umol/mol)
14	-0.45	2.52				
16	-0.42	2.64				
18	-0.60	2.53				
20	-0.05	2.78	1.8	223	9	
22	-0.03	2.65				
24	-0.26	2.51	1.8	196	6	
26	-0.44	2.28				
28	-0.74	2.70	1.7	197	5	
30	-0.76	2.56				
32	-0.47	2.37	1.8	247	2	
34	-0.47	1.86				
36	-0.45	2.24	1.8	190	7	
38	-0.38	2.19				
40	-0.23	1.94	1.7	190	7	
42	-0.05	2.03				
44	0.35	2.29	1.7	193	2247	
46	0.28	2.53				
48	0.59	2.23	1.7	196	7	
50	0.49	2.09				
52	0.48	2.39	1.7	163	3	
54	0.29	2.23				
56	0.30	2.33	1.9	213	9	
58	0.25	2.25				
60	0.01	1.88	2.1	190	6	
62	-0.15	1.93				
64	-0.38	1.80	2.1	200	13	
66	-0.54	1.75				
68	-0.81	1.98	2.0	190	18	
70	-0.88	1.90				
72	-0.98	2.08	2.0	195	9	
74	-0.71	1.84				
76	-0.42	2.14	2.0	215	9	
78	-0.47	1.92				
80	-0.46	2.10	2.1	255	8	
82	-0.25	1.89				
84	-0.16	1.58	2.4	207	9	
86	-0.58	1.24				
88	-0.65	1.22	2.4	204	7	
90	-1.55	1.14				
92	-1.42	1.34	2.1	159	2	
94	-1.00	1.56				
96	-0.93	1.84	2.3	184	33493	
98	-1.39	1.61				
100	-1.39	1.51	2.3	220	543	
102	-1.18	1.64				
104	-1.38	1.44	2.4	204	12	
106	-1.32	1.19				
108	-1.50	1.19	2.3	197	30	
110	-1.41	1.40				
112	-1.60	1.11	2.7	219	22	
114	-1.82	0.98				
116	-0.78	2.96	2.3	223	19	
118	-0.87	2.79				
120	-1.15	2.70	2.1	237	8	

Length from apex (mm)	$\delta^{13}C$ (‰)	$\delta^{18}O$ (‰)	Sr/Ca (mmol/ mol)	P/Ca (umol/ mol)	Fe/Ca (umol/ mol)	U/Ca (umol/ mol)
124	-1.48	1.99	2.1	230	8	
126	-1.25	2.30				
128	-1.20	2.30	2.0	211	9	
130	-1.44	2.51				
132	-1.45	2.17	1.9	212	15	
134	-1.10	2.31				
136	-1.00	2.31	2.0	199	6	
138	-1.02	2.03				
140	-1.15	2.16	2.1	190	8	
142	-1.13	2.05				
144	-1.01	2.34	2.3	205	8	
146	-1.11	2.18				
148	-1.30	1.83	2.1	218	22	
150	-1.40	0.99				
152	-1.89	0.84	2.8	203	5	
156	-1.46	0.89				
158	-1.52	0.79	2.7	195	8	
160	-1.37	1.10				
162	-1.44	0.93	3.0	193	5	
0	-1.20	2.07				
3	-0.97	1.89				
6	-1.89	1.61				
9	-1.30	1.37				
12	-1.12	0.91				
15	-1.40	1.10				
18	-1.22	0.87				
21	-1.56	0.73				
24	-1.35	1.07				
27	-1.10	1.12				
30	-1.16	1.34				
33	-1.61	1.51				
36	-1.25	2.02				
39	-0.06	2.89				
42	0.40	2.81	2.0	217	15	
45	-0.98	2.37	1.8	18634	28	
48	-1.17	2.27	1.7	224	10	
51	-0.90	2.36	1.6	222	6	
54	-1.08	2.38	1.6	207	7	
57	-1.47	2.21	1.7	204	6	
60	-1.28	1.95	1.6	192	6	
63	-0.96	2.16	1.6	190	7	
66	-1.06	2.09	1.5	303	6	
69	-0.92	1.83	1.5	206	5	
72	-0.89	1.50	1.6	198	5	
75	-1.28	1.49	1.8	201	4	
78	-0.83	0.91	1.8	190	6	
81	-0.59	0.65	2.0	198	5	
84	-0.70	0.67	2.0	183	11	
87	-0.71	0.43	2.2	186	11	
90	-0.89	0.09	2.4	186	5	
93	-0.58	0.52	2.6	176	4	
96	-0.42	0.94	2.6	165	6	
99	-1.30	1.23	2.3	209	6	
102	-0.98	1.55	2.3	191	6	

Length from apex (mm)	$\delta^{13}C$ (‰)	$\delta^{18}O$ (‰)	Sr/Ca (mmol/mol)	P/Ca (umol/mol)	Fe/Ca (umol/mol)	U/Ca (umol/mol)
108	-1.32	2.84	1.8	1518	6	
111	-0.95	2.91	1.7	209	8	
114	-0.95	2.62	1.6	197	6	
117	-1.07	2.69	1.5	213	6	
120	-0.67	2.66	1.6	205	6	
123	-0.73	2.94	1.7	213	5	
126	-1.78	3.24	1.7	195	5	
129	-1.40	2.53	1.7	198	4	
132	-1.81	1.91	1.8	186	4	
135	-1.92	1.65	2.0	182	5	
138	-1.46	0.80	2.2	175	7	
141	-1.63	0.76	2.6	170	13	
144	-1.54	0.85	2.6	185	12	
147	-1.77	1.39	2.5	176	6	
150	-1.86	1.38	2.5	189		
153	-1.56	2.27	2.4	193		
0.0	1.44	1.77				
0.8			1.8			533
1.5	1.52	1.58				
2.3			1.8			635
3.0	1.39	1.60				
3.8			1.8			522
4.5	1.46	1.51				
5.5	1.51	1.48				
6.3			1.4			989
7.0	1.40	1.75				
8.2	1.31	1.63				
9.2	1.63	1.71				
9.9			1.8			749
10.6	2.00	2.59				
11.6			1.6			811
12.5	1.81	2.05				
13.3			1.6			636
14.1	1.93	2.07				
15.0			1.5			824
15.9	1.93	2.23				
16.6			1.7			615
17.3	1.39	2.02				
18.0			1.6			486
18.6	1.54	1.47				
19.4			1.6			683
20.1	1.53	1.80				
21.1			1.7			813
22.0	1.64	1.93				
23.0			1.7			644
23.9	1.49	1.80				
23.9	1.56	1.84				
24.8			1.7			828
25.7	1.26	1.49				
25.7	1.67	2.00				
26.6			2.1			838
27.4	1.49	1.74				
27.4	1.53	1.82				
28.6			1.6			877

Length from apex (mm)	$\delta^{13}C$ (‰)	$\delta^{18}O$ (‰)	Sr/Ca (mmol/mol)	P/Ca (umol/mol)	Fe/Ca (umol/mol)	U/Ca (umol/mol)
29.7	1.33	1.68				
30.7			1.7			943
31.7	1.24	1.37				
32.6			2.0			869
33.4	1.07	1.64				
33.4	1.17	1.50				
34.4			2.0			638
35.4	1.23	1.80				
35.4	1.26	1.58				
36.5			1.8			873
37.6	1.41	1.62				
37.6	1.30	1.31				
38.8			1.9			932
40	1.54	1.23				
40	1.45	1.26				
42.3	1.73	1.51				
42.3	1.45	1.45				
44.1	1.67	1.60				
45.8	1.31	1.67				
45.8	1.12	1.10				
47.5	1.29	1.33				
48.5			2.3			710
49.5	1.60	1.56				
49.5	1.20	1.20				
50.5			2.2			941
51.5	1.25	1.21				
52.8			2.1			728
54	1.33	1.54				
55.0			1.9			1456
55.9	1.46	2.12				
55.9	1.63	2.28				
57.1			1.6			939
58.3	1.67	2.71				
58.3	1.68	2.76				
59.4			1.7			561
60.4	1.78	2.70				
60.4	1.67	2.57				
62.6	1.17	1.50				
62.6	1.38	1.81				
63.6			1.6			786
64.5	1.08	1.98				
65.6			1.6			730
66.7	1.10	1.82				
66.7	0.99	1.86				
67.7			1.7			772
68.6	0.65	1.26				
68.6	0.71	1.79				
69.4			2.0			755
70.1	0.90	1.31				
71.9	1.24	1.17				
71.9	1.13	1.19				
72.7			2.2			772
73.5	1.48	1.42				
73.5	1.36	1.34				

Length from apex (mm)	$\delta^{13}C$ (‰)	$\delta^{18}O$ (‰)	Sr/Ca (mmol/mol)	P/Ca (umol/mol)	Fe/Ca (umol/mol)	U/Ca (umol/mol)
75.4	1.17	1.24				
75.4	1.19	1.42				
76.1			2.4			598
76.8	1.16	1.24				
77.5			2.3			874
78.2	1.13	1.33				
78.2	1.21	1.76				
79.1			2.1			840
79.9	1.20	1.49				
80.6			2.0			814
81.3	1.00	1.26				
81.3	1.08	1.47				
82.2			2.1			878
83.1	1.00	1.30				
83.1	1.10	1.33				
83.9			2.0			1140
84.6	1.12	1.13				
84.6	1.17	1.47				
85.5			2.0			1113
86.4	0.85	0.68				
86.4	1.09	1.05				
87.3			2.0			1068
88.2	0.92	1.11				
89.1			2.0			998
89.9	1.11	1.41				
89.9	1.07	1.67				
90.7			2.0			1035
91.4	1.20	1.55				
92.2			1.7			838
92.9	1.19	2.51				
92.9	1.27	2.52				
93.5			1.7			636
94.1	1.16	2.55				
94.1	1.17	2.66				
95.2			1.9			392
96.3	0.48	1.75				
96.3	0.51	1.77				
96.9			2.2			309
97.5	0.36	1.59				
97.5	0.63	1.86				
0	1.79	-0.42				
1.3	1.82	-0.34				
2.3			2.2			192
3.1	1.94	-0.28				
5.3	1.86	-0.35				
6.9	1.75	-0.49				
8.8	2.04	-0.38				
11.1	1.90	-0.46				
12.1			2.3			37
13.2	1.90	-0.49				
15.1	2.03	-0.43				
17.5	2.15	-0.52				
19.7	2.07	-0.42				
21.1			2.1			160

Length from apex (mm)	$\delta^{13}C$ (‰)	$\delta^{18}O$ (‰)	Sr/Ca (mmol/mol)	P/Ca (umol/mol)	Fe/Ca (umol/mol)	U/Ca (umol/mol)
24.2	2.02	-0.43				
25.7	2.03	-0.34				
26.4			2.2			468
27.4	1.99	-0.26				
29	2.08	-0.57				
30.7	1.99	-0.51				
31.8			2.1			167
32.8	1.90	-0.35				
34.9	2.21	-0.46				
37	2.03	-0.47				
38.1			2.2			48
39.1	2.10	-0.55				
41.2	2.04	-0.50				
43	2.14	-0.38				
44.1			2.2			162
44.9	2.18	-0.44				
47.4	2.18	-0.50				
49.9	2.27	-0.39				
51.2			2.3			51
52.2	2.28	-0.39				
54.6	2.19	-0.36				
57.5	2.10	-0.52				
59.3			2.3			138
60.5	2.14	-0.40				
63	2.13	-0.39				
65.3	1.95	-0.40				
65.6			2.3			273
67.8	2.10	-0.28				
70.3	1.85	-0.30				
71.8			2.4			144
72.8	1.73	-0.48				
75.3	1.65	-0.73				
77.9	1.77	-0.37				
79.9			2.4			153
80.9	1.61	-0.62				
83.9	1.78	-0.46				
86.8	1.86	-0.52				
88.8			2.3			270
90.1	2.30	-0.21				
92.6	2.29	-0.16				
95.2	2.18	-0.16				
96.9			2.5			141
97.8	2.23	-0.11				
100.7	2.07	0.11				
103.3	2.21	0.12				
103.6			2.5			192
105.9	2.21	-0.09				
108.5	2.16	0.03				
108.8			2.5			135
111.1	2.12	0.17				
113.7	2.29	0.57				
114.1			2.4			75
116.5	2.52	1.01				
118.9	2.10	0.49				

Length from apex (mm)	$\delta^{13}C$ (‰)	$\delta^{18}O$ (‰)	Sr/Ca (mmol/mol)	P/Ca (umol/mol)	Fe/Ca (umol/mol)	U/Ca (umol/mol)
121.9	1.89	-0.08				
124.4	2.24	-0.43				
126.5			2.5			72
127.8	2.29	0.00				
130.3	2.17	-0.72				
132.5	2.17	-0.78				
134.3			2.4			169
135.4	2.04	-0.92				
138.1	2.16	-0.72				
141.1	2.16	-1.23				
142.3			2.4			289
143.1	2.02	-1.01				
145.7	1.89	-0.87				
147.9	1.85	-1.03				
148.1			2.2			286
150.2	1.86	-0.92				
0	1.87	-0.52				
2	2.00	-0.55				
3			2.5		128	370
5	2.25	-0.62				
7	2.30	-0.66				
9	2.07	-0.57				
11	2.27	-0.58				
13	2.11	-0.40				
13			2.5		31	248
15	2.18	-0.38				
17	2.12	-0.39				
19	2.16	-0.34				
21	2.12	-0.48				
23	1.86	-0.34				
23			2.5		58	254
25	2.11	-0.46				
27	2.14	-0.35				
29	2.21	-0.28				
31	2.10	-0.43				
33	2.10	-0.36				
33			2.3		2	257
35	2.38	-0.46				
37	2.27	-0.50				
39	2.22	-0.34				
41	2.21	-0.37				
43	2.20	-0.28				
43			2.3		-1	156
45	2.24	-0.46				
47	2.22	-0.27				
49	2.08	-0.26				
51	2.17	-0.20				
53	2.19	-0.23				
53			2.5		0	204
55	2.21	-0.13				
57	2.02	-0.23				
59	1.95	-0.26				
61	1.95	-0.30				
63	1.69	-0.31				

Length from apex (mm)	$\delta^{13}C$ (‰)	$\delta^{18}O$ (‰)	Sr/Ca (mmol/mol)	P/Ca (umol/mol)	Fe/Ca (umol/mol)	U/Ca (umol/mol)
65	1.78	-0.37				
67	1.88	-0.21				
69	1.79	-0.22				
71	1.54	-0.36				
73	2.17	-0.27				
72			2.4		17	218
74	2.05	-0.33				
76	2.03	-0.27				
78	2.14	-0.11				
80	1.95	-0.35				
80			2.2		3	130
82	2.29	0.04				
84	2.38	0.22				
86	2.38	0.64				
88	2.27	0.62				
88			2.4		0	145
90	2.17	0.58				
92	1.94	0.37				
94	2.20	0.67				
95			2.3		1	147
97	2.20	0.66				
99	2.20	0.90				
101	2.25	1.06				
101			2.5		14	152
103	1.95	0.67				
105	2.20	1.59				
107	2.18	1.55				
106			2.4		2	113
108	2.00	2.01				
110	1.66	1.86				
110			2.4		4	111
112	1.66	0.02				
114	1.91	-0.03				
115			2.5		9	137
117	1.89	0.14				
119	1.87	-0.19				
121	1.77	-0.21				
120			2.6		4	121
122	1.92	-0.25				
124	1.83	-0.23				
126	1.75	-0.10				
128	1.98	-0.18				
130	1.76	-0.36				
132	2.04	-0.26				
134	1.81	-0.39				
136	1.56	-0.33				
138	1.83	-0.19				
0	1.85	-0.58				
1.2	2.01	-0.60				
2.3	2.14	-0.56				
5.2	2.01	-0.39				
6.3	2.27	0.15				
7.8	2.10	0.49				
8.9	2.24	0.97				

Length from apex (mm)	$\delta^{13}C$ (‰)	$\delta^{18}O$ (‰)	Sr/Ca (mmol/mol)	P/Ca (umol/mol)	Fe/Ca (umol/mol)	U/Ca (umol/mol)
11.8	2.49	1.54				
14.6	2.24	1.01				
15.8	2.36	0.99				
17	2.30	0.94				
18.5	2.07	0.92				
19.5	1.91	0.62				
20.6	2.11	0.58				
21.7	2.05	0.49				
22.9	2.02	0.53				
24	1.89	0.49				
25.1	1.84	0.48				
26.4	1.99	0.56				
27.7	1.87	0.57				
28.6	1.86	0.54				
29.6	1.86	0.48				
31.5	1.64	0.54				
32.5	1.88	0.47				
34	1.96	0.38				
35	1.94	0.52				
36.4	1.89	0.34				
37.8	1.85	0.30				
39.6	1.91	0.40				
41	1.91	0.28				
42.7	1.85	0.25				
44.4	1.83	0.30				
45.6	1.90	0.27				
47	1.88	0.14				
48.5	1.93	0.18				
50.1	1.98	0.20				
52.3	2.03	0.01				
53.5	2.19	0.21				
55	2.11	0.06				
56.5	2.00	-0.02				
58	1.94	0.13				
59.7	1.79	0.05				
61.9	1.60	-0.01				
63.2	1.53	0.11				
65.3	1.56	-0.07				
67.1	1.61	-0.10				
68.9	1.60	-0.15				
70.3	1.46	-0.22				
71.7	1.33	-0.17				
73.4	1.65	-0.32				
75.5	1.70	-0.22				
76.7	1.64	-0.05				
78.7	1.55	-0.13				
80.6	1.63	-0.11				
82.5	1.52	-0.12				
83.9	1.65	-0.27				
85.9	1.58	-0.26				
87.6	1.64	-0.08				
89.1	1.50	-0.21				
90.6	1.62	-0.30				
92.4	2.05	-0.08				

Length from apex (mm)	$\delta^{13}C$ (‰)	$\delta^{18}O$ (‰)	Sr/Ca (mmol/mol)	P/Ca (umol/mol)	Fe/Ca (umol/mol)	U/Ca (umol/mol)
96.7	2.44	-0.01				
98.4	2.63	-0.08				
99.9	2.53	0.01				
0	0.37	-1.02				
3	1.89	-1.02				
7	2.12	-1.69				
9	1.90	-1.44				
13	2.20	-1.03				
17	2.38	-1.13				
20	2.37	-0.92				
24	2.02	-0.72				
28	2.24	-0.58				
31	2.45	-0.49				
35	2.28	-0.09				
39	2.44	0.24				
43	2.89	0.93				
47	2.57	0.69				
52	2.59	0.63				
55	2.26	0.13				
59	2.59	0.73				
62	2.51	1.10				
66	2.53	0.62				
70	2.70	0.63				
74	2.16	0.51				
78	2.50	0.26				
82	2.30	-0.03				
85	2.40	0.20				
89	2.51	-0.02				
92	2.12	0.01				
96	1.95	-0.31				
99	1.38	-0.28				
103	1.69	-0.20				
106	1.53	-0.71				
110	1.41	-0.76				
113	1.65	-0.76				
116	1.51	-0.99				
120	1.48	-0.86				
123	2.28	-0.82				
127	1.91	-1.00				
130	1.32	-1.01				
134	1.18	-1.14				
138	1.19	-0.98				
141	1.41	-1.20				
144	1.38	-0.94				
148	1.35	-0.93				
152	1.32	-1.22				
155	1.22	-1.02				
159	1.39	-1.20				
163	1.86	-1.17				
166	1.65	-0.94				
170	1.67	-1.03				
174	2.02	-0.89				
177	1.55	-0.93				
180	1.58	-1.27				

Length from apex (mm)	$\delta^{13}C$ (‰)	$\delta^{18}O$ (‰)	Sr/Ca (mmol/mol)	P/Ca (umol/mol)	Fe/Ca (umol/mol)	U/Ca (umol/mol)
186	1.29	-0.92				
190	1.69	-0.79				
194	1.41	-0.67				
198	1.59	-0.01				
201	1.22	0.03				
204	0.95	-0.16				
207	0.80	0.51				
210	1.30	0.18				
214	1.25	-0.71				
217	1.30	-1.22				
221	1.31	-1.34				
224	1.13	-1.20				
228	1.00	-1.34				
232	1.08	-1.33				
236	1.02	-1.11				
240	1.24	-1.05				
243	1.06	-1.10				
247	1.17	-1.12				
250	0.82	-0.46				
254	0.71	0.05				
257	1.01	1.11				
261	1.47	-1.05				
264	1.36	-0.98				
0	2.65	-0.26				
1.2	2.57	-0.37				
2.9	2.39	-0.50				
4.3	2.41	-0.61				
5.9	2.34	-0.79				
7.2	2.51	-0.86				
8.4	2.49	-0.82				
10.1	2.11	-1.09				
11.5	2.27	-1.12				
12.9	1.76	-1.15				
14.8	1.54	-1.02				
16.7	1.53	-0.93				
19.5	1.40	-0.94				
21.7	1.91	-1.05				
23.9	1.83	-1.13				
26.1	2.05	-1.11				
28	2.03	-0.88				
29.9	2.12	-0.56				
31.9	1.93	-0.28				
33.9	1.73	-0.18				
35.9	2.37	-0.47				
38.4	2.65	-0.41				
40.7	2.64	-0.59				
43.3	2.49	-0.69				
45.4	2.55	-0.42				
47.8	2.50	-0.33				
50.3	2.14	-0.24				
52.3	1.54	0.28				
55	1.56	0.21				
57.2	1.61	-0.11				
59.3	1.78	0.23				

Length from apex (mm)	$\delta^{13}C$ (‰)	$\delta^{18}O$ (‰)	Sr/Ca (mmol/mol)	P/Ca (umol/mol)	Fe/Ca (umol/mol)	U/Ca (umol/mol)
63.7	2.31	0.62				
65.9	2.41	0.96				
68.2	2.33	0.98				
70.5	2.12	1.11				
73.5	2.20	0.74				
76	2.48	0.47				
78.3	1.88	-0.57				
80.1	2.15	-0.80				
82.4	2.05	-0.83				
84.5	1.91	-0.93				
86.8	1.09	-1.65				
89.7	1.41	-0.98				
92	1.47	-1.04				
94.3	1.37	-0.67				
96.4	1.38	-1.70				
98.5	1.48	-1.10				
101.4	1.41	-0.97				
104.1	1.44	-1.05				
106.5	1.52	-1.20				
109.5	1.36	-1.80				
112.8	1.85	-0.89				
116.1	1.67	-1.02				
119.3	1.87	-0.95				
121.6	1.81	-1.14				
124.2	1.66	-0.63				
126.8	1.45	-0.58				
128.9	1.62	-0.25				
131.4	1.65	0.16				
-1.0			2.0		218	16331
0	2.15	-0.72				
0.6			1.9		312	15368
1.2	2.22	-0.50				
2.4			2.1		356	10696
3.5	1.78	-0.88				
4.5			2.2		202	7600
5.4	1.82	-0.85				
6.1			2.3		261	6686
6.8	1.80	-0.85				
7.8			1.9		298	6835
8.8	1.76	-0.86				
9.6			1.8		197	7777
10.3	1.62	-1.03				
11.5			1.5		187	13644
12.6	2.18	0.80				
13.6			1.5		226	13260
14.5	2.61	0.55				
15.6			1.9		203	13082
16.7	2.73	0.36				
17.7			1.9		216	15108
18.6	2.28	-0.05				
20.1	2.19	-0.26				
22.2	2.29	-0.45				
24.7	2.21	-0.38				
27	2.42	-0.37				

Length from apex (mm)	$\delta^{13}C$ (‰)	$\delta^{18}O$ (‰)	Sr/Ca (mmol/mol)	P/Ca (umol/mol)	Fe/Ca (umol/mol)	U/Ca (umol/mol)
29.9	2.71	-0.50				
31.0			2.2			7744
32.1	2.21	-0.64				
32.9			2.2			7262
33.7	2.42	-0.67				
35.3			2.2			8413
36.9	2.16	-0.66				
37.9			2.2			11177
38.8	2.16	-0.61				
39.8			2.2			14112
40.8	1.91	-0.77				
41.9			2.0			13480
42.9	2.23	-0.65				
43.8			2.0			11283
44.7	2.18	-0.45				
46.5	2.32	-0.28				
47.6			1.8		55	11394
48.7	2.58	-0.23				
49.5			1.8		69	11522
50.3	2.51	-0.25				
51.5			1.6		87	12906
52.7	2.30	-0.18				
53.5			1.6		188	14396
54.2	2.55	0.25				
55.4			1.7		137	10751
56.6	2.47	0.73				
57.9			1.6			8060
59.1	2.18	0.43				
59.9			1.7			7662
60.6	1.89	0.37				
62.0			1.8			6498
63.3	2.39	-0.07				
64.6			1.9			4630
65.8	2.49	-0.24				
67.0			2.0			7998
68.1	2.42	-0.30				
69.3			2.0			7386
70.4	2.37	-0.34				
71.5			2.0			10460
72.5	2.30	-0.51				
73.8			2.1			13025
75.1	2.48	-0.59				
76.4			2.2			10432
77.7	1.70	-0.59				
78.7			2.2			13025
79.7	1.48	-0.24				
80.6			2.2		125	12299
81.5	1.58	-0.40				
82.6			2.0		35	9053
83.7	1.73	-0.49				
84.9			2.0		82	11699
86.1	1.64	-0.38				
87.3			1.8		36	10037
88.5	1.56	-0.30				

Length from apex (mm)	$\delta^{13}C$ (‰)	$\delta^{18}O$ (‰)	Sr/Ca (mmol/mol)	P/Ca (umol/mol)	Fe/Ca (umol/mol)	U/Ca (umol/mol)
91.1	1.69	-0.06				
92.1			1.7		117	12611
93.1	1.69	-0.08				
94.3			2.0		32	9866
95.5	2.17	0.29				
0	2.51	0.35				
4	2.51	0.54				
8	2.31	0.46				
15	2.09	0.55				
20	2.26	0.84				
24	2.33	0.63				
28	1.44	0.00				
32	1.39	-0.13				
37	2.13	0.06				
41	2.15	0.04				
47	2.11	0.69				
52	2.23	1.29				
57	1.86	0.31				
63	2.35	-0.98				
69	2.19	-0.96				
75	2.57	-1.06				
81	1.86	-0.63				
86	1.61	-0.46				
91	2.04	0.05				
96	2.20	0.28				
101	1.88	0.73				
107	2.02	0.90				
113	2.29	1.59	1.9	287	90	
119	1.89	0.93	1.9	265	18	
124	2.23	0.20	1.8	269	17	
129	2.47	0.05	1.9	235	178	
134	1.92	0.83	1.8	247	95	
139	2.19	0.25	1.8	267	50	
145	1.81	0.67	1.8	227	24	
150	1.82	-0.48	2.1	401	14	
155	2.20	-0.60	2.1	270	17	
160	2.07	-0.68	2.0	249	16	
165	1.75	-0.90	2.0	245	16	
171	1.68	-0.45	2.0	192	3	
176	1.76	-0.05	2.1	310	15	
181	1.84	0.46	2.0	287	9	
186	1.79	0.66	1.8	288	11	
191	1.88	0.85	1.8	274	13	
196	1.92	0.92	1.9	239	4	
202	1.98	0.99	1.8	263	16	
207	2.25	0.38	2.0	177	2	
212	2.13	-0.03	1.9	115	2	
217	2.56	0.17	2.0	241	14	
222	2.58	0.12	1.9	227	19	
228	2.50	-0.09	2.1	229	13	
233	2.13	-0.85	2.2	238	19	
238	2.10	-0.83	2.1	242	12	
243			2.1	247	11	
248	1.83	-0.58	2.1	251	13	

Length from apex (mm)	$\delta^{13}C$ (‰)	$\delta^{18}O$ (‰)	Sr/Ca (mmol/ mol)	P/Ca (umol/ mol)	Fe/Ca (umol/ mol)	U/Ca (umol/ mol)
259	1.82	0.46	1.9	336	204	
264	1.92	1.12	1.9	328	19	
269	2.27	0.02	2.0	511	38	
274	2.12	0.10	2.0	272	192	
279	2.18	0.07	1.9	250	8	
284	2.08	-0.26	2.0	265	15	
290	2.01	-0.76	2.3	254	50	
295	1.96	-0.10	2.2	247	17	
300	1.79	-0.17	2.0	257	10	
305	1.80	0.78	1.9	266	16	
310	2.15	0.49	2.0	246	17	
315	2.28	-0.07	2.1	289	15	
320	2.45	-0.06	2.1	209	4	
325	2.26	0.56	2.0	266	19	
330	1.58	-0.76	2.1	251	22	
336	2.17	-1.02	2.1	235	22	
341	1.44	-1.04	2.0	167	5	
346	1.40	-0.44	1.8	270	22	
351	1.57	-0.05				
356	1.66	0.78	1.6	287	24	
361	1.34	0.89	1.8	2381	39	
367	1.48	0.43	2.0	315	37	
373	1.35	0.12	2.0	4302	87	
378	1.43	-0.46	2.1	219	9	
383	1.54	-0.91	2.2	245	38	
388	1.13	-0.28	2.0	293	18	

APPENDIX 2

STABLE ISOTOPE ANALYSES OF MODERN AND FOSSIL PANAMA SAMPLES

Sample ID	Length from apex (mm)	$\delta^{13}C$	$\delta^{18}O$
TA06-294A	74.0	2.10	-1.01
TA06-294A	72.0	1.87	-0.97
TA06-294A	70.0	1.70	-0.82
TA06-294A	68.0	2.22	-0.81
TA06-294A	66.0	2.56	-0.78
TA06-294A	64.0	2.26	-0.64
TA06-294A	62.0	2.05	-0.72
TA06-294A	60.0	2.10	-0.80
TA06-294A	58.0	1.68	-0.73
TA06-294A	56.0	2.09	-0.72
TA06-294A	54.0	2.38	-0.78
TA06-294A	52.0	2.63	-0.62
TA06-294A	50.0	2.55	-0.62
TA06-294A	48.0	2.64	-0.89
TA06-294A	46.0	2.66	-0.67
TA06-294A	44.0	2.53	-0.50
TA06-294A	42.0	2.48	-0.80
TA06-294A	40.0	2.56	-1.23
TA06-294A	38.0	2.59	-1.02
TA06-294A	36.0	2.56	-1.06
TA06-294A	34.0	2.67	-1.02
TA06-294A	32.0	2.49	-1.14
TA06-294A	30.0	2.62	-1.03
TA06-294A	28.0	2.41	-1.12
TA06-294A	26.0	2.44	-1.08
TA06-294A	24.0	2.28	-1.30
TA06-294A	22.0	2.46	-0.87
TA06-294A	20.0	2.44	-1.00
TA06-294A	18.0	2.30	-0.95
TA06-294A	16.0	2.41	-1.19
TA06-294A	14.0	2.38	-0.95
TA06-294A	12.0	2.42	-1.09
TA06-294A	10.0	2.25	-1.33
TA06-294A	8.0	2.36	-1.16
TA06-294A	6.0	2.22	-1.08
TA06-294A	4.0	2.07	-1.08
TA06-294A	2.0	1.95	-0.94
TA06-294A	0.0	2.23	-0.80
TA06-294B	22.5	1.46	-0.58
TA06-294B	21.0	1.68	-0.58
TA06-294B	19.5	1.67	-0.49

Sample ID	Length from apex (mm)	$\delta^{13}C$	$\delta^{18}O$
TA06-294B	18.0	1.74	-0.65
TA06-294B	16.5	1.76	-0.51
TA06-294B	15.0	1.74	-0.59
TA06-294B	13.5	1.85	-0.47
TA06-294B	12.0	1.90	-0.52
TA06-294B	10.5	1.92	-0.57
TA06-294B	9.0	1.96	-0.47
TA06-294B	7.5	1.75	-0.62
TA06-294B	6.0	1.96	-0.66
TA06-294B	4.5	1.83	-0.60
TA06-294B	3.0	1.72	-0.90
TA06-294B	1.5	1.77	-0.78
TA06-294B	0.0	1.70	-0.86
SB95-1	55.5	1.97	-2.49
SB95-1	54.0	1.78	-2.11
SB95-1	52.5	1.99	-1.74
SB95-1	51.0	1.97	-1.68
SB95-1	49.5	1.28	-1.85
SB95-1	48.0	1.35	-1.61
SB95-1	46.5	1.58	-1.00
SB95-1	45.0	1.35	-1.12
SB95-1	43.5	1.38	-1.08
SB95-1	42.0	1.62	-0.86
SB95-1	40.5	1.66	-1.25
SB95-1	39.0	1.55	-1.46
SB95-1	37.5	1.61	-1.63
SB95-1	36.0	1.75	-1.46
SB95-1	34.5	1.63	-1.82
SB95-1	33.0	1.91	-1.55
SB95-1	31.5	1.88	-1.88
SB95-1	30.0	1.87	-1.81
SB95-1	28.5	1.96	-1.65
SB95-1	27.0	1.91	-1.85
SB95-1	25.5	1.95	-1.41
SB95-1	24.0	2.01	-1.46
SB95-1	22.5	1.82	-1.70
SB95-1	21.0	1.86	-1.98
SB95-1	19.5	1.71	-1.92
SB95-1	18.0	1.77	-1.89
SB95-1	16.5	2.07	-1.47
SB95-1	15.0	1.92	-1.56
SB95-1	13.5	2.22	-1.51
SB95-1	12.0	2.03	-1.50
SB95-1	10.5	2.13	-1.27
SB95-1	9.0	2.17	-1.22
SB95-1	7.5	2.23	-1.28
SB95-1	6.0	2.20	-1.36

Sample ID	Length from apex (mm)	$\delta^{13}C$	$\delta^{18}O$
SB95-1	4.5	2.28	-1.03
SB95-1	3.0	1.90	-1.65
SB95-1	1.5	1.99	-1.35
SB95-1	0.0	1.87	-1.81
TA04-10A	51.0	0.76	-1.10
TA04-10A	49.5	0.82	-0.70
TA04-10A	48.0	1.10	-0.65
TA04-10A	46.5	1.11	-0.91
TA04-10A	45.0	0.79	-0.87
TA04-10A	43.5	1.13	-1.05
TA04-10A	42.0	0.73	-0.97
TA04-10A	40.5	1.15	-0.85
TA04-10A	39.0	1.25	-0.71
TA04-10A	37.5	1.16	-0.89
TA04-10A	36.0	1.22	-0.83
TA04-10A	34.5	1.31	-0.97
TA04-10A	33.0	1.58	-0.81
TA04-10A	31.5	1.35	-0.82
TA04-10A	30.0	1.25	-0.79
TA04-10A	28.5	1.37	-0.85
TA04-10A	27.0	1.12	-0.90
TA04-10A	25.5	0.80	-0.66
TA04-10A	24.0	1.24	-0.70
TA04-10A	22.5	1.44	-0.62
TA04-10A	21.0	1.25	-0.79
TA04-10A	19.5	1.03	-0.52
TA04-10A	18.0	1.21	-0.85
TA04-10A	16.5	1.20	-0.55
TA04-10A	15.0	1.50	-0.71
TA04-10A	13.5	1.53	-0.64
TA04-10A	12.0	1.53	-0.66
TA04-10A	10.5	1.46	-0.93
TA04-10A	9.0	1.51	-0.78
TA04-10A	7.5	1.43	-0.88
TA04-10A	6.0	1.54	-0.74
TA04-10A	4.5	1.57	-0.79
TA04-10A	3.0	1.72	-1.12
TA04-10A	1.5	1.57	-1.37
TA04-10A	0.0	1.46	-0.83
TA04-10B	52.0	1.50	-1.22
TA04-10B	50.0	1.31	-0.99
TA04-10B	48.0	1.35	-0.99
TA04-10B	46.0	1.36	-1.17
TA04-10B	44.0	1.70	-1.03
TA04-10B	42.0	1.15	-1.07
TA04-10B	40.0	1.16	-0.99

Sample ID	Length from apex (mm)	$\delta^{13}C$	$\delta^{18}O$
TA04-10B	38.0	1.44	-1.07
TA04-10B	36.0	1.48	-0.75
TA04-10B	34.0	1.15	-0.92
TA04-10B	32.0	1.04	-0.95
TA04-10B	30.0	1.01	-0.67
TA04-10B	28.0	1.68	-0.49
TA04-10B	26.0	1.78	-0.59
TA04-10B	24.0	1.65	-0.50
TA04-10B	22.0	1.66	-0.56
TA04-10B	20.0	1.74	-0.62
TA04-10B	18.0	1.88	-0.62
TA04-10B	16.0	1.76	-1.05
TA04-10B	14.0	1.80	-0.68
TA04-10B	12.0	1.91	-0.85
TA04-10B	10.0	1.76	-1.11
TA04-10B	8.0	1.67	-0.98
TA04-10B	6.0	1.43	-1.06
TA04-10B	4.0	1.75	-0.84
TA04-10B	2.0	1.79	-1.02
TA04-10B	0.0	1.60	-1.24
TA04-10C	50.0	0.14	-1.22
TA04-10C	48.0	0.49	-1.09
TA04-10C	46.0	1.08	-0.95
TA04-10C	44.0	1.08	-0.98
TA04-10C	42.0	1.22	-1.41
TA04-10C	40.0	0.95	-1.43
TA04-10C	38.0	0.55	-1.38
TA04-10C	36.0	1.03	-1.27
TA04-10C	34.0	1.01	-1.47
TA04-10C	32.0	1.22	-1.35
TA04-10C	30.0	1.13	-1.33
TA04-10C	28.0	1.16	-1.52
TA04-10C	26.0	0.83	-1.95
TA04-10C	24.0	0.89	-1.39
TA04-10C	22.0	0.99	-1.56
TA04-10C	20.0	0.88	-1.30
TA04-10C	18.0	1.04	-1.22
TA04-10C	16.0	0.93	-1.06
TA04-10C	14.0	0.94	-1.06
TA04-10C	12.0	0.67	-1.08
TA04-10C	10.0	0.48	-0.91
TA04-10C	8.0	0.83	-1.34
TA04-10C	6.0	0.91	-1.20
TA04-10C	4.0	0.80	-1.42
TA04-10C	2.0	0.82	-1.26
TA04-10C	0.0	0.91	-1.31

Sample ID	Length from apex (mm)	$\delta^{13}C$	$\delta^{18}O$
GP97-17A	160.9	1.39	-1.61
GP97-17A	157.9	1.51	-1.47
GP97-17A	155.0	1.19	-2.20
GP97-17A	152.1	1.17	-2.12
GP97-17A	149.2	0.97	-2.33
GP97-17A	146.3	1.24	-1.83
GP97-17A	143.4	1.33	-1.66
GP97-17A	140.5	1.49	-1.21
GP97-17A	137.6	1.76	-0.29
GP97-17A	134.8	1.80	-0.62
GP97-17A	132.3	1.98	-0.49
GP97-17A	129.3	1.69	-0.43
GP97-17A	126.8	1.95	-0.56
GP97-17A	124.1	1.95	-1.98
GP97-17A	121.6	1.92	-2.64
GP97-17A	118.9	1.95	-2.13
GP97-17A	116.2	2.01	-2.66
GP97-17A	113.4	2.03	-2.11
GP97-17A	111.0	2.06	-2.03
GP97-17A	108.5	2.14	-2.34
GP97-17A	106.1	1.98	-2.53
GP97-17A	103.1	1.91	-2.87
GP97-17A	100.1	2.04	-2.41
GP97-17A	97.7	2.04	-2.73
GP97-17A	94.9	2.07	-2.70
GP97-17A	92.4	2.21	-3.51
GP97-17A	89.9	2.17	-2.77
GP97-17A	87.4	2.18	-2.64
GP97-17A	84.9	1.48	-2.77
GP97-17A	82.4	1.99	-2.69
GP97-17A	79.6	2.15	-2.74
GP97-17A	77.3	2.30	-2.72
GP97-17A	74.7	2.49	-2.43
GP97-17A	72.1	2.26	-3.02
GP97-17A	69.8	2.14	-2.91
GP97-17A	67.2	2.39	-2.79
GP97-17A	64.9	2.52	-2.69
GP97-17A	62.3	2.53	-2.76
GP97-17A	60.0	2.46	-2.41
GP97-17A	57.7	2.06	-3.19
GP97-17A	55.3	2.58	-2.50
GP97-17A	53.2	2.56	-2.54
GP97-17A	50.6	2.63	-1.98
GP97-17A	48.3	2.50	-2.21
GP97-17A	46.0	2.42	-2.13
GP97-17A	43.7	2.77	-2.02
GP97-17A	41.4	2.72	-1.71
GP97-17A	39.1	2.63	-2.04

Sample ID	Length from apex (mm)	$\delta^{13}C$	$\delta^{18}O$
GP97-17A	36.8	2.48	-2.37
GP97-17A	34.5	2.71	-2.31
GP97-17A	32.2	2.64	-2.17
GP97-17A	29.9	2.59	-2.06
GP97-17A	27.6	2.51	-2.06
GP97-17A	25.3	2.45	-2.24
GP97-17A	23.0	2.52	-2.31
GP97-17A	20.7	2.29	-2.53
GP97-17A	18.4	2.50	-2.41
GP97-17A	16.1	2.61	-2.02
GP97-17A	13.8	2.62	-1.94
GP97-17A	11.5	2.54	-1.74
GP97-17A	9.2	2.37	-1.46
GP97-17A	6.9	2.39	-1.38
GP97-17A	4.6	2.40	-1.24
GP97-17A	2.3	2.34	-0.81
GP97-17B	71.5	0.72	-1.45
GP97-17B	70.0	0.73	-1.35
GP97-17B	68.5	0.96	-1.58
GP97-17B	66.7	0.94	-1.96
GP97-17B	65.2	1.25	-1.79
GP97-17B	63.6	0.91	-1.74
GP97-17B	62.1	0.97	-1.19
GP97-17B	60.4	0.66	-1.30
GP97-17B	58.5	0.79	-1.46
GP97-17B	57.0	0.84	-1.21
GP97-17B	55.2	0.81	-1.20
GP97-17B	53.8	0.79	-1.66
GP97-17B	52.4	0.70	-2.21
GP97-17B	51.1	0.31	-2.18
GP97-17B	49.3	0.56	-1.71
GP97-17B	47.3	0.81	-1.54
GP97-17B	45.6	1.01	-1.44
GP97-17B	43.9	0.92	-1.58
GP97-17B	42.3	0.98	-1.23
GP97-17B	40.9	0.76	-1.99
GP97-17B	39.4	0.38	-2.38
GP97-17B	38.0	0.54	-2.13
GP97-17B	36.5	0.85	-1.82
GP97-17B	35.0	0.97	-1.53
GP97-17B	33.1	0.76	-1.35
GP97-17B	31.5	0.94	-1.11
GP97-17B	30.0	1.17	-1.22
GP97-17B	28.4	0.90	-1.56
GP97-17B	26.8	0.61	-1.64
GP97-17B	25.4	0.67	-1.74
GP97-17B	23.9	0.65	-2.16

Sample ID	Length from apex (mm)	$\delta^{13}C$	$\delta^{18}O$
GP97-17B	21.8	0.84	-2.17
GP97-17B	19.7	0.60	-2.50
GP97-17B	17.6	0.43	-2.90
GP97-17B	15.5	0.75	-2.99
GP97-17B	13.4	0.61	-3.27
GP97-17B	11.8	0.82	-2.67
GP97-17B	10.2	0.68	-3.36
GP97-17B	8.5	0.53	-3.30
GP97-17B	6.8	0.65	-3.40
GP97-17B	5.1	1.29	-2.83
GP97-17B	3.4	0.84	-2.65
GP97-17B	1.7	0.98	-2.55
GP97-17B	0.0	0.94	-2.22
GC97-80A	121.9	2.44	-0.01
GC97-80A	119.8	2.48	0.08
GC97-80A	117.0	2.29	-0.53
GC97-80A	114.5	2.60	0.51
GC97-80A	112.5	2.48	0.41
GC97-80A	109.8	2.42	0.29
GC97-80A	107.4	2.44	0.19
GC97-80A	104.9	2.39	0.28
GC97-80A	102.0	2.48	-0.04
GC97-80A	99.6	2.36	0.37
GC97-80A	96.9	2.34	0.21
GC97-80A	94.5	2.19	-0.04
GC97-80A	91.9	2.11	-0.07
GC97-80A	89.4	2.31	0.07
GC97-80A	87.0	2.20	0.08
GC97-80A	84.2	2.19	0.43
GC97-80A	81.4	2.07	0.40
GC97-80A	78.4	2.08	0.41
GC97-80A	76.1	2.03	0.31
GC97-80A	73.5	2.08	0.23
GC97-80A	70.6	2.03	0.17
GC97-80A	68.0	1.99	-0.11
GC97-80A	65.7	1.88	0.14
GC97-80A	62.6	1.81	-0.36
GC97-80A	60.1	1.93	-0.06
GC97-80A	57.4	1.87	-0.22
GC97-80A	54.7	1.87	0.60
GC97-80A	51.9	1.84	0.51
GC97-80A	48.9	1.81	0.61
GC97-80A	46.5	1.90	0.13
GC97-80A	43.6	1.75	0.19
GC97-80A	40.7	1.83	-0.11
GC97-80A	37.8	1.79	-0.06
GC97-80A	35.0	1.64	-0.17

Sample ID	Length from apex (mm)	$\delta^{13}C$	$\delta^{18}O$
GC97-80A	32.5	1.64	-0.09
GC97-80A	30.6	1.77	-0.26
GC97-80A	27.9	1.58	-0.02
GC97-80A	25.1	1.40	0.19
GC97-80A	22.4	1.31	0.24
GC97-80A	19.6	1.30	0.49
GC97-80A	17.0	1.38	0.56
GC97-80A	14.4	1.25	0.75
GC97-80A	11.8	1.22	0.79
GC97-80A	9.1	1.44	0.45
GC97-80A	6.9	1.62	0.44
GC97-80A	4.6	1.61	0.52
GC97-80A	2.3	1.86	0.74
GC97-80A	0.0	1.82	0.48
GC97-80B	67.7	1.04	0.33
GC97-80B	65.8	0.99	0.31
GC97-80B	63.2	0.95	0.11
GC97-80B	61.1	1.16	0.71
GC97-80B	58.3	1.18	0.81
GC97-80B	55.8	1.65	0.60
GC97-80B	53.7	1.74	0.50
GC97-80B	51.7	1.84	0.11
GC97-80B	49.3	1.92	0.12
GC97-80B	47.3	1.97	0.23
GC97-80B	45.0	2.03	-0.02
GC97-80B	42.4	1.94	0.24
GC97-80B	39.8	2.04	-0.05
GC97-80B	36.8	1.97	0.24
GC97-80B	34.6	2.21	0.15
GC97-80B	32.5	2.08	-0.01
GC97-80B	29.9	2.15	-0.21
GC97-80B	27.1	1.88	-0.02
GC97-80B	25.0	1.95	0.07
GC97-80B	22.5	1.99	0.35
GC97-80B	20.0	1.87	-0.12
GC97-80B	17.6	2.06	0.33
GC97-80B	15.5	2.00	0.40
GC97-80B	13.3	2.00	0.43
GC97-80B	11.1	1.85	0.69
GC97-80B	8.9	1.31	0.88
GC97-80B	6.5	1.26	1.06
GC97-80B	4.1	1.32	1.14
GC97-80B	2.2	1.48	1.10
GC97-80B	0.0	1.76	0.66
310474	140.2	1.58	-0.78
310474	137.8	1.50	-2.44

Sample ID	Length from apex (mm)	$\delta^{13}C$	$\delta^{18}O$
310474	135.3	1.48	-3.17
310474	133.0	1.24	-2.67
310474	131.0	1.41	-3.18
310474	128.4	0.95	-3.39
310474	125.9	1.50	-2.86
310474	123.5	1.71	-2.56
310474	120.8	1.56	-2.79
310474	117.9	1.56	-2.78
310474	115.7	1.56	-2.86
310474	113.6	1.73	-2.59
310474	111.3	1.76	-2.60
310474	109.1	1.85	-2.37
310474	106.9	2.15	-1.85
310474	104.4	2.18	-1.89
310474	102.4	2.06	-1.35
310474	99.6	2.15	-1.30
310474	97.7	2.08	-1.28
310474	95.0	2.05	-0.63
310474	92.9	1.88	-1.21
310474	90.1	1.96	-1.21
310474	87.9	2.07	-1.36
310474	86.8	2.07	-2.04
310474	85.7	2.06	-2.39
310474	83.5	1.85	-2.37
310474	81.0	2.09	-2.90
310474	78.6	2.09	-2.67
310474	76.2	2.03	-2.72
310474	73.0	1.97	-2.82
310474	70.4	1.84	-2.76
310474	67.8	1.80	-3.06
310474	65.5	2.00	-3.08
310474	62.6	2.07	-2.99
310474	60.4	2.15	-3.04
310474	57.5	1.99	-3.05
310474	54.7	1.90	-2.94
310474	52.5	1.81	-2.96
310474	50.2	1.91	-3.13
310474	47.2	2.10	-2.86
310474	45.1	2.17	-3.03
310474	42.1	1.89	-2.95
310474	39.2	2.05	-2.86
310474	36.6	2.02	-2.87
310474	33.8	1.90	-2.91
310474	31.3	1.76	-2.70
310474	28.7	2.29	-2.64
310474	25.6	2.11	-2.63
310474	23.4	2.35	-2.29
310474	20.5	2.47	-2.31

Sample ID	Length from apex (mm)	$\delta^{13}C$	$\delta^{18}O$
310474	18.3	2.12	-2.47
310474	15.3	2.43	-2.27
310474	12.4	2.33	-1.73
310474	9.6	2.43	-1.61
310474	7.0	2.45	-1.56
310474	4.4	2.39	-1.49
310474	2.0	2.36	-1.14
310474	0.0	2.35	-1.26
301490A	123.0	2.09	0.18
301490A	120.6	2.14	-0.80
301490A	118.7	2.17	-0.94
301490A	116.7	2.17	-0.87
301490A	114.8	2.46	-1.32
301490A	112.9	2.17	0.17
301490A	110.7	1.98	-1.47
301490A	108.7	2.06	-1.77
301490A	107.4	2.21	-2.38
301490A	104.4	2.00	-0.86
301490A	102.1	2.04	0.02
301490A	99.7	2.01	-0.57
301490A	97.3	1.39	-2.03
301490A	95.3	1.42	-1.90
301490A	93.1	1.49	-1.20
301490A	89.8	1.74	-0.08
301490A	86.9	1.77	-0.94
301490A	84.7	1.62	-0.79
301490A	81.8	1.41	-2.24
301490A	78.9	1.60	-2.19
301490A	76.9	1.86	-1.91
301490A	74.6	1.78	-1.50
301490A	72.7	1.68	-1.32
301490A	70.3	1.65	-1.32
301490A	68.0	1.78	-0.40
301490A	65.8	1.81	0.01
301490A	62.8	2.02	-1.19
301490A	60.4	1.75	-1.28
301490A	57.7	1.75	-1.94
301490A	55.0	1.59	-2.38
301490A	52.4	1.73	-2.31
301490A	50.0	1.90	-2.27
301490A	47.5	1.93	-2.21
301490A	45.0	2.26	-2.35
301490A	42.5	2.19	-2.15
301490A	40.0	2.30	-2.03
301490A	37.2	2.17	-1.76
301490A	35.0	2.26	-1.14
301490A	32.9	2.15	-0.57

Sample ID	Length from apex (mm)	$\delta^{13}C$	$\delta^{18}O$
301490A	29.9	1.97	-0.44
301490A	26.9	1.86	-0.26
301490A	24.2	2.09	-1.38
301490A	21.7	2.00	-1.86
301490A	19.2	1.83	-2.12
301490A	16.2	2.25	-2.38
301490A	13.7	2.15	-2.46
301490A	11.1	1.88	-2.22
301490A	8.7	2.26	-2.03
301490A	5.6	2.08	-1.45
301490A	2.5	2.23	-1.24
301490A	0.0	2.03	-0.62
301490B	71.7		
301490B	71.7	1.11	-2.86
301490B	70.0	1.45	-2.77
301490B	68.2	1.46	-2.72
301490B	65.7	1.44	-2.33
301490B	64.0	1.48	-2.36
301490B	62.2	1.31	-2.13
301490B	60.0	1.30	-1.35
301490B	57.7	1.58	-0.94
301490B	55.7	1.31	-0.93
301490B	53.5	1.36	-1.53
301490B	51.0	1.34	-2.61
301490B	48.9	1.64	-2.33
301490B	46.3	1.53	-2.33
301490B	44.0	1.61	-2.29
301490B	41.8	1.49	-2.00
301490B	39.4	1.57	-2.14
301490B	36.9	1.58	-2.22
301490B	34.5	1.44	-2.23
301490B	32.0	1.77	-2.11
301490B	29.6	1.74	-2.18
301490B	27.3	1.55	-1.83
301490B	24.9	1.46	-1.48
301490B	22.3	1.43	-1.67
301490B	19.7	1.32	-0.67
301490B	16.8	1.31	-0.55
301490B	14.0	1.32	-0.54
301490B	11.5	1.33	-0.98
301490B	8.9	1.16	-1.86
301490B	5.9	1.13	-1.78
301490B	3.0	1.06	-1.62
301490B	0.0	1.23	-1.78
JL06-33-1C	87.5	2.27	0.24
JL06-33-1C	85.1	2.12	-0.13

Sample ID	Length from apex (mm)	$\delta^{13}C$	$\delta^{18}O$
JL06-33-1C	82.6	2.31	-0.07
JL06-33-1C	80.1	2.39	0.02
JL06-33-1C	77.7	2.38	0.34
JL06-33-1C	75.2	2.28	0.00
JL06-33-1C	72.3	2.12	-0.16
JL06-33-1C	69.5	2.23	-0.13
JL06-33-1C	67.9	2.17	-0.37
JL06-33-1C	65.0	2.19	-0.32
JL06-33-1C	62.5	1.79	-0.25
JL06-33-1C	59.8	2.01	-0.38
JL06-33-1C	57.2	2.11	-0.25
JL06-33-1C	54.9	2.23	0.12
JL06-33-1C	53.0	1.92	-0.20
JL06-33-1C	51.5	2.10	0.13
JL06-33-1C	49.7	2.05	0.12
JL06-33-1C	47.1	2.09	0.31
JL06-33-1C	44.3	2.25	0.34
JL06-33-1C	42.1	2.14	0.41
JL06-33-1C	39.5	2.11	0.45
JL06-33-1C	36.4	2.23	0.12
JL06-33-1C	33.6	2.33	0.29
JL06-33-1C	30.5	2.34	0.04
JL06-33-1C	27.7	2.01	0.04
JL06-33-1C	25.5	2.13	-0.02
JL06-33-1C	22.8	2.02	-0.04
JL06-33-1C	20.2	1.96	0.26
JL06-33-1C	17.9	2.04	0.15
JL06-33-1C	15.5	1.98	-0.06
JL06-33-1C	14.2	1.81	-0.21
JL06-33-1C	12.8	1.88	-0.44
JL06-33-1C	11.6	1.78	-0.06
JL06-33-1C	10.5	1.75	0.35
JL06-33-1C	7.8	2.04	0.05
JL06-33-1C	5.2	2.09	0.06
JL06-33-1C	4.0	1.88	0.18
JL06-33-1C	2.7	1.91	-0.20
JL06-33-1C	1.4	1.92	0.30
JL06-33-1C	0.0	2.11	0.08
JL06-33-1F	79.0	1.96	0.29
JL06-33-1F	76.0	1.67	0.21
JL06-33-1F	73.6	1.59	-0.10
JL06-33-1F	70.6	1.75	0.37
JL06-33-1F	68.4	1.64	-0.18
JL06-33-1F	65.9	1.62	-0.12
JL06-33-1F	63.4	1.69	-0.17
JL06-33-1F	60.2	2.00	0.30
JL06-33-1F	57.7	1.67	-0.12

Sample ID	Length from apex (mm)	$\delta^{13}C$	$\delta^{18}O$
JL06-33-1F	55.3	1.63	-0.19
JL06-33-1F	52.9	1.87	-0.19
JL06-33-1F	50.8	1.89	0.06
JL06-33-1F	48.2	1.69	-0.21
JL06-33-1F	45.8	1.58	-0.32
JL06-33-1F	43.3	1.27	-0.54
JL06-33-1F	40.9	1.45	-0.38
JL06-33-1F	38.3	1.55	0.02
JL06-33-1F	35.4	1.80	0.37
JL06-33-1F	32.8	1.76	0.35
JL06-33-1F	30.5	1.58	-0.08
JL06-33-1F	28.2	1.97	0.32
JL06-33-1F	25.6	1.70	-0.10
JL06-33-1F	22.8	1.73	-0.14
JL06-33-1F	20.5	1.70	0.09
JL06-33-1F	18.0	1.71	0.36
JL06-33-1F	16.0	1.83	0.29
JL06-33-1F	13.7	1.72	0.15
JL06-33-1F	11.8	1.77	0.27
JL06-33-1F	9.5	1.66	0.57
JL06-33-1F	6.9	1.56	0.12
JL06-33-1F	4.7	1.51	-0.03
JL06-33-1F	2.3	1.53	-0.11
JL06-33-1F	0.0	1.67	0.18
JL06-6-1	85.8	1.18	-0.07
JL06-6-1	83.7	0.93	0.25
JL06-6-1	82.1	1.02	0.05
JL06-6-1	80.7	1.42	0.23
JL06-6-1	78.8	1.16	-0.03
JL06-6-1	76.1	1.13	-0.18
JL06-6-1	74.0	1.32	0.02
JL06-6-1	71.2	1.19	-0.37
JL06-6-1	68.5	0.91	-0.44
JL06-6-1	66.4	0.90	-0.11
JL06-6-1	64.2	0.86	-0.17
JL06-6-1	61.7	1.05	0.01
JL06-6-1	59.7	1.07	-0.11
JL06-6-1	57.9	1.15	-0.13
JL06-6-1	55.4	1.11	0.10
JL06-6-1	53.0	1.01	-0.03
JL06-6-1	51.2	0.99	-0.10
JL06-6-1	48.7	1.03	-0.19
JL06-6-1	46.7	0.94	0.03
JL06-6-1	44.8	1.07	-0.03
JL06-6-1	43.4	0.97	-0.13
JL06-6-1	41.6	1.11	-0.24
JL06-6-1	39.8	1.26	0.23

Sample ID	Length from apex (mm)	$\delta^{13}C$	$\delta^{18}O$
JL06-6-2	38.7	1.29	-0.02
JL06-6-1	37.6	1.23	-0.32
JL06-6-1	35.7	1.02	0.03
JL06-6-1	34.0	1.29	-0.41
JL06-6-1	32.8	0.88	-0.37
JL06-6-1	31.5	0.97	-0.13
JL06-6-1	30.1	1.36	-0.12
JL06-6-1	28.3	0.90	-0.05
JL06-6-1	26.2	1.14	-0.24
JL06-6-1	23.9	1.06	-0.18
JL06-6-1	22.0	1.30	-0.23
JL06-6-1	20.2	1.30	-0.53
JL06-6-1	18.5	1.33	-0.21
JL06-6-1	16.8	1.10	-0.22
JL06-6-1	15.1	1.38	-0.11
JL06-6-1	13.0	1.31	-0.26
JL06-6-1	10.8	1.22	-0.41
JL06-6-1	8.7	1.28	-0.30
JL06-6-1	6.8	1.21	-0.03
JL06-6-1	5.0	1.36	-0.01
JL06-6-1	3.6	1.60	-0.04
JL06-6-1	1.9	1.13	-0.09
JL06-6-1	0.0	1.36	-0.28
JL06-29-1A	99.0	0.71	-0.68
JL06-29-1A	97.3	0.85	-0.79
JL06-29-1A	95.1	1.67	-0.28
JL06-29-1A	93.2	1.63	-0.90
JL06-29-1A	91.6	1.37	-0.80
JL06-29-1A	89.6	1.77	-0.93
JL06-29-1A	88.5	1.70	-0.75
JL06-29-1A	86.3		-0.99
JL06-29-1A	85.4	1.91	-0.61
JL06-29-1A	83.2	1.87	-0.55
JL06-29-1A	80.8	1.64	-0.34
JL06-29-1A	79.0	1.33	-0.73
JL06-29-1A	76.5	1.46	-0.86
JL06-29-1A	74.0	1.37	-0.99
JL06-29-1A	71.1	1.44	-1.38
JL06-29-1A	68.0	1.38	-1.21
JL06-29-1A	64.8		-1.18
JL06-29-1A	63.6	1.53	-0.76
JL06-29-1A	61.0	1.31	-0.57
JL06-29-1A	59.7	1.46	-0.57
JL06-29-1A	53.1	1.21	-0.88
JL06-29-1A	50.7	1.33	-0.92
JL06-29-1A	49.4	1.18	-1.02
JL06-29-1A	47.3		-1.08

Sample ID	Length from apex (mm)	$\delta^{13}C$	$\delta^{18}O$
JL06-29-1A	45.0	1.38	-0.66
JL06-29-1A	42.5	1.85	-0.65
JL06-29-1A	40.1	1.68	-1.00
JL06-29-1A	37.6	1.58	-1.08
JL06-29-1A	34.7	1.82	-1.20
JL06-29-1A	32.2	1.95	-1.06
JL06-29-1A	29.9	1.99	-0.96
JL06-29-1A	27.2	1.67	-0.91
JL06-29-1A	24.5	1.88	-0.75
JL06-29-1A	23.0	1.66	-0.72
JL06-29-1A	21.5		-0.86
JL06-29-1A	18.7		-0.98
JL06-29-1A	15.9	1.75	-0.66
JL06-29-1A	13.2	2.14	-1.05
JL06-29-1A	10.6	2.29	-1.13
JL06-29-1A	7.7	2.13	-0.82
JL06-29-1A	4.5	2.15	-1.09
JL06-29-1A	2.3	2.28	-1.08
JL06-29-1A	0.0	2.10	-1.15
JL06-29-1B	84.0	1.03	-0.81
JL06-29-1B	82.7	0.84	-0.72
JL06-29-1B	80.1	1.17	-0.40
JL06-29-1B	79.0	1.18	-0.49
JL06-29-1B	77.0	1.39	-0.54
JL06-29-1B	75.1	1.11	-0.50
JL06-29-1B	73.0	1.24	-0.78
JL06-29-1B	70.8	1.36	-0.88
JL06-29-1B	68.8	1.32	-1.19
JL06-29-1B	65.8	0.81	-1.17
JL06-29-1B	63.4	0.88	-0.75
JL06-29-1B	61.1	1.10	-1.04
JL06-29-1B	58.8	0.51	-1.04
JL06-29-1B	53.4	1.28	-1.00
JL06-29-1B	51.1	1.47	-1.03
JL06-29-1B	48.9	1.30	-0.98
JL06-29-1B	46.6	1.20	-0.72
JL06-29-1B	43.7	1.13	-1.07
JL06-29-1B	40.9	1.02	-1.12
JL06-29-1B	38.9	1.42	-1.04
JL06-29-1B	36.8	1.49	-0.64
JL06-29-1B	34.6	1.42	-0.77
JL06-29-1B	32.4	0.91	-0.83
JL06-29-1B	29.8	1.01	-1.06
JL06-29-1B	27.7	1.23	-1.04
JL06-29-1B	25.6	0.59	-0.94
JL06-29-1B	23.0	1.50	-0.67
JL06-29-1B	20.8	1.51	-0.69

Sample ID	Length from apex (mm)	$\delta^{13}C$	$\delta^{18}O$
JL06-29-1B	18.1	1.65	-0.68
JL06-29-1B	15.5	1.95	-0.71
JL06-29-1B	13.1	2.15	-0.67
JL06-29-1B	10.7	1.79	-0.68
JL06-29-1B	8.3	1.70	-0.91
JL06-29-1B	5.9	2.18	-1.09
JL06-29-1B	3.0	1.71	-1.07
AT06-5-1A	241.3	1.20	-0.55
AT06-5-1A	238.8	1.58	-0.56
AT06-5-1A	235.2	1.68	-0.35
AT06-5-1A	231.5	1.63	-0.37
AT06-5-1A	228.8	1.89	-0.38
AT06-5-1A	226.0	1.90	0.11
AT06-5-1A	223.4	1.39	-0.65
AT06-5-1A	220.6	1.77	-0.33
AT06-5-1A	217.4	1.77	-0.02
AT06-5-1A	214.3	1.85	-0.39
AT06-5-1A	211.4	1.54	-0.71
AT06-5-1A	208.3	1.73	-0.40
AT06-5-1A	205.2	1.67	-0.27
AT06-5-1A	202.4	1.56	-0.37
AT06-5-1A	199.6	1.66	-0.58
AT06-5-1A	196.6	1.86	-0.81
AT06-5-1A	193.4	1.98	-0.19
AT06-5-1A	190.6	2.16	-0.46
AT06-5-1A	187.3	2.25	-0.65
AT06-5-1A	184.8	2.17	-1.07
AT06-5-1A	182.1	1.79	-1.25
AT06-5-1A	179.1	1.73	-1.18
AT06-5-1A	175.9	2.10	-0.44
AT06-5-1A	173.4	2.51	-0.39
AT06-5-1A	170.4	2.43	-0.33
AT06-5-1A	167.8	2.56	-0.73
AT06-5-1A	165.6	2.34	-1.32
AT06-5-1A	162.4	2.36	-1.11
AT06-5-1A	159.9	2.41	-1.24
AT06-5-1A	157.4	2.73	-1.02
AT06-5-1A	153.8	2.60	-1.51
AT06-5-1A	150.7	2.21	-1.25
AT06-5-1A	148.0	2.30	-0.79
AT06-5-1A	145.7	1.97	-1.00
AT06-5-1A	142.6	1.97	-0.49
AT06-5-1A	140.1	1.98	-0.67
AT06-5-1A	137.1	1.90	-0.99
AT06-5-1A	134.2	1.47	-1.17
AT06-5-1A	130.7	2.04	-1.49
AT06-5-1A	127.8	2.45	-1.17

Sample ID	Length from apex (mm)	$\delta^{13}C$	$\delta^{18}O$
AT06-5-1A	125.4	2.47	-1.46
AT06-5-1A	122.4	3.04	-1.07
AT06-5-1A	120.2	2.71	-0.80
AT06-5-1A	117.0	2.73	-0.76
AT06-5-1A	114.2	2.83	-0.70
AT06-5-1A	111.5	2.62	-0.76
AT06-5-1A	108.8	2.54	-0.82
AT06-5-1A	105.4	2.37	-0.92
AT06-5-1A	102.8	2.48	-0.22
AT06-5-1A	100.9	2.43	-0.35
AT06-5-1A	98.6	2.65	-0.64
AT06-5-1A	96.4	2.50	-0.83
AT06-5-1A	93.5	2.49	-0.96
AT06-5-1A	91.2	2.60	-1.19
AT06-5-1A	88.7	2.45	-1.33
AT06-5-1A	85.6	2.47	-1.39
AT06-5-1A	83.2	2.65	-1.32
AT06-5-1A	80.5	2.58	-1.90
AT06-5-1A	78.2	2.46	-1.80
AT06-5-1A	76.0	2.58	-1.89
AT06-5-1A	73.3	2.61	-1.11
AT06-5-1A	71.1	2.49	-1.00
AT06-5-1A	68.1	2.71	-1.22
AT06-5-1A	65.0	2.61	-1.39
AT06-5-1A	62.3	2.73	-0.91
AT06-5-1A	59.8	2.44	-0.97
AT06-5-1A	57.8	2.64	-0.65
AT06-5-1A	55.0	2.60	-0.86
AT06-5-1A	52.6	2.71	-0.60
AT06-5-1A	49.7	2.39	-0.56
AT06-5-1A	47.4	2.85	-0.46
AT06-5-1A	45.3	2.87	-0.48
AT06-5-1A	42.7	2.93	-0.38
AT06-5-1A	39.7	2.61	-0.45
AT06-5-1A	36.9	2.88	-0.64
AT06-5-1A	34.1	2.69	-0.55
AT06-5-1A	31.0	2.44	-0.32
AT06-5-1A	28.3	2.63	-0.62
AT06-5-1A	25.7	2.52	-0.27
AT06-5-1A	23.4	2.63	-0.63
AT06-5-1A	20.9	2.69	-0.34
AT06-5-1A	18.3	2.58	-0.72
AT06-5-1A	15.7	2.56	-1.32
AT06-5-1A	12.8	2.46	-1.18
AT06-5-1A	10.2	2.50	-1.13
AT06-5-1A	7.6	2.51	-1.04
AT06-5-1A	5.1	2.44	-1.40
AT06-5-1A	2.5	2.40	-0.94

Sample ID	Length from apex (mm)	$\delta^{13}C$	$\delta^{18}O$
AT06-5-1A	0.0	2.39	-0.99
AT06-5-1B	88.0	2.52	-0.17
AT06-5-1B	86.9	2.46	-0.70
AT06-5-1B	85.7	2.63	-0.39
AT06-5-1B	84.2	2.63	-0.30
AT06-5-1B	82.7	2.35	-0.26
AT06-5-1B	81.2	2.42	-0.32
AT06-5-1B	79.6	2.24	-0.51
AT06-5-1B	77.6	2.33	-0.95
AT06-5-1B	75.8	2.71	-0.81
AT06-5-1B	74.0	2.74	-1.03
AT06-5-1B	71.6	2.69	-1.00
AT06-5-1B	69.5	2.64	-1.30
AT06-5-1B	67.9	2.57	-1.03
AT06-5-1B	66.2	2.71	-0.68
AT06-5-1B	60.4	2.70	-0.07
AT06-5-1B	58.2	2.68	0.04
AT06-5-1B	56.3	2.90	0.18
	55.3	2.82	-0.13
AT06-5-1B	54.3	2.95	-0.43
AT06-5-1B	52.0	2.62	-0.41
AT06-5-1B	49.5	2.71	-0.17
AT06-5-1B	46.3	2.71	-0.29
AT06-5-1B	44.0	2.74	-0.09
AT06-5-1B	41.6	3.01	-0.14
AT06-5-1B	39.4	3.08	-0.27
AT06-5-1B	36.9	3.02	-0.09
AT06-5-1B	34.1	3.06	-0.12
AT06-5-1B	31.4	2.81	-0.02
AT06-5-1B	28.8	2.72	-0.16
AT06-5-1B	26.1	2.93	-0.27
AT06-5-1B	23.5	2.67	-0.22
AT06-5-1B	21.6	2.83	0.08
AT06-5-1B	19.4	3.02	-0.46
AT06-5-1B	17.2	2.63	0.19
AT06-5-1B	14.9	2.31	-0.51
AT06-5-1B	12.3	2.79	-0.72
AT06-5-1B	9.9	2.76	-0.26
AT06-5-1B	7.5	2.84	-0.85
AT06-5-1B	5.0	2.58	-1.05
AT06-5-1B	2.5	2.54	-1.13
AT06-19-1	78.3	2.11	0.86
AT06-19-1	76.5	2.18	1.33
AT06-19-1	74.5	2.08	1.38
AT06-19-1	72.1	2.20	1.12
AT06-19-1	69.9	1.85	0.70

Sample ID	Length from apex (mm)	$\delta^{13}C$	$\delta^{18}O$
AT06-19-1	68.1	1.87	0.52
AT06-19-1	66.0	2.06	0.89
AT06-19-1	63.1	2.09	0.91
AT06-19-1	60.7	2.34	1.01
AT06-19-1	58.3	2.37	1.03
AT06-19-1	55.6	2.41	1.05
AT06-19-1	53.0	2.48	0.73
AT06-19-1	50.6	2.45	1.11
AT06-19-1	47.7	2.41	0.91
AT06-19-1	45.3	2.32	0.86
AT06-19-1	43.0	2.33	0.78
AT06-19-1	41.0	2.39	1.02
AT06-19-1	39.0	2.23	0.85
AT06-19-1	37.0	2.09	0.72
AT06-19-1	34.9	2.17	0.72
AT06-19-1	32.7	2.21	0.56
AT06-19-1	30.7	2.39	0.51
AT06-19-1	28.0	2.30	0.64
AT06-19-1	25.3	2.35	0.63
AT06-19-1	23.5	2.30	0.40
AT06-19-1	21.3	2.24	0.34
AT06-19-1	19.2	2.31	0.56
AT06-19-1	16.2	2.25	0.34
AT06-19-1	13.9	2.15	0.47
AT06-19-1	11.7	1.97	0.75
AT06-19-1	9.7	2.09	0.38
AT06-19-1	8.1	2.19	0.28
AT06-19-1	6.2	2.04	0.24
AT06-19-1	4.3	1.95	0.04
AT06-19-1	2.2	2.05	0.16
AT06-19-1	0.0	1.94	0.50
JL06-15-1	179.8	0.64	-0.22
JL06-15-1	177.8	-0.02	-0.66
JL06-15-1	175.8	1.00	-0.24
JL06-15-1	173.3	0.10	-0.28
JL06-15-1	170.5	-0.35	-0.38
JL06-15-1	168.6	-0.58	-0.33
JL06-15-1	166.6	0.38	-0.34
JL06-15-1	164.5	-0.29	-0.38
JL06-15-1	162.2	0.72	-0.37
JL06-15-1	159.8	-0.29	-0.66
JL06-15-1	157.0	1.24	-0.57
JL06-15-1	154.9	-0.10	-0.35
JL06-15-1	152.6	-0.10	-0.40
JL06-15-1	150.4	-0.59	-0.50
JL06-15-1	148.2	-0.99	-0.40
JL06-15-1	145.9	-0.17	-0.56

Sample ID	Length from apex (mm)	$\delta^{13}C$	$\delta^{18}O$
JL06-15-1	143.6	0.37	-0.76
JL06-15-1	141.6	0.25	-0.66
JL06-15-1	139.6	-0.26	-0.59
JL06-15-1	137.4	-0.50	-0.63
JL06-15-1	135.1	-0.26	-0.83
JL06-15-1	132.5	-0.10	-0.59
JL06-15-1	130.1	0.53	-0.84
JL06-15-1	128.2	0.00	-0.95
JL06-15-1	125.9	-0.42	-0.96
JL06-15-1	124.0	0.01	-0.81
JL06-15-1	122.0	-0.29	-0.76
JL06-15-1	119.9	-0.22	-0.84
JL06-15-1	116.9	-0.10	-0.39
JL06-15-1	114.6	-0.32	-0.60
JL06-15-1	112.2	-1.08	-0.85
JL06-15-1	110.7	-0.58	-0.81
JL06-15-1	108.1	-0.42	-0.91
JL06-15-1	106.4	-0.58	-0.91
JL06-15-1	104.6	-1.34	-1.01
JL06-15-1	102.6	-1.12	-1.32
JL06-15-1	99.8	-1.34	-0.77
JL06-15-1	97.7	-1.31	-0.75
JL06-15-1	95.1	-0.79	-0.91
JL06-15-1	93.0	-0.40	-0.84
JL06-15-1	90.7	-0.31	-0.62
JL06-15-1	88.5	0.87	-0.53
JL06-15-1	86.8	0.64	-0.79
JL06-15-1	85.2	-0.09	-0.54
JL06-15-1	82.8	0.78	-0.57
JL06-15-1	80.6	1.05	-0.52
JL06-15-1	78.7	0.15	-0.52
JL06-15-1	76.2	1.43	-0.54
JL06-15-1	74.3	0.43	-0.76
JL06-15-1	72.6	0.78	-0.46
JL06-15-1	70.0	0.65	-0.53
JL06-15-1	67.7	0.38	-0.59
JL06-15-1	65.4	0.59	-0.63
JL06-15-1	63.3	-0.17	-0.68
JL06-15-1	61.3	0.50	-0.63
JL06-15-1	59.5	-0.35	-0.81
JL06-15-1	57.7	0.33	-0.84
JL06-15-1	55.5	0.03	-1.01
JL06-15-1	53.1	0.41	-1.16
JL06-15-1	51.4	0.86	-1.19
JL06-15-1	49.1	0.60	-0.89
JL06-15-1	46.5	0.83	-0.70
JL06-15-1	44.0	1.33	-0.70
JL06-15-1	41.6	0.76	-0.80

Sample ID	Length from apex (mm)	$\delta^{13}C$	$\delta^{18}O$
JL06-15-1	39.0	0.61	-0.89
JL06-15-1	36.5	0.47	-0.89
JL06-15-1	33.6	0.76	-0.70
JL06-15-1	31.0	0.99	-0.72
JL06-15-1	29.1	1.25	-0.65
JL06-15-1	26.7	0.99	-0.64
JL06-15-1	23.3	1.07	-0.66
JL06-15-1	20.5	1.37	-0.55
JL06-15-1	18.1	1.35	-0.47
JL06-15-1	15.2	0.88	-0.71
JL06-15-1	12.3	0.97	-0.72
JL06-15-1	9.9	0.76	-0.56
JL06-15-1	7.6	1.44	-0.56
JL06-15-1	5.4	1.20	-0.58
JL06-15-1	2.8	1.09	-0.62
JL06-15-1	0.0	1.43	-0.50
AT06-22-1A	67.7	1.30	-0.03
AT06-22-1A	66.0	1.57	-0.22
AT06-22-1A	64.8	1.53	0.03
AT06-22-1A	63.6	1.77	0.07
AT06-22-1A	62.4	1.71	0.06
AT06-22-1A	60.8	1.66	-0.04
AT06-22-1A	59.1	1.75	-0.11
AT06-22-1A	57.5	1.96	0.14
AT06-22-1A	56.0	1.91	0.27
AT06-22-1A	54.1	1.36	-0.02
AT06-22-1A	52.6	1.81	0.06
AT06-22-1A	50.9	2.11	-0.07
AT06-22-1A	49.2	2.52	0.28
AT06-22-1A	47.2	2.56	0.20
AT06-22-1A	45.4	2.59	0.34
	44.5	2.17	0.19
AT06-22-1A	43.7	2.02	0.21
AT06-22-1A	42.0	2.03	0.18
AT06-22-1A	40.5	2.13	0.10
AT06-22-1A	39.0	1.96	0.09
AT06-22-1A	37.5	2.11	-0.08
AT06-22-1A	36.2	1.87	0.00
AT06-22-1A	34.5	1.96	0.16
AT06-22-1A	33.1	2.04	-0.02
AT06-22-1A	31.7	2.23	-0.04
	31.0	2.23	0.04
AT06-22-1A	30.4	1.90	-0.03
AT06-22-1A	29.0	2.00	-0.02
AT06-22-1A	27.8	2.02	-0.16
AT06-22-1A	26.7	2.09	-0.02
AT06-22-1A	25.5	2.00	0.00

Sample ID	Length from apex (mm)	$\delta^{13}C$	$\delta^{18}O$
AT06-22-1A	23.2	2.13	0.07
AT06-22-1A	21.0	2.34	0.32
AT06-22-1A	19.8	2.48	0.06
AT06-22-1A	17.7	2.04	-0.02
AT06-22-1A	15.5	2.19	0.14
AT06-22-1A	13.4	1.97	-0.04
AT06-22-1A	11.4	2.51	0.08
AT06-22-1A	9.4	2.60	0.21
AT06-22-1A	7.5	2.54	0.30
AT06-22-1A	5.7	2.31	0.20
AT06-22-1A	3.5	2.34	0.26
AT06-22-1A	1.8	2.36	0.17
AT06-22-1A	0.0	2.32	0.29
GFG-A	127.3	1.84	-0.12
GFG-A	125.5	1.80	-0.57
GFG-A	123.0	1.83	-0.97
GFG-A	121.4	1.71	-0.75
GFG-A	119.3	1.96	-0.38
GFG-A	117.4	1.77	-0.51
GFG-A	115.2	1.81	-0.22
GFG-A	113.7	1.76	-0.42
GFG-A	111.6	1.73	-0.79
GFG-A	109.3	1.44	-0.95
GFG-A	107.2	1.45	-0.64
GFG-A	105.6	1.52	-0.60
GFG-A	104.0	1.69	-0.16
GFG-A	101.6	1.70	-0.20
GFG-A	99.8	1.70	-0.50
GFG-A	96.6	1.78	-0.31
GFG-A	94.2	1.95	-0.29
GFG-A	91.7	1.95	-0.34
GFG-A	89.7	1.83	-0.51
GFG-A	86.9	1.71	-0.53
GFG-A	84.7	1.81	-0.55
GFG-A	83.3	1.97	-0.82
GFG-A	80.8	1.81	-0.86
GFG-A	78.6	1.54	-0.82
GFG-A	76.4	1.88	-0.44
GFG-A	74.4	1.82	0.10
GFG-A	72.4	1.83	-0.36
GFG-A	70.2	1.85	-0.44
GFG-A	68.2	1.79	-0.51
GFG-A	66.3	2.10	-0.47
GFG-A	64.1	2.28	-0.66
GFG-A	61.8	2.46	-0.48
GFG-A	59.8	2.43	-0.45
GFG-A	57.5	2.31	-0.73

Sample ID	Length from apex (mm)	$\delta^{13}C$	$\delta^{18}O$
GFG-A	54.9	2.24	-0.62
GFG-A	53.0	2.19	-0.59
GFG-A	50.9	2.19	-0.40
GFG-A	48.7	2.18	-0.54
GFG-A	46.2	2.63	-0.49
GFG-A	43.9	2.44	-0.52
GFG-A	41.5	2.30	-0.78
GFG-A	39.1	2.23	-0.90
GFG-A	36.7	2.09	-1.18
GFG-A	34.2	1.87	-0.29
GFG-A	31.6	2.17	-0.73
GFG-A	29.0	2.18	-0.68
GFG-A	26.7	1.94	-0.85
GFG-A	24.3	2.10	-0.82
GFG-A	21.9	2.13	-0.53
GFG-A	19.5	2.05	-0.74
GFG-A	16.8	2.23	-0.96
GFG-A	13.9	2.04	-0.91
GFG-A	11.3	1.87	-0.85
GFG-A	8.9	2.13	-0.64
GFG-A	6.9	2.02	-0.68
GFG-A	4.4	2.28	-0.75
GFG-A	2.3	1.87	-0.75
GFG-A	0.0	1.92	-0.91
GFS-2A	100.5	2.12	-1.03
GFS-2A	98.9	2.51	-1.08
GFS-2A	97.4	2.68	-1.05
GFS-2A	95.3	2.51	-0.96
GFS-2A	93.5	2.63	-0.95
GFS-2A	91.8	2.26	-0.94
GFS-2A	89.4	1.76	-1.21
GFS-2A	87.9	1.91	-1.23
GFS-2A	85.9	2.13	-1.07
GFS-2A	84.5	2.05	-1.10
GFS-2A	82.9	2.41	-0.85
GFS-2A	81.0	2.74	-0.84
GFS-2A	79.6	2.41	-1.05
GFS-2A	77.7	2.71	-1.07
GFS-2A	75.8	3.09	-1.06
GFS-2A	74.0	3.15	-1.02
GFS-2A	72.5	3.11	-1.06
GFS-2A	70.5	2.96	-1.06
GFS-2A	68.4	2.85	-0.94
GFS-2A	66.4	2.68	-1.13
GFS-2A	64.1	2.85	-1.17
GFS-2A	62.3	2.82	-1.15
GFS-2A	60.7	2.78	-1.05

Sample ID	Length from apex (mm)	$\delta^{13}C$	$\delta^{18}O$
GFS-2A	58.3	2.68	-0.98
GFS-2A	56.2	2.75	-1.02
GFS-2A	52.3	2.77	-1.25
GFS-2A	50.6	3.02	-1.28
GFS-2A	48.9	2.84	-1.27
GFS-2A	46.8	2.92	-1.33
GFS-2A	44.8	2.93	-1.41
GFS-2A	43.2	2.93	-1.39
GFS-2A	41.5	2.70	-1.57
GFS-2A	39.8	2.74	-1.78
GFS-2A	38.2	2.88	-1.31
GFS-2A	36.9	2.76	-1.41
GFS-2A	35.3	2.89	-1.51
GFS-2A	33.5	3.04	-1.54
GFS-2A	31.3	3.08	-1.36
GFS-2A	29.1	2.92	-1.30
GFS-2A	26.8	3.01	-1.37
GFS-2A	24.5	2.93	-1.45
GFS-2A	21.8	2.64	-1.04
GFS-2A	19.4	2.82	-1.00
GFS-2A	16.8	2.77	-1.12
GFS-2A	14.4	2.64	-0.90
GFS-2A	11.9	2.57	-0.64
GFS-2A	9.6	2.60	-0.76
GFS-2A	7.1	2.66	-1.01
GFS-2A	4.4	2.75	-1.15
GFS-2A	2.5	2.85	-1.25
GFS-2A	0.0	2.90	-0.98
GFS-3A	67.8	2.02	-0.93
GFS-3A	64.8	2.17	-1.72
GFS-3A	63.0	2.14	-1.98
GFS-3A	60.9	2.33	-1.38
GFS-3A	59.2	2.32	-1.09
GFS-3A	57.6	2.31	-1.04
GFS-3A	55.3	1.99	-1.02
GFS-3A	53.3	1.76	-0.63
GFS-3A	51.0	1.87	-1.13
GFS-3A	49.1	1.82	-1.06
GFS-3A	47.4	1.88	-1.29
GFS-3A	45.9	2.05	-1.13
GFS-3A	43.6	2.45	-1.57
GFS-3A	41.8	2.18	-1.54
GFS-3A	39.5	2.17	-2.03
GFS-3A	37.6	2.00	-1.70
GFS-3A	35.7	2.09	-1.38
GFS-3A	33.9	1.94	-0.77
GFS-3A	31.4	1.82	-0.37

Sample ID	Length from apex (mm)	$\delta^{13}C$	$\delta^{18}O$
GFS-3A	29.5	1.97	-1.00
GFS-3A	27.2	2.08	-0.77
GFS-3A	25.0	2.16	-1.01
GFS-3A	22.9	2.13	-1.02
GFS-3A	21.0	2.22	-1.11
GFS-3A	19.1	2.16	-0.91
GFS-3A	17.1	1.95	-0.22
GFS-3A	14.9	2.20	-0.28
GFS-3A	12.8	2.03	-0.87
GFS-3A	10.6	2.29	-0.96
GFS-3A	8.3	2.15	-1.09
GFS-3A	6.0	2.18	-1.09
GFS-3A	3.8	2.26	-1.50
GFS-3A	1.9	2.31	-1.35
GFS-3A	0.0	2.37	-1.42
GFS-3B	84.8	2.47	-1.23
GFS-3B	82.8	2.28	-1.62
GFS-3B	80.3	2.36	-1.10
GFS-3B	78.4	2.44	-1.02
GFS-3B	76.8	2.47	-1.00
GFS-3B	74.4	2.77	-1.17
GFS-3B	71.6	2.49	-1.13
GFS-3B	69.4	2.98	-1.26
GFS-3B	67.1	2.98	-1.51
GFS-3B	65.5	3.05	-1.64
GFS-3B	62.9	2.70	-1.50
GFS-3B	60.1	2.93	-1.54
GFS-3B	57.5	2.28	-1.38
GFS-3B	55.0	1.99	-1.27
GFS-3B	52.7	2.54	-1.18
GFS-3B	50.7	2.50	-1.10
GFS-3B	47.7	2.72	-1.13
GFS-3B	45.3	2.57	-1.13
GFS-3B	43.4	2.38	-0.99
GFS-3B	41.2	2.32	-0.84
GFS-3B	39.2	2.09	-0.87
GFS-3B	36.7	2.47	-0.93
GFS-3B	34.1	2.26	-0.95
GFS-3B	32.0	2.65	-0.84
GFS-3B	29.9	2.58	
GFS-3B	28.0	3.10	-0.92
GFS-3B	25.7	2.88	-0.93
GFS-3B	23.4	2.46	-0.82
GFS-3B	20.9	2.89	-1.00
GFS-3B	18.5	2.82	-1.22
GFS-3B	16.2	2.96	-1.69
GFS-3B	14.0	2.92	-1.66

Sample ID	Length from apex (mm)	$\delta^{13}C$	$\delta^{18}O$
GFS-3B	11.7	3.12	-1.64
GFS-3B	9.4	2.75	-1.67
GFS-3B	7.1	2.67	-1.72
GFS-3B	4.8	2.42	-1.69
GFS-3B	2.4	2.81	-1.36
GFS-3B	0.0	2.59	-1.23
GFS-3F	87.1	1.80	-1.09
GFS-3F	85.9	1.78	-1.13
GFS-3F	84.1	2.09	-1.57
GFS-3F	81.8	1.83	-0.99
GFS-3F	79.5	2.08	-0.94
GFS-3F	78.1	1.98	-1.10
GFS-3F	76.4	1.97	-1.60
GFS-3F	75.0	2.17	-1.57
GFS-3F	73.2	2.04	-1.40
GFS-3F	71.2	1.92	-1.32
GFS-3F	69.6	2.00	-1.29
GFS-3F	67.8	2.04	-1.12
GFS-3F	65.9	2.20	-1.04
GFS-3F	63.8	2.18	-0.80
GFS-3F	61.2	2.06	-0.70
GFS-3F	58.9	2.10	-1.13
GFS-3F	57.0	2.14	-1.08
GFS-3F	55.3	1.99	-1.25
GFS-3F	52.7	2.53	-1.94
GFS-3F	50.3	2.55	-1.79
GFS-3F	48.9	2.59	-1.69
GFS-3F	46.9	2.44	-1.59
GFS-3F	44.4	2.49	-1.39
GFS-3F	42.0	2.11	-1.16
GFS-3F	39.9	2.23	-1.07
GFS-3F	38.2	2.44	-1.15
GFS-3F	36.2	2.04	-0.96
GFS-3F	34.3	2.20	-0.94
GFS-3F	32.1	2.26	-0.94
GFS-3F	30.0	2.60	-1.10
GFS-3F	27.7	2.35	-1.01
GFS-3F	25.5	2.30	-1.41
GFS-3F	23.9	2.85	-1.60
GFS-3F	22.2	2.77	-1.73
GFS-3F	20.5	3.34	-1.57
GFS-3F	18.9	3.21	-1.60
GFS-3F	17.2	3.06	-1.54
GFS-3F	15.4	3.07	-1.31
GFS-3F	13.5	3.06	-1.43
GFS-3F	11.4	2.97	-1.39
GFS-3F	9.4	2.56	-1.44

Sample ID	Length from apex (mm)	$\delta^{13}C$	$\delta^{18}O$
GFS-3F	7.4	2.59	-1.24
GFS-3F	5.5	2.45	-1.00
GFS-3F	3.7	2.89	-0.99
GFS-3F	1.9	2.64	-0.94
GFS-3F	0.0	2.99	-0.88
GPR-A	108.6	1.96	-0.53
GPR-A	107.0	1.84	-0.67
GPR-A	105.5	2.22	-0.71
GPR-A	103.9	2.26	-0.89
GPR-A	102.1	2.05	-0.73
GPR-A	100.6	1.94	-0.98
GPR-A	98.9	2.17	-1.37
GPR-A	97.1	1.70	-1.33
GPR-A	94.8	1.48	-0.96
GPR-A	92.6	1.40	-1.20
GPR-A	91.1	1.93	-1.08
GPR-A	89.3	1.73	-0.82
GPR-A	87.1	1.89	-0.58
GPR-A	85.4	2.12	-0.58
GPR-A	84.2	2.23	-1.60
GPR-A	83.0	1.84	-1.60
GPR-A	81.1	1.80	-0.76
GPR-A	79.3	1.79	-0.58
GPR-A	77.2	2.17	-0.73
GPR-A	74.9	2.32	-1.05
GPR-A	73.1	2.25	-1.31
GPR-A	71.3	2.00	-1.64
GPR-A	70.4	1.70	-0.93
GPR-A	69.5	1.79	-0.61
GPR-A	67.7	1.83	-0.74
GPR-A	65.7	1.57	-0.70
GPR-A	64.3	1.72	-0.84
GPR-A	62.1	2.15	-1.10
GPR-A	60.1	2.31	-1.45
GPR-A	58.4	2.22	-1.67
GPR-A	56.2	1.99	-1.46
GPR-A	54.0	1.80	-1.50
GPR-A	51.7	1.87	-0.85
GPR-A	49.6	1.73	-0.90
GPR-A	47.3	1.71	-0.78
GPR-A	45.1	1.72	-0.59
GPR-A	43.1	1.95	-1.17
GPR-A	41.1	2.05	-0.67
GPR-A	39.1	2.45	-0.73
GPR-A	37.3	2.46	-0.79
GPR-A	35.4	2.39	-0.63
GPR-A	33.5	2.37	-0.77

Sample ID	Length from apex (mm)	$\delta^{13}C$	$\delta^{18}O$
GPR-A	31.8	2.67	-0.66
GPR-A	30.2	2.75	-0.88
GPR-A	28.6	2.45	-0.97
GPR-A	26.9	2.58	-0.94
GPR-A	25.3	2.37	-1.39
GPR-A	23.6	2.08	-1.46
GPR-A	22.0	2.32	-1.71
GPR-A	20.3	2.62	-1.32
GPR-A	18.5	2.58	-1.54
GPR-A	16.8	2.41	-1.50
GPR-A	15.1	2.86	-1.56
GPR-A	11.8	2.68	-1.39
GPR-A	10.2	2.60	-1.38
GPR-A	8.9	2.63	-1.15
GPR-A	7.3	2.09	-1.01
GPR-A	5.0	2.21	-0.90
GPR-A	2.7	2.06	-0.93
GPR-A	0.0	2.67	-0.96

APPENDIX 3

CALCULATION OF PALEO-SSTS AND BASELINE $\delta^{18}O$ VALUES AND ERROR ANALYSES OF THE PANAMA SAMPLES

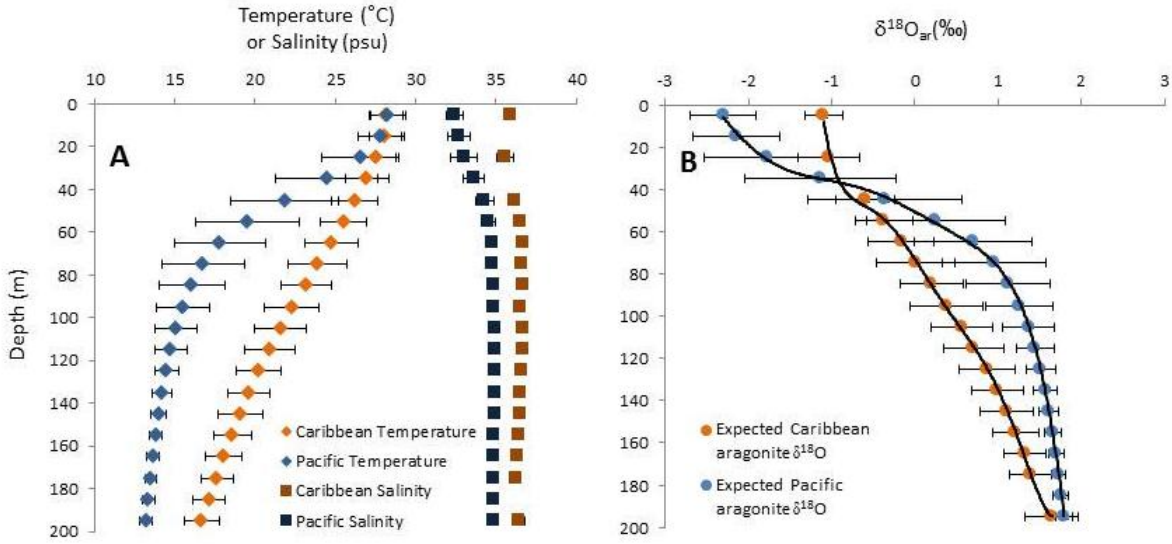

APPENDIX FIGURE 1—(A) Modern seawater temperature and salinity and (B) expected aragonite $\delta^{18}O$ values ($\delta^{18}O_{ar}$) versus depth. Temperature and salinity data are from WOD 2009 data set and equilibrium $\delta^{18}O_{ar}$ determined using the Grossman and Ku (1986) equation.

Calculation of baseline $\delta^{18}O$ values, the reference from which seasonal upwelling and freshwater input are quantified, requires open ocean $\delta^{18}O$ values free of upwelling and local freshwater influences. These $\delta^{18}O$ values are based on planktonic foraminiferal $\delta^{18}O$ values from DSDP and ODP cores. However, to correct for paleo-depth differences between the planktonic foraminifera and the mollusk shells, foraminiferal $\delta^{18}O$ data and paleo-SST proxies are used to calculate seawater $\delta^{18}O$ from foraminiferal $\delta^{18}O$. Modern

temperature and seawater $\delta^{18}O$ profiles are then used to determine the depth correction, followed by the calculation of baseline $\delta^{18}O$ values for *Conus* aragonite. These steps are detailed below.

1. The seawater $\delta^{18}O$ values are derived from Eq. (1), which has two quadratic roots:

$$\delta^{18}O_w = \delta^{18}O_{cl} - \frac{4.36 \pm \sqrt{4.36^2 - 0.48(15.7 - T)}}{0.24} \qquad (2)$$

where cl is planktonic foraminiferal calcite. Both $\delta^{18}O_{cl}$ and T are averaged values of each sample's age interval. Only one of the roots generate reasonable $\delta^{18}O_w$ values, which is

$$\delta^{18}O_w = \delta^{18}O_{cl} - \frac{4.36 - \sqrt{4.36^2 - 0.48(15.7 - T)}}{0.24} \qquad (3)$$

2. Depth correction of the molluscan $\delta^{18}O$ values are derived from the regression fits of the modern SWC and TEP $\delta^{18}O_{ar\text{-}depth}$ derived from WOD 2009 data and shown in Appendix Figure 1, which are:

$$\delta^{18}O_{SWC} = 1.2636\times10^{-12}d^6 - 8.0582\times10^{-10}d^5 + 2.0336\times^{-7}d^4 - 2.5819\times10^{-5}d^3 + 1.6731\times10^{-3}d^2 - 2.9989\times10^{-2}d - 0.986 \quad (R^2=0.9999) \qquad (4)$$

$$\delta^{18}O_{TEP} = 3.8680\times10^{-12}d^6 - 2.6737\times10^{-9}d^5 + 7.1863\times^{-7}d^4 - 9.2724\times10^{-5}d^3 + 5.4887\times10^{-3}d^2 - 7.8116\times10^{-2}d - 2.012 \quad (R^2=0.9993) \qquad (5)$$

where d is the depth of each specimen. These equations assume that the Neogene $\delta^{18}O_{ar\text{-}depth}$ profiles are same to those in the modern.

3. The paleo-SSTs are calculated from Grossman and Ku (1986; modified by Hudson and Arthur, 1989), which is:

$$T\ (°C) = 19.7 - 4.34(\delta^{18}O_{ar\text{-}corr} - \delta^{18}O_w) \qquad (6)$$

Note that $\delta^{18}O_{ar\text{-}corr}$ is the $\delta^{18}O$ value of gastropod shell after depth correction.

4. Calculation of error in the paleo-SST calculation comes from errors in the

determination of $\delta^{18}O_{ar\text{-}corr}$ and $\delta^{18}O_w$, and the error of the $\delta^{18}O_w$ comes primarily from $\delta^{18}O_{cl}$, so the entire error can be derived from:

$$\varepsilon(T) = 4.34\sqrt{\varepsilon(\delta^{18}O_{ar})^2 + \varepsilon\left(\delta^{18}O_{depth-corr}\right)^2 + \varepsilon(\delta^{18}O_{cl})^2} \qquad (7)$$

where the depth correction error comes from the error in temperature and salinity of each depth and the error from the uncertainty of depth determination.

5. The baseline shell $\delta^{18}O$ values ($\delta^{18}O_{bl}$) for each sample location are derived from the depth-corrected temperature and seawater $\delta^{18}O$ using the Grossman and Ku (1986) equation:

$$\delta^{18}O_{bl} = \frac{19.7-T}{4.34} + \delta^{18}O_w \qquad (8)$$

6. The normalized shell $\delta^{18}O$ is then calculated as following:

$$\delta^{18}O_{norm} = \delta^{18}O_{shell} + \delta^{18}O_{depth-corr} - \delta^{18}O_{bl} \qquad (9)$$

7. The normalized ΔT during the upwelling event and normalized ΔS associated with freshwater input is determined from Grossman and Ku (1986) and Fairbanks et al. (1992), respectively:

$$\Delta T = -4.34\delta^{18}O_{norm} \qquad (10)$$

$$\Delta S_{TEP} = \frac{1}{0.26}\delta^{18}O_{norm} \qquad (11)$$

$$\Delta S_{SWC} = \frac{1}{0.19}\delta^{18}O_{norm} \qquad (12)$$

8. The error in the normalized shell $\delta^{18}O$ comes from depth correction, literature temperature, and $\delta^{18}O_w$:

$$\varepsilon(\delta^{18}O_{norm}) = \sqrt{\varepsilon(\delta^{18}O_{shell})^2 + \varepsilon\left(\delta^{18}O_{depth-corr}\right)^2 + \left(\frac{\varepsilon(T)}{4.34}\right)^2 + \varepsilon(\delta^{18}O_{cl})^2} \qquad (13)$$

VITA

Kai Tao, of Wuhu, China, received his Bachelor of Science degree in geochemistry from University of Science and Technology of China in 2004. He began graduate Study at the Department of Geology and Geophysics at Texas A&M University in August, 2004. He graduated from Texas A&M University in 2012. His research interests include using stable isotope geochemistry to study nutrient sources on high-productivity regions, particularly in the low-latitude coastal seas. He plans a career in academia.

Mail to Mr. Tao can be sent to his advisor Dr. Ethan Grossman at Department of Geology and Geophysics, MS 3119, TAMU, College Station, TX 77845. Mr. Tao's email is taokai@gmail.com.